

Aus dem Pathologischen Institut  
der Ludwig-Maximilians-Universität München  
Direktor: Prof. Dr. med. Thomas Kirchner

# **Deciphering the role of the developmental transcription factor *SOX6* in tumorigenesis and progression of Ewing sarcoma**



**Dissertation**

Zum Erwerb des Doctor of Philosophy (Ph.D)  
an der Medizinischen Fakultät der  
Ludwig-Maximilians-Universität zu München

Vorgelegt von

**Aruna Marchetto**

aus München

2020

**Mit Genehmigung der Medizinischen Fakultät der Universität München**

Supervisor(s): PD Dr. med. Thomas Grünewald, Ph.D.

Prof. Dr. med. Thomas Kirchner

Dean: Prof. Dr. med. dent. Reinhard HICKEL

Day of oral defense: 18.05.2020

*Per i miei genitori*



## Affidavit

Pathologisches Institut der LMU  
**Marchetto, Aruna**  
Thalkirchner Str. 36  
80337 München

I hereby declare, that the submitted thesis entitled

**„Deciphering the roles of the developmental transcription factor *SOX6* in tumorigenesis and progression of Ewing sarcoma“**

is my own work. I have only used the sources indicated and have not made unauthorized use of services of a third party. Where the work of others has been quoted or reproduced, the source is always given.

I further declare that the submitted thesis or parts thereof have not been presented as part of an examination degree to any other university.

Munich, 20.05.2020

Aruna Marchetto

## **Confirmation of congruency between printed and electronic version of the doctoral thesis**

Pathologisches Institut der LMU  
**Marchetto, Aruna**  
Thalkirchner Str. 36  
80337 München

I hereby declare that the electronic version of the submitted thesis, entitled

**„Deciphering the roles of the developmental transcription factor *SOX6* in tumorigenesis and progression of Ewing sarcoma“**

is congruent with the printed version both in content and format.

Munich, 20.05.2020

Aruna Marchetto

**Table of contents**

Summary .....	V
1. Introduction.....	1
1.1 Ewing Sarcoma .....	1
1.1.1 Origin .....	1
1.1.2 Molecular and genetic profile of EwS .....	1
1.1.3 Clinical aspects: epidemiology, diagnosis and therapy .....	2
1.2 SRY-related HMG-box 6 (SOX6).....	4
1.2.1 SOX family of transcription factors .....	4
1.2.2 SOX6 gene: Structure and regulation .....	5
1.2.3 SOX6 function in vertebrate development .....	7
1.2.4 Role of SOX6 in endochondral ossification .....	8
1.2.5 SOX6 expression in tumors and other malignancies.....	10
1.3 Oxidative stress and the role of TXNIP .....	11
2 Research objectives and scientific aims .....	13
2.2 Research objectives.....	13
2.3 Scientific aims.....	13
3. Materials and methods .....	14
3.1 Materials.....	14
3.1.1 List of manufacturers .....	14
3.1.2 General materials .....	15
3.1.3 Mice strains .....	16
3.1.4 Instruments and equipment.....	16
3.1.5 Chemicals.....	17
3.1.6 Biological reagents .....	18
3.1.7 Commercial kits .....	19
3.1.8 Restriction enzymes .....	20
3.1.9 Primary and Secondary antibodies for Western blot and immunohistochemistry .....	20
3.1.9.1 Western blot.....	20
3.1.9.2 Immunohistochemistry .....	20
3.1.10 Buffer and solutions .....	20
3.1.11 SDS-PAGE gel compositions.....	21
3.1.12 Sequences.....	21
3.1.12.1 shRNA sequences for pLKO-Tet-On cloning .....	21
3.1.12.2 Sequences for pCDH vector cloning .....	22

---

3.1.12.3	Primer .....	22
3.1.12.4	Sequencing primer .....	23
3.1.12.5	Sequences for small interfering RNAs (siRNA) .....	23
3.1.13	Vectors.....	23
3.1.14	Software .....	23
3.2	Methods .....	24
3.2.1	Microbiology.....	24
3.2.1.1	Cloning with the pGL3-Promotor vector .....	24
3.2.1.2	Cloning with the pLKO-Tet-On system .....	28
3.2.1.3	Cumate-inducible pCDH-CuO-MCS-EF1 $\alpha$ CymR-T2A-Puro.....	31
3.2.1.4	Transformation of <i>E.coli</i> and colony PCR .....	33
3.2.1.5	Sequencing of pGL3-mSat, pLKO-shSOX6/shCtrl and pCDH-TXNIP constructs.....	36
3.2.2	Cell culture.....	37
3.2.2.1	Cell lines.....	37
3.2.2.2	Cell culture methods .....	38
3.2.2.3	Transduction of pLKO-shSOX6 and pLKO-shSOX6-pCDH-TXNIP in EwS cell lines .....	38
3.2.2.4	Transfection.....	39
3.2.3	Molecular biology.....	40
3.2.3.1	Isolation of total RNA, cDNA synthesis and quantitative real time PCR (qRT-PCR) .....	40
3.2.3.2	DNA extraction .....	41
3.2.4	Biochemistry.....	41
3.2.4.1	Generation of cell lysates and Bradford assay .....	41
3.2.4.2	SDS-PAGE and Western Blot.....	42
3.2.5	Cell-based assays.....	42
3.2.5.1	Cell proliferation.....	42
3.2.5.2	Clonogenic (2D) and sphere (3D) assay.....	44
3.2.5.3	Cell cycle analysis with propidium iodide.....	44
3.2.5.4	Determination of apoptosis with Annexin V staining .....	45
3.2.5.5	Drug-response assay .....	46
3.2.5.6	Detection of oxidative stress by DCF-DA fluorescence .....	47
3.2.5.7	Detection of mitochondrial ROS (mito-ROS) by MitoSOX Red fluorescence .....	47
3.2.5.8	Luciferase assay .....	48
3.2.6	Histology.....	49
3.2.6.1	Immunohistochemistry of cleaved caspase 3, SOX6, Ki67, 8-OHG and TXNIP.....	49
3.2.6.2	Quantification of immunohistological stainings.....	50

---

3.2.6.3	Human samples and ethics approval .....	51
3.2.7	Survival analysis.....	51
3.2.8	<i>In vivo</i> models.....	51
3.2.8.1	Xenograft subcutaneous murine model.....	51
3.2.8.2	Intravenous injection of Elesclomol .....	52
3.2.8.3	Orthotopic bone injection model.....	52
3.2.8.4	Patient-derived xenograft (PDX) model .....	53
3.2.9	Bioinformatic data analyses .....	54
3.2.9.1	Analysis of published DNase sequencing (DNase-Seq) and chromatin immuno-precipitation DNA sequencing (ChIP-Seq) data .....	54
3.2.9.2	Analysis of <i>SOX6</i> expression levels in human embryoid bodies.....	54
3.2.9.3	Analysis of copy-number-variation and promoter methylation in primary EwS .....	55
3.2.9.4	Transcriptome and splicing analyses.....	55
3.2.9.5	Gene expression and drug response correlation .....	57
3.2.10	Statistical analysis.....	57
4.	Results .....	58
4.1	<i>SOX6</i> is highly expressed in EwS compared to other sarcomas .....	58
4.2	<i>SOX6</i> does not correlate with EwS patient survival .....	61
4.3	Functional analysis of <i>SOX6</i> <i>in vitro</i> and <i>in vivo</i> .....	62
4.3.1	<i>SOX6</i> is induced by <i>EWSR1-FLI1</i> via an intronic enhancer-like GGAA-mSat .....	62
4.3.2	<i>SOX6</i> contributes to proliferation, cell-cycle progression and anchorage-independent colony-formation <i>in vitro</i> .....	65
4.3.3	Knockdown of <i>SOX6</i> inhibits tumorigenicity <i>in vivo</i> .....	69
4.3.4	Correlation of tumor growth in PDX of EwS patients with <i>SOX6</i> expression.....	71
4.4	Therapeutic aspect of <i>SOX6</i> .....	72
4.4.1	<i>SOX6</i> expression confers sensitivity toward small-molecule Elesclomol.....	72
4.4.2	Elesclomol induces apoptosis <i>in vitro</i> and necrosis <i>in vivo</i> .....	74
4.4.3	<i>SOX6</i> expression is associated with oxidative stress levels in EwS .....	76
4.4.4	<i>SOX6</i> regulates Elesclomol sensitivity via <i>TXNIP</i> .....	80
5.	Discussion .....	84
6.	Conclusions and limitations.....	88
6.1	Conclusions.....	88
6.2	Limitations .....	88
7.	References .....	90
8.	Appendix.....	101

---

8.1	1-kb sequence from the reference genome containing SOX6-mSat.....	101
8.2	List of GGAA-repeats of the <i>SOX6</i> -associated GGAA-mSat with different <i>SOX6</i> expressions and its corresponding enhancer activity .....	101
8.3	List of analyzed splicing events by microarray .....	102
8.4	List of differentially expressed genes (DEGs) .....	102
8.5	List of Gene Set Enrichment Analysis of DEGs.....	104
8.6	List of matched gene expression data with drug response data .....	105
8.7	List of figures .....	106
8.8	List of tables.....	107
8.9	List of abbreviations .....	108
9.	Acknowledgement.....	110
10.	Publications .....	111

## Summary

The aim of this thesis was to functionally characterize the role of the transcription factor *SOX6* in Ewing Sarcoma (EwS), since preliminary findings revealed that *SOX6* is highly expressed in EwS patients.

EwS is a bone or soft tissue tumor characterized by a fusion oncogene called *EWSR1-FLI1* that has been shown to regulate its target genes through GGAA-microsatellites (mSat). So far, it has been demonstrated that *SOX6* is actively expressed and it is essential for bone development during the endochondral ossification step, suggesting the importance of further analysis of this gene in a bone tumor such as EwS.

In fact, the presented data in this thesis revealed a new insight into the regulation of the transcription factor *SOX6* and its therapeutic vulnerability toward the oxidative stress-inducing drug Elesclomol.

Preliminary experiments showed, that the transcription factor *SOX6* is highly expressed in EwS patients, whereas its overexpression did not correlate with patient's survival.

For functional experiments, EwS cell lines were generated to induce *SOX6* knockdown via a doxycycline (Dox)-inducible shRNA against *SOX6*. Reporter assays demonstrated that *EWSR1-FLI1* hijacks *SOX6* via its binding to an intronic GGAA-mSat. Transcriptome-profiling and Gene Set Enrichment analysis (GSEA) offered valuable clues about the role of *SOX6* in EwS resulting in proliferation-related signatures, which were confirmed by functional assays. *SOX6* appears to be involved in cell cycle progression *in vitro* and in the promotion of tumor growth *in vivo*. Further analyses in combination with drug-screening data pointed out a strong sensitivity of EwS cells toward the oxidative stress-inducing small molecule Elesclomol. This drug is known to be an oxidative-stress inducing agent that exerts its potency by binding copper and transporting it into the mitochondria. There it produces free radicals inside the cell leading to mitochondrial apoptosis. In addition, transcriptome-profiling analysis revealed that the second most downregulated gene, upon *SOX6* knockdown, is thioredoxin-inhibitor protein (*TXNIP*), which may partially explain the observed sensitivity toward Elesclomol. As part of the antioxidant system TXNIP regulates the oxidative stress levels within the cell by inhibiting thioredoxin. In agreement to this, the data reported in this thesis demonstrated that constitutively high *SOX6* expression promotes elevated levels of oxidative stress that create a therapeutic vulnerability toward Elesclomol in EwS.



## 1. Introduction

### 1.1 Ewing Sarcoma

#### 1.1.1 Origin

Ewing sarcoma was first described as a “diffuse endothelioma of the bone” by James Ewing in 1921 (Ewing, 1921) and only later became known as Ewing sarcoma (EWS).

Ewing sarcoma family of tumors are grouped together based on morphological and immunohistological features as well as the presence of a common chromosomal translocation (mainly *EWSR1-FLI1*). They include the classical *osseous* Ewing sarcoma, *extraosseus* Ewing sarcoma, *Askin* tumor and *peripheral primitive neuroectodermal tumors* (PNET) (Kovar, 1998).

Although the origin of this tumor is still debated, there is evidence of being potentially originated from a mesenchymal stem cell with an osteo-chondrogenic progenitor (Tanaka et al., 2014; Tirode et al., 2007). Tirode and colleagues showed that upon *EWSR1-FLI1* silencing, EwS cell lines cultured in the appropriate differentiation medium, were able to differentiate into different lineages showing a more mesenchymal stem cell expression profile (Tirode et al., 2007). Additionally, Riggi and colleagues showed that ectopical expression of *EWSR1-FLI1* in human mesenchymal stem cells resembles EwS cells (Riggi et al., 2008) and the ectopic expression of *EWSR1-FLI1* on murine primary bone-derived stem cells induces Ewing sarcoma-like tumors *in vivo* (Castillero-Trejo et al., 2005; Riggi et al., 2005).

#### 1.1.2 Molecular and genetic profile of EwS

Generally, EwS is characterized by a somatic chromosomal *in frame* translocation of the 5′–EWS gene (*EWSR1*, Ewing sarcoma breakpoint region 1) with one of the 3′–ETS family of transcription factor members (*FLI1*, *ERG*, *ETV1*, *ETV4*, *FEV*, *PATZ1*, *SP3*, *NFATC2*, *SMARCA5*, *E1AF*, *ZSG*). The resulting translocations are present in sarcomas, exclusively (Riggi and Stamenkovic, 2007). In 85% of EwS cases the *EWSR1* gene on p22q12 is fused with the *FLI1* gene on p11q24 resulting in a chimeric fusion transcript *EWSR1-FLI1* (Anderson et al., 2018; Delattre et al., 1992).

The characteristic *EWSR1* gene on chromosome 22 belongs to the TET protein family and contains a protein-RNA binding domain (Bertolotti et al., 1996). On the other hand, the ETS transcription factors bind to promoters resulting in transcriptional activation or repression of their target genes. They preferentially bind to a DNA core motifs of 5'-GGAA/T-3' (Dittmer, 2011). The Friend leukemia integration 1 gene (*FLI1*) is a member of the ETS factors and is mostly expressed in hematopoietic cells in adult tissue (Ben-David et al., 1991). This fusion oncogene is known not only to bind GGAA-core motifs but also consecutive GGAA-repeats so-called GGAA-microsatellites (mSats), whose enhancer activity increases with the number of consecutive GGAA-motifs (Boulay et al., 2017; Gangwal and Lessnick, 2008; Gangwal et al., 2008; Guillon et al., 2009; Riggi et al., 2014). Thus, *EWSR1-FLI1* partly regulates some of its target genes (*ERG*, *MYBL2* and *NROB1*) and mediates EwS tumorigenesis (Grünewald et al., 2015; Kinsey et al., 2006; Musa et al., 2019).

The chromosomal translocation between *EWSR1* and *FLI1* mostly occurs in two modalities: Exon 7 of *EWSR1* fuses to exon 6 of *FLI1* (type 1) or exon 7 of *EWSR1* fuses to exon 5 of *FLI1* (type 2), the latter accounting for 85% of cases (Delattre et al., 1992, 1994; Turc-Carel et al., 1988). In contrast to earlier assumptions, both fusion types have the same prognostic outcome (Le Deley et al., 2010). In 10–15% of EwS cases gene on p22q12 is fused to p21q12 resulting in the *EWSR1-ERG* chimeric gene (Sorensen et al., 1994). The generated fusion protein is an aberrantly expressed oncogenic transcription factor.

### **1.1.3 Clinical aspects: epidemiology, diagnosis and therapy**

After osteosarcoma, EwS represents the second most common bone and soft-tissue tumor (Grünewald et al., 2018) in children, adolescents and young adults (Esiashvili et al., 2008), accounting for 3% of all pediatric cancers (Resnick and Kransdorf, 2005). The incidence of this rare disease is ~1.5 cases per 1.000.000 each year and is more common in Caucasian than African or Asian populations (Beck et al., 2012; Esiashvili et al., 2008; Khoury, 2005; Paulussen et al., 2009). The average peak age is 10–24 years and males are slightly more affected than females at a ratio of about 3:2 (Paulussen et al., 2008a).

Although EwS can virtually arise from every part of the body, the most common sites are Pelvis (25%), Femur (16%), Ribs (12%) and Tibia (8%). Interestingly, it can also develop in soft tissues without direct affection of the bone (Cotterill et al., 2000; Resnick and Kransdorf, 2005).

Molecular analysis of EwS can be done by immunohistochemistry (IHC). This trend-setting method is based on the detection of CD99, a surface antigen that is expressed in 90% of EwS cases (Khoury, 2005). Diagnosis based on the conventional immunohistochemical marker CD99 is however unspecific as it can be detected in other small round cell tumors such as lymphoblastic lymphoma, rhabdomyosarcoma, synovial sarcoma, mesenchymal chondrosarcoma, blastemal component of Wilms tumor, and rarely in desmoplastic small round cell tumors (DSRCT) (Folpe et al., 2000). In the backlight of this, Baldauf and colleagues recently suggested three potential biomarkers (BCL11B, GLG1 and ATP1A1) that could help to reduce misdiagnosis due to the aforementioned poor specificity of CD99 (Baldauf et al., 2018a). Currently, the final diagnosis of EwS is made by detecting the fusion oncogene *EWSR1-ETS* using PCR or FISH methods.

Especially in the case of metastatic or recurrent disease, the effectiveness of EwS patient treatment remains dismal (Gaspar et al., 2015). The survival and treatment options heavily depend on the fact of whether patients already present metastasis at diagnosis or not. The 5-year survival rate of patients with localized tumors is approximately 70–80% after diagnosis (Grier et al., 2003; Le Deley et al., 2010; Paulussen et al., 2008b; Womer et al., 2012). The current treatment for localized tumors is surgery and/or radiotherapy (Cotterill et al., 2000; Gaspar et al., 2015; Grünewald et al., 2018).

In 20–25% of the cases, EwS patients have metastasis at diagnosis in bone, bone marrow or lungs and are unfortunately resistant to established treatment regimes. Their 5-year survival rate drops dramatically compared to localized tumors onto < 30%, whereas patients with restricted lung metastasis have a survival rate of ~ 50% (Cotterill et al., 2000; Gaspar et al., 2015).

Treatment options include high dose of polychemotherapy (Doxorubicin, Etoposide, Ifosfamide and Vincristin) in combination with radiotherapy and surgical resection (Gaspar et al., 2015).

However, the efficacy of these treatments is limited for patients with metastatic or recurrent tumors (Gaspar et al., 2015). In fact, approximately 30–40% of the EwS patients suffer from recurrent tumors and their survival rate is devastating with less than 20–25% (Ahrens et al., 1999). There is no specific treatment protocol for recurrent tumors, but current practices include resection, chemotherapy and radiotherapy. This highlights the urgency of novel therapeutic options that are needed to improve the outcomes of these patients.

## **1.2 SRY-related HMG-box 6 (SOX6)**

### **1.2.1 SOX family of transcription factors**

The SOX (SRY-related HMG-box) family genes encode an important group of transcription factors (TF). They harbor a conserved high mobility group (HMG) DNA binding domain that was originally identified in the mouse and human testis-determining gene *Sry* residing on the Y-chromosome (Berta et al., 1990; Cohen-Barak et al., 2001; Gubbay et al., 1990).

The HMG-box is a 79 amino-acid DNA binding domain (DBD) that is highly conserved (Stros et al., 2007) among SOX gene family members of vertebrate and invertebrates. All proteins that share at least 50% similarity to the HMG box of *Sry* are referred to as SOX proteins. All SOX family genes have a crucial role in cell fate decision during development (Sarkar and Hochedlinger, 2013).

Based on sequence homology, SOX genes can be further categorized into six subfamilies (Cohen-Barak et al., 2001; Pevny and Lovell-Badge, 1997) one of these is the SOXD subfamily, which comprises the transcription factors *SOX5*, *SOX6* and *SOX13*. Interestingly, SOXD subfamily proteins do not possess a known trans-activation or trans-repression domain (Han and Lefebvre, 2008; Lefebvre et al., 1998). Additionally, SOXD proteins possess uniquely two highly conserved leucine-zipper coiled-coil domains that allows homo-dimerization resulting in high-efficiency binding on DNA (Lefebvre et al., 2007).

### 1.2.2 *SOX6* gene: Structure and regulation

In this thesis, the focus will be set mainly on the transcription factor *SOX6*. The transcription factor SRY-box 6 (*SOX6*) was discovered to be located on the 16 exon-containing human chromosome 11p15.3-p15.2 (Cohen-Barak et al., 2001). *SOX6* is a 92 kDa protein that was initially isolated from an adult mouse testis cDNA library and comprises three isoforms (Denny et al., 1992).

As part of the SOXD subfamily, *SOX6* is forced to homo- or heterodimerize with other proteins and various cofactors (Hagiwara, 2011) in order to activate or repress gene expression (Kamachi et al., 2000; Lefebvre et al., 1998). The SOXE subfamily, including Sox8/9/10, contain an activator domain and represent an important interacting partner of *SOX6* (Kamachi et al., 2000; Wegner, 1999).

The SOXD family member *SOX5*, a cofactor of *SOX6*, shares sequence similarity (Hagiwara, 2011; Koopman et al., 2004). Both act together with redundant functions in chondrogenesis and oligodendrocyte development (Hagiwara, 2011; Smits et al., 2001; Stolt et al., 2006). Moreover, it has been demonstrated in mice that Sox5/6 complex interact together with Sox9, which possess an activator domain, to promote cartilage specific genes (Akiyama et al., 2002; Hagiwara, 2011; Han and Lefebvre, 2008; Kamachi et al., 2000; Lefebvre et al., 1998; Stolt et al., 2006). Contrarily, Sox5/Sox6 antagonize Sox9 as an activator during oligodendrocyte development (Stolt et al., 2006).

Among the SOX family of transcription factors, especially *SOX6* is considered functionally very versatile due to its unique structure:

1) *SOX6* does not contain any known regulatory domain; instead it utilizes various cofactors (listed in (Hagiwara, 2011)). 2) *SOX6* possesses a long 3'–UTR region (Bartel, 2009) containing multiple micro RNA (miRNA) target sequences that enable the tissue-specific microRNAs to control *SOX6* expression in certain tissues (**Table 1**):

miRNA	Function	Reference
miR-16	Suppresses cell apoptosis while promoting cell proliferation in esophageal squamous cell carcinoma.	(Zhu et al., 2014)
miR-18a	Targets SOX6 in cervical cancer.	(Dong et al., 2018)
miR-19b	Promotes cell proliferation during cardiac differentiation by targeting Sox6 expression.	(Han et al., 2018)
miR-96	Targets SOX6 and promotes proliferation, migration and invasion of hepatocellular carcinoma.	(Li and Wang, 2017)
miR-103	Inhibits chondrocyte proliferation in osteoarthritis development.	(Chen and Wu, 2019)
miR-122	Targets SOX6 and promotes carcinogenesis of glioma cells.	(Chen et al., 2019)
miR-129-5p	Alleviates nerve injury and inflammatory response of Alzheimer's disease via SOX6 downregulation.	(Zeng et al., 2019)
miR-132-3p	Inhibits osteogenic differentiation of ligamentum flavum cells by targeting SOX6.	(Qu et al., 2016)
miR-135a-5p	Regulates Sox6 expression in neuronal differentiation.	(Li et al., 2019)
miR-155	Aberrant expression of microRNA-155 may accelerate cell proliferation by targeting sex-determining region Y box 6 in hepatocellular carcinoma.	(Xie et al., 2012)
miR-181b	Targets SOX6 to decrease proliferation and metastasis in lung cancer cells.	(Zhou et al., 2019)
miR-202	Promotes endometriosis by regulating SOX6 expression.	(Zhang et al., 2015)
miR-208	Represses SOX6 expression in human esophageal squamous cell carcinoma.	(Li et al., 2014)
miR-208a,b	Involved in cardiac hypertrophy by targeting Sox6	(Soci et al., 2016)
miR-219	Required for normal oligodendrocyte differentiation and myelination.	(Dugas et al., 2010; Zhao et al., 2010)
miR-499	Regulates cell proliferation and apoptosis during late-stage cardiac differentiation via Sox6 and cyclin D1.	(Li et al., 2013)
miR-499-5p	Regulates porcine myofiber specification by controlling Sox6 expression.	(Wang et al., 2017)
miR-508-3p	Targets SOX6 in melanogenesis.	(Liu et al., 2018)
miR-671	Promotes prostate cancer cell proliferation by inhibiting SOX6.	(Yu et al., 2018)
miR-765	Regulates proliferation and apoptosis in multiple myeloma.	(Long et al., 2019)
miR-766	Regulation of cell proliferation in human colorectal cancer.	(Li et al., 2015)
miR-1269a	Regulation of SOX6 expression in non-small cell lung cancer	(Jin et al., 2018)

**Table 1:** Overview of microRNAs (miRNA) that regulate SOX6 expression in different tissues or tumor entities.

Besides its role as a DNA-binding transcription factor, SOX6 also emerges as an RNA-binding and bending factor that controls pre-mRNA splicing and mRNA translation (Ohe et al., 2009). All these facts underline the role of SOX6 as a multifaceted protein.

### 1.2.3 SOX6 function in vertebrate development

Previous studies have suggested that Sox6 plays a role in the development of the central nervous system (CNS) (Dugas et al., 2010; Stolt et al., 2006; Zhao et al., 2010) and chondrogenesis in mice embryos (Akiyama et al., 2002; Lefebvre and Smits, 2005; Lefebvre et al., 1998; Smits et al., 2001, 2004). However, most of the SOX genes, especially Sox6, are differentially expressed in multiple development stages of different tissues with different effects at each step (Akiyama et al., 2002; Hagiwara, 2011; Lefebvre and Smits, 2005) (**Table 2**).

In mice, Sox6 is expressed in the central nervous system (CNS) during embryogenesis, but later on decreases in the adult CNS (Azim et al., 2009). In humans, SOX6 is expressed in the brain during embryogenesis and remains at only very low levels in the adult brain (Ueda et al., 2004a, 2004b).

What?	Function	Reference
<b>Differentiation of mesenchymal tissues</b>		
<b>Chondrocyte</b>	Sox5/Sox6 regulates proliferative chondroblasts during cartilage differentiation.	(Akiyama et al., 2002; Lefebvre and Smits, 2005; Lefebvre et al., 1998; Smits et al., 2001, 2004)
<b>Skeletal muscle</b>	Sox6 is involved in specification of muscle fiber types.	(Hagiwara et al., 2007; von Hofsten et al., 2008)
<b>Development of central nervous system (CNS)</b>		
<b>Oligodendrocyte</b>	Sox5/Sox6 regulates proliferative oligodendrocyte progenitor cells differentiation.	(Dugas et al., 2010; Stolt et al., 2006; Zhao et al., 2010)
<b>Neurons</b>	Sox6 specifies post-mitotic interneurons.	(Azim et al., 2009)

Differentiation of other cell and tissues		
<b>Erythropoiesis</b>	Sox6 regulates proliferation and maturation of red blood cells.	(Cohen-Barak et al., 2007; Dumitriu, 2006; Dumitriu et al., 2010; Xu et al., 2010; Yi et al., 2006)
<b>Pancreatic <math>\beta</math>-cells</b>	Sox6 regulates glucose-stimulated insulin secretion from $\beta$ -cells.	(Iguchi et al., 2005, 2007)
<b>Cardiomyocyte</b>	Sox6 regulates proliferative cardiomyocyte progenitor cells.	(Sluijter et al., 2010)
<b>Testis</b>	Sox6 regulates proliferation in spermatogenesis.	(Hagiwara, 2011; Yamashita et al., 2000)

**Table 2:** Sox6 function in mesenchymal differentiation, development of the CNS or in differentiation of different tissues.

In mice, Sox6 appears to be mainly involved in the proliferation process of cardiomyo-, chondro and oligodendrocytes progenitor cells, but not in post-mitotic differentiating cells. Controversially, Sox6 may be involved in differentiation of post-mitotic interneurons (Azim et al., 2009; Batista-Brito et al., 2009) and specification of muscle fiber types (Hagiwara et al., 2007).

Depending on the cellular context, SOX6 has two major functions: 1) to control the cell cycle exit during terminal differentiation and 2) to regulate terminal differentiation of post-mitotic cells (Hagiwara, 2011).

#### 1.2.4 Role of SOX6 in endochondral ossification

Among the several functions of SOX6, the major interest of this thesis is its role in endochondral ossification, because dysfunction of this process might promote development and progression of a bone-related tumor such as EwS.

Endochondral ossification (**Figure 1**) is driving formation and growth of long bones (vertebrae, ribs and limbs) as well as promoting the healing of bone fractures. This ossification pathway is characterized by

mesenchymal stem cell (MSC) progenitors going through a cartilage intermediate and finally transforming into new bone tissue (Horton et al., 1988; Quintana et al., 2009).

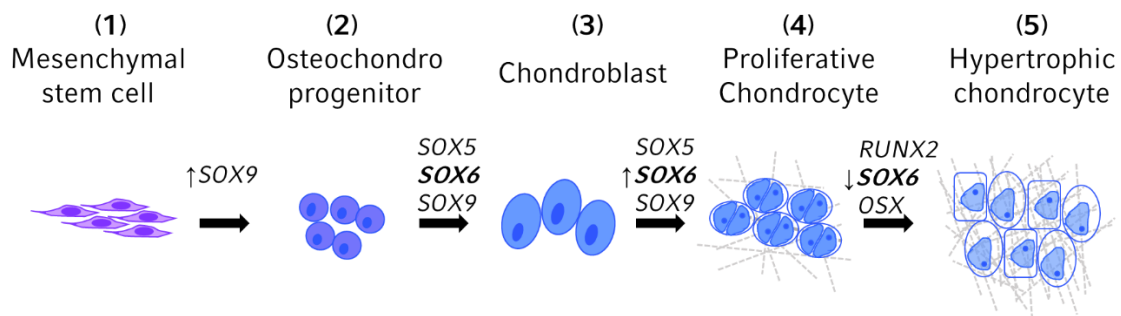


**Figure 1: Main steps in endochondral ossification (1 – 5) and key transcription factors.**

Chondrogenesis is a crucial step in endochondral ossification and starts with the condensation and growth arrest of mesenchymal progenitors to the osteo-/chondrogenic progenitor cells (**Figure 1(2)**), through migration to the sites where bone will develop. For this step, proliferation associated genes are downregulated, whereas differentiation-associated genes are expressed to induce chondrogenic differentiation (**Figure 1(1)**). The whole bone development is controlled by many signaling molecules such as TGF- $\beta$ , BMPs or the Indian hedgehog (Ihh) pathway.

The chondrogenic differentiation pathway is regulated by the transcription factor *SOX9* that allows the proliferation and differentiation of MSC into chondroblasts (Akiyama et al., 2002; Bi et al., 1999). Those progenitors keep expressing *SOX9* to form a dense structure mass by producing collagens.

The additional time-restricted co-expression of the *SOX5/SOX6* genes (then referred to as SOX-trio) (**Figure 1(3)**) enable chondroblasts to proliferate (**Figure 1(4)**) to start synthesizing/ secreting extracellular matrix (ECM) components to form a scaffold for osteoblasts (Hagiwara, 2011; Lefebvre et al., 1998; Quintana et al., 2009).

At a certain timepoint, when the SOX-trio level decreases (**Figure 1(5)**), and other factors important for differentiation such as *RUNX2* or *OSX* are upregulated, chondroblasts undergo chondrocyte maturation (Lefebvre et al., 1998; Quintana et al., 2009). The regulation of proliferating chondroblasts is under control of *SOX6*, which inhibits the precocious exit from the cell cycle, thereby preventing

chondroblasts from entering pre-hypertrophic stage too early (Hagiwara, 2011; Lefebvre et al., 1998; Smits et al., 2004).

Chondrocytes exit the cell cycle, become hypertrophic and initiate the endochondral ossification process mainly by degrading the ECM. This step includes among others the mineralization of the cartilage matrix with calcium salts (Quintana et al., 2009). Subsequently, hypertrophic chondrocytes undergo apoptosis to form a cartilaginous scaffold for blood vessels carrying osteoblastic progenitors (Quintana et al., 2009) (**Figure 1(5)**).

So far, it has been reported that Sox6 single-knockout mice die prematurely and showed mild skeletal abnormalities compared to mice with Sox5/Sox6 double-knockout, that revealed severe chondrodysplasia (Smits et al., 2001). Thus, although Sox5 and Sox6 have redundant functions both are essential for endochondral ossification (Smits et al., 2001).

### **1.2.5 SOX6 expression in tumors and other malignancies**

The transcription factor SOX6 is mostly expressed during the development of the CNS and in the early stages of chondrogenesis. In adult tissues, SOX6 is thought to maintain functionality of specific tissues but its role in adults is still unclear (Hagiwara, 2011). The enormous versatility of SOX6 is also mirrored by its role in tumorigenesis, where it can act either as an oncogene or as a tumor suppressor gene, depending on the cellular context.

On the one hand, it has been reported that the expression of SOX6 acts as a tumor suppressor in esophageal squamous cell carcinoma (Qin et al., 2011) and hepatocellular carcinoma (Guo et al., 2013).

On the other hand, SOX6 was found to be overexpressed in melanoma cells compared to neural-crest deriving melanocytes probably supporting an oncogenic role (Le Douarin and Kalcheim, 1999).

Additionally, Ueda and colleagues, discovered that SOX6 is overexpressed in glioma tissues including glioblastoma, oligodendroglioma and astrocytoma (Ueda et al., 2004a). Interestingly, over-expression

of SOX6 was not found in more differentiated brain tumors indicating that the effect of SOX6 become apparent in multipotent cells that are still prone to differentiation.

In addition to that, as previously mentioned, the transcription factor *SOX6* is known to be involved in cell cycle progression during cartilage differentiation. This observation and the fact that EwS is characterized as an immature and highly proliferative bone-associated tumor makes *SOX6* an interesting variable to analyze in the context of EwS progression.

### **1.3 Oxidative stress and the role of TXNIP**

Tumors are typically characterized by higher oxidative stress levels than non-malignant cells through increased metabolic activity. This observation holds true for EwS, generally displaying heightened oxidative stress levels compared to normal tissues (Benz and Yau, 2008; Grünewald et al., 2012).

On the one hand elevated oxidative stress levels are important to maintain tumor properties but on the other hand an extensive oxidative stress production make them susceptible to specific drugs that are able to induce oxidative stress (Trachootham et al., 2009). Therapeutically, utilizing the properties of the oxidative stress mechanism within tumor cells appears to be a promising option. Successful trials have already been able to exploit this mechanism by increasing the levels of oxidative stress over a tolerable dose in form of an anticancer therapy (Gibellini et al., 2010).

The electron respiratory chain in mitochondria is the predominant source of aerobic energy production in mammalian cells and also the main location of oxidative stress production. Normal cells maintain a redox homeostasis as balanced levels of oxidative stress are important for certain cellular processes such as gene expression, cell proliferation and signal transduction (Mikkelsen and Wardman, 2003). Hence, a functional antioxidant machinery is crucial to maintain this homeostasis as increased oxidative stress levels interact with lipids, proteins, nucleic acids and cell death programs, thereby damaging the cells.

One of these antioxidant machineries is the thioredoxin system. The thioredoxin system is composed of thioredoxin (Trx), thioredoxin reductase (TrxR), the coenzyme  $\alpha$ -nicotinamide adenine dinucleotide

phosphate (NADPH) and the thioredoxin-interacting protein (TXNIP). Two thioredoxin antioxidant machineries are present within the cell; Trx1 is located in the cytoplasm whereas Trx2 is only located in the mitochondria.

TXNIP was originally identified as Vitamin D3 upregulated protein 1 (VUP1) (Chen and DeLuca, 1994) and is known to be mainly involved in the redox system and apoptosis, but it has become clear that the role of TXNIP extends beyond the Trx antioxidant system. In fact, in the last few years this protein has emerged as a regulator of lipid and glucose metabolism and become linked to diabetes mellitus. Mainly, TXNIP is involved in the redox antioxidant system where it inhibits Trx, consequently leading to an oxidative stress accumulation within the cell. The ability of TXNIP to induce oxidative stress-mediated apoptosis and the fact that TXNIP is often reduced in tumor tissues such as hepatocellular, breast and bladder carcinoma (Zhou and Chng, 2013), suggest that TXNIP is indeed a tumor suppressor.

## 2 Research objectives and scientific aims

### 2.2 Research objectives

EwS seems to arise from osteo-/chondrogenic progenitor cells and those are characterized as highly proliferative and undifferentiated cells. Therefore, the underlying hypothesis was that SOX6, being highly overexpressed in EwS, is critical for EWSR1-FLI1 mediated arrest of EwS cells in an early-committed differentiation state and that SOX6 is part of the EWSR1-FLI1-induced transformation program.

This PhD project aimed at functionally characterizing the mechanism by which *EWSR1-FLI1* drives *SOX6* expression and at unveiling the role of SOX6 in tumorigenesis and progression of EwS *in vitro* and *in vivo*. Moreover, it was hypothesized that SOX6 might serve as a valuable biomarker for EwS treatment.

### 2.3 Scientific aims

- 1<sup>st</sup> aim: Assessment of the enhancer activity and *EWSR1-FLI1* occupancy of the *SOX6* GGAA-microsatellite.
- 2<sup>nd</sup> aim: Analysis of the effect of *SOX6* on the phenotype of EwS *in vitro*.
- 3<sup>rd</sup> aim: Analysis of the *SOX6* effect on the differentiation capacity of EwS cells.
- 4<sup>th</sup> aim: Evaluation of the impact of *SOX6* on the phenotype of EwS in a xenograft model.
- 5<sup>th</sup> aim: Identification and validation of indirect and direct *SOX6* target genes.
- 6<sup>th</sup> aim: Exploration of a therapeutic vulnerability due to *SOX6* in EwS.

### 3. Materials and methods

#### 3.1 Materials

##### 3.1.1 List of manufacturers

<b>Manufacturer</b>	<b>Location</b>
(Carl) Roth	Karlsruhe, Germany
Abcam	Cambridge, UK
Agilent Technologies	Santa Clara, USA
Alpha Innotech	Kasendorf, Germany
Applied Biosystems	Darmstadt, Germany
ATCC	Rockyville, Maryland, USA
Atlas Antibodies	Bromma, Sweden
B. Braun Melsungen AG	Melsungen, Germany
BD Biosciences Europe	Heidelberg, Germany
Beckman Coulter	Palo Alto, California, USA
Bela-Pharm	Vechta, Germany
Berthold detection systems	Pforzheim, Germany
Biochrom	Berlin, Germany
BioRad	Richmond, California, USA
BIOTECH (siTOOLS)	Munich, Germany
Biozym	Hess. Olendorf, Germany
Beurer GmbH	Ulm, Germany
Brand	Wertheim, Germany
Braun Biotech international GmbH	Melsungen, Germany
Cell Marque Corporation	Rocklin, California, USA
Cell Signaling Technology	Frankfurt a. M., Germany
Corning incorporated	New York, USA
Dechra Veterinary Products	Aulendorf, Germany
Eppendorf	Hamburg, Germany
Falcon	Oxnard, California, USA
Fischer Scientific	Schwerte, Germany
Fryka	Esslingen am Neckar, Germany
GE Healthcare	Freiburg, Germany
Gilson Incorporated	Middleton, USA
Greiner	Nürtingen, Germany
Hamilton Company	Nevada, USA
Hartenstein	Würzburg, Germany
Heidolph Instruments	Schwabach, Germany
Heraeus	Hanau, Germany
HP Labortechnik	München, Germany
INTEGRA biosciences	Zizers, Switzerland
Invitrogen	Karlsruhe, Germany
InVivoGen	San Diego, California, USA
Julabo	Seelbach, Germany
Leica Biosystems	Wetzlar, Germany
LI-COR	Nebraska, USA

Life Technologies	California, USA
Macherey-Nagel	Düren, Germany
Merck Millipore	Burlington, Massachusetts, USA
Mergo GmbH & Ko KG	Wesel, Germany
New England BioLabs	Frankfurt a. M., Germany
Nordcap	Bremen, Germany
Nunc	Naperville, USA
OriGene Technologies	Rockville, Maryland, USA
Pechiney Plastic Packaging	Menasha, Wisconsin, USA
Prodivet pharmaceuticals	Raeren, Belgium
PJK GmbH	Kleinblittersdorf, Germany
Promega	Madison, Wisconsin, USA
Qiagen	Chatsworth, California, USA
OriGene Technologies	Rockville, USA
Quartett Biochemicals	Berlin, Germany
Richter Pharma AG	Wels, Austria
Roche	Mannheim, Germany
Santa Cruz Biotechnology	Heidelberg, Germany
Sartorius	Göttingen, Germany
Scientific industries	New York, USA
Selleckchem	Munich, Germany
Sigma	St. Louis, Missouri, USA
System Biosciences	Palo Alto, California, USA
Taconic Denmark ApS	Silkeborg, Denmark
The Jackson Laboratory	Bar Harbor, USA
Takara Bio Europe	Saint-Germain-en-Laye, France
Thermo Fisher Scientific	Ulm, Germany
Thermo Scientific	Braunschweig, Germany
Vector Laboratories	California, USA
Whatman	Dassel, Germany
WTW	Weilheim, Germany
Zeiss	Oberkochen, Germany

### 3.1.2 General materials

Material	Manufacturer
6, 12, 24 and 96-well-plate	Corning Incorporated
96-well-plate (white)	Corning Incorporated
Amersham Protran 0.45 nitrocellulose Western blotting membranes	GE Healthcare
Blotting paper	Hartenstein
Cell culture flasks (150, 75, 25 cm <sup>2</sup> )	Corning Incorporated
Cell scraper	Corning Incorporated
Costar Ultralow attachment plates 96-well	Corning Incorporated
CryoGen	Hartenstein
Eppendorf Tubes (1.5 and 2 ml)	Hartenstein
Falcon Tubes (15 ml and 50 ml PP or PS)	Falcon
HandyStep electronic	Brand

Heating lamp	Beurer GmbH
Needle for orthotopic injection (Small Hub RN Needle (28/20/4) and syringe)	Hamilton Company
Nunclon cell culture dish (10 cm <sup>2</sup> )	Thermofisher
Optical adhesive film for 96er PCR-Plates	Fisher Scientific
Parafilm	Pechiney Plastic Packaging
Pasteur Pipette	Hartenstein
PCR-Plates (96-well)	Fisher Scientific
Pipetboy	INTEGRA Biosciences
Pipette tips (10 µl, 20 µl, 100 µl, 200 µl, 1000 µl)	Biozym
Pipettes (0.5-10 µl, 10-100 µl, 100-1000 µl)	Gilson
Scalpels	Mergo GmbH & Ko KG
Stripette (2, 5, 10, 25 and 50 ml)	Corning Incorporated
Needle and syringe for intravenous injection (BD MicroFine™+ Insulin)	BD Biosciences
Syringes for viruses (0,45µm)	(Carl) Roth

### 3.1.3 Mice strains

Mouse strain	Manufacturer
NSG (NOD.CG-SCID): NOD-scid IL2Rgammanull, NOD-scid IL2Rgnull, NSG, NOD scid gamma	The Jackson Laboratory
NOD/SCID: NOD/MrkBomTac-Prkdcscid	Taconia Denmark ApS

### 3.1.4 Instruments and equipment

Device	Specification	Manufacturer
Affymetrix-Gene Chip	Human Clariom™ D	Thermofischer
Autoclave	Varioklav	HP Laborartorteknik
Bacteria incubator	Kelvitron	Heraeus
Bacteria shaker	Certomat IS	Braun BioTech internat.
Bioanalyzer	2100	Agilent Technologies
Cell counter	Countess II	Thermofischer
Centrifuge	Heraeus™ Megafuge™ 40	Heraeus
Centrifuge	Centrifuge (5424 R and 5430)	Eppendorf
Controlled-freezing box	Mr. Frosty	Nalgene
Electrophoresis	Mini Trans-Blot	Biorad
ELISA reader	Varioskan™ LUX	Thermofisher
Flow Cytometer	BD Accuri™ C6	BD Biosciences
Freezer (-20°C)	No Frost	Siemens
Freezer (-80°C)	B 35-50	Fryka
Gel documentation	Multi Image Light Cabinet	Alpha Innotech
Hemocytometer	C-Chip	Biochrom
Ice maker	SPR 80	Nordcap
Incubator	Heracell™ 240i CO <sub>2</sub> incubator	Thermofisher

Luminometer	Orion II	Berthold
Microscope (fluorescence)	Axivert200	Zeiss
Microscope (TMA)	Axioplan 2 imaging	Zeiss
Multichannel pipette	Transferpette-12 electronic	Brand
Nanodrop	Nanodrop ND-1000 UV/Vis	Thermofischer
pH-meter	pH-197	WtW
Power Supply	PowerPac™	Biorad
RT-qPCR software	Bio-Rad CFX Connect™	Biorad
Scale	GE1302	Sartorius
SDS-PAGE chamber	Mini Trans-Blot	Biorad
Shaker	Unimax 1010 DT	Heidolph Instruments
Sterile bench	Maxisafe2020	Thermofisher
Thermocycler	T100 TM Thermal Cyclers	Biorad
Thermomixer	Thermomixer comfort	Eppendorf
Vortex	Vortex-Genie 2	Scientific Industries
Waterbath	ED-5	Julabo
Western blot documentation	Image Studion Ver 5.2	LI-COR

### 3.1.5 Chemicals

Chemicals	Manufacturer
Acrylamid/Bisacrylamid	(Carl) Roth
Agar	Sigma-Aldrich
Agarose	Sigma-Aldrich
Ammonium Perisulfate (APS)	Sigma-Aldrich
Ampicillin	Sigma-Aldrich
Atipamezole hydrochloride	Prodivet pharmaceuticals
BelaDox®	Bela-pharm
Bovine albumin (BSA)	Sigma-Aldrich
Buprenorphin hydrochloride	Richter Pharma AG
BRD56491	Sigma-Aldrich
Cumate solution	System Biosciences
DC_AC50	Sigma-Aldrich
Dimethylsulfoxid (DMSO)	Sigma-Aldrich
Dithiothreitol (DTT)	Sigma-Aldrich
Doxycycline Hyclate (HPLC)	Sigma-Aldrich
Elesclomol (STA-4783)	Selleckchem
Ethanol (99%)	(Carl) Roth
Fentanyl	Dechra Veterinary Products
Glacial acetic acid	Sigma-Aldrich
Glycine	(Carl) Roth
H <sub>2</sub> O <sub>2</sub> 30% (w/w)	Sigma-Aldrich
H <sub>2</sub> DCFDA (DCF-DA)	Invitrogen
Isopropanol	(Carl) Roth
L-glutamine	Sigma-Aldrich
LB-Medium	(Carl) Roth
Menadione	Sigma-Aldrich
Midazolam	Roche

Medetomidin hydrochlorid	Prodivet pharmaceuticals
Methanol (100%)	(Carl) Roth
Milk powder	(Carl) Roth
MitoSOX Red and MitoTracker green	Thermofisher
N-acetylcysteine (Nac)	Sigma-Aldrich
Naloxon hydrochloride	B. Braun Melsungen AG
Sodium hydroxide (NaOH)	Sigma-Aldrich
Resazurin	Sigma-Aldrich
Sodium Chloride (NaCl)	(Carl) Roth
Sodium Deoxycholate	Sigma-Aldrich
Sodium dodecyl sulfate (SDS)	Sigma-Aldrich
Sodium Orthovanadate (Na <sub>3</sub> VO <sub>4</sub> )	Sigma-Aldrich
Target Retrieval Solution	Agilent Technologies
TEMED	Sigma-Aldrich
Tiron (disodium 4,5-dihydroxy-1,3-benzenedisulfonate)	Sigma-Aldrich
TRIS-Base	Sigma-Aldrich
Tween-20	Sigma-Aldrich
Tween-80	Sigma-Aldrich

### 3.1.6 Biological reagents

Reagents	Manufacturer
1-kbp DNA-ladder	(Carl) Roth
4% Formalin	Sigma-Aldrich
Accutase	Sigma-Aldrich
AEC+ Substrate-Chromogen	Agilent Technologies
Agel-HF	New England BioLabs
β-FGF	Life Technologies
Bradford reagent	Biorad
Crysatl violet	Sigma-Aldrich
DAB+ Substrate-Chromogen	Agilent Technologies
Deoxynucleotide triphosphates (dNTPs)	Sigma-Aldrich
Dh5α competent cells	Thermofisher
DMEM with 3.7 g/l NaHCO <sub>3</sub> , with 1.0 g/l D-glucose	Biochrom
Ethidiumbromide	Sigma-Aldrich
EcoRV-HF	New England BioLabs
Fetal bovine serum (Tetracycline-free)	Sigma-Aldrich
Geltrex LDEV-Free Reduced Growth Factor Basement Membrane Matrix	Thermofisher
GeneRuler 100 bp Plus DNA Ladder	Life Technologies
GoTaq G2 Hot Start Polymerase	Promega
Hematoxylin	Vector Laboratories
Hexadimethrinbromide (polybren)	Sigma-Aldrich
HindIII-HF	New England BioLabs
HiPerFect	Qiagen
Immobilon Western HRP Substrate	Merck
Lipofectamine LTX Reagent with PLUSReagent	Invitrogen

Lipofectamine LTX with Plus Reagent	Thermofisher
Lipofectamine RNAiMax	Invitrogen
Maxima Hot Start Taq DNA Polymerase	Thermo Scientific
Maxima Hot Start Taq Polymerase	Thermo scientific
Opti-MEM Medium	Life Technologies
PageRuler Prestained Protein Ladder	Thermofisher
Penicillin/Streptomycin	Biochrom
Penicillin-Streptomycin-Glutamine (100x)	Life Technologies
Phosphate Buffered Saline (PBS)	Biochrom
Phusion High-Fidelity DNA Polymerase	Thermo Scientific
Plasmocure	InVivoGen
Poly-Ethylene-Glycol (PEG)	Sigma-Aldrich
Propidium-iodide	Sigma-Aldrich
Protease inhibitor cocktail	Sigma-Aldrich
Puromycin	InVivoGen
Quick Start Bovine Serum Albumin Standard	Biorad
Beetle- and Renilla-Juice	PJK
Streptavidin HRP	Leica Biosystems
RNase	Thermofisher
RPMI 1640 with 2.0 g/l NaHCO <sub>3</sub> 500 ml	Biochrom
Sipool	BIOTECH (siTools)
Stellar competent cells	Takara
Sucrose > 99.5% (GC)	Sigma-Aldrich
SYBR SELECT Master Mix	Life Technologies
T <sub>4</sub> Ligase	Thermo Scientific
Target Retrieval Solution	Agilent Technologies
Trypanblue	Sigma-Aldrich
Trypsin/EDTA (10x)	Biochrom
XhoI	Thermo Scientific
α-Medium (no nucleosides)	Biochrom
ProTaq <sub>s</sub> II Antigen Enhancer	Quartett Biochemicals

### 3.1.7 Commercial kits

Kit	Manufacturer	Reference
NucleoSpin Gel and PCR Clean-up	Macherey-Nagel	740609
ReliaPrep miRNA Cell and Tissue Miniprep System	Promega	Z621
High-Capacity cDNA Reverse Transcription Kit	Applied Biosystems	4368814
NucleoSpin RNA	Macherey-Nagel	740955
NucleoSpin Tissue/DNA	Macherey-Nagel	740952
In-Fusion HD Cloning Kit	Takara	639646
PureYield Plasmid Midiprep System	Promega	A2495
FITC Annexin V Apoptosis Detection kit I	BD Biosciences	556547
ImmPRESS HRP anti-rabbit IgG Polymer Detection Kit	Vector Laboratories	MP-7401
ImmPRESS HRP Anti-Mouse IgG IgG Polymer Detection Kit	Vector Laboratories	MP-7402

### 3.1.8 Restriction enzymes

Name	Sequence (5'→3')	Manufacturer	Reference
XhoI-HF (20U)	CTCGAG	New England BioLabs	R0146S
EcoRV-HF (20U)	GATATC	New England BioLabs	R3195S
HindIII-HF (20U)	AAGCTT	New England BioLabs	R3104S
AgeI-HF (20U)	ACCGGT	New England BioLabs	R3552S
EcoRI-HF (20U)	GAATTC	New England BioLabs	R3101S
NotI-HF (20U)	GCGGCCGC	New England BioLabs	R3189S
AvrII-HF (5U)	CCTAGG	New England BioLabs	R0174S
SbfI-HF (10U)	CCTGCAGG	New England BioLabs	R3642S
BamHI-HF (20U)	GGATCC	New England BioLabs	R3136S
PacI-HF (10U)	TTAATTAA	New England BioLabs	R0547S

### 3.1.9 Primary and Secondary antibodies for Western blot and immunohistochemistry

#### 3.1.9.1 Western blot

Antibody	Manufacturer	Reference
Mouse monoclonal anti-GAPDH	Santa Cruz	Sc-32233
Mouse monoclonal anti-SOX6	Santa Cruz	Sc-393314
Goat polyclonal anti-rabbit IgG-HRP	OriGene EU	R1364HRP
Goat polyclonal anti-mouse IgG(H+L)-HRP	Promega	W402B
Rabbit monoclonal anti-TXNIP	Abcam	ab188865

#### 3.1.9.2 Immunohistochemistry

Antibody	Manufacturer	Reference
Rabbit polyclonal anti-SOX6	Atlas Antibodies	HPA003908
Rabbit monoclonal anti-Ki67	Cell marque	275R-15
Mouse monoclonal anti-8-OHG	OriGene Technologies	AM03160PU-N
Rabbit polyclonal anti-Cleaved Caspase 3	Cell Signaling	9661
Rabbit monoclonal anti-TXNIP	Abcam	ab188865
Biotinylated anti-rat IgG mouse adsorbed	Vector Laboratories	BA 4001

### 3.1.10 Buffer and solutions

Solution	Composition
10× RIPA Buffer	150 mM NaCl; 1% triton X-100; 0.5% sodium deoxycholate; 0.1% SDS; 50 mM Tris-HCl, pH = 8
Freezing solution	10% DMSO, 45% FCS and 45% normal medium
1× TBS	100 ml 10× TBS; 900 ml H <sub>2</sub> O
1× TBST	100 ml 10× TBS; 900 ml H <sub>2</sub> O; 1 ml Tween-20
10× Running/Blotting buffer (10× R/B buffer) (pH = 8.3)	30g Tris-Base; 144g glycine
1× Running buffer	100 ml 10× R/B buffer; 900 ml H <sub>2</sub> O; 10 ml 10% SDS

1× Blotting buffer	100 ml 10× R/B buffer; 700 ml H <sub>2</sub> O; 200 ml methanol
Loading dye	312.5 mM Tris-HCl (pH = 6.8); 10% SDS; 50% glycerol; bromphenolblue
4× Loading dye	250 mM DTT to 1 ml loading dye
10% SDS	10g SDS; 100 ml H <sub>2</sub> O
Blocking buffer	5% non-fat dried milk or 5% BSA in 1x TBST
10% APS	1g ammonium persulfate; 10 ml H <sub>2</sub> O
Na <sub>3</sub> VO <sub>4</sub> (pH = 10)	200 mM Na <sub>3</sub> VO <sub>4</sub>
10× annealing buffer	1 M NaCl, 100 mM Tris-HCl, pH = 7.4
RPMI medium	500 ml RPMI 1640 medium, 10% FCS, 1% Penicillin/Streptomycin (P/S)
DMEM medium	500 ml DMEM medium, 10% FCS, 1% P/S
α-medium	500 ml α-medium, 10% FCS, 1% P/S, 2 ng/ml β-FGF
10× TAE electrophoresis buffer	48.4g Tris-Base, 11.4 ml glacial acetic acid, 3.7g EDTA, fill up to 1L with H <sub>2</sub> O
Electrophoresis gel	100 ml 1× TAE buffer, X% agarose, 4 μl EtBr
10× TBS (pH = 7.3)	24g Tris-Base; 88g NaCl
1 M Tris-HCl; pH = 6.8	30.3g Tris up to 250 ml H <sub>2</sub> O
1.5 M Tris-HCl; pH = 8.8	45.4g Tris up to 250 ml H <sub>2</sub> O

### 3.1.11 SDS-PAGE gel compositions

Resolving gel (7.5 ml)	5%	7%	10%	12%
H <sub>2</sub> O	4.2 ml	3.7 ml	2.9 ml	2.4 ml
1.5 M Tris-HCl (pH = 8.8)	2 ml	2ml	2ml	2ml
30% (w/v) Acrylamid/Bisacrylamid	1.3 ml	1.8 ml	2.5 ml	3 ml
10% (w/v) SDS	75 μl	75 μl	75 μl	75 μl
10% (w/v) APS	40 μl	40 μl	40 μl	40 μl
TEMED	10 μl	10 μl	10 μl	10 μl

Stacking gel (5ml)	3%
H <sub>2</sub> O	3.5 ml
1 M Tris-HCl (pH = 6.8)	860 μl
30% (w/v) Acrylamid/Bisacrylamid	500 μl
10% (w/v) SDS	48 μl
10% (w/v) APS	40 μl
TEMED	10 μl

### 3.1.12 Sequences

#### 3.1.12.1 shRNA sequences for pLKO-Tet-On cloning

Oligoname	Hairpin sequence (5' → 3')	TRCN-Number
sh_Control top	CCGGCAACAAGATGAAGAGCACCAACTCGAGTTGGTGTCTTCATCTTGTTG	
sh_Control bottom	AATTCAAAAACAACAAGATGAAGAGCACCAACTCGAGTTGGTGCTCTTCATCTTGTTG	

shRNA_SOX6_1 top	CCGGCCAGCCCTGTAAGTCAAGTTACTCGAGTAACTTGAGTT ACAGGGCTGGTTTTTG	0000085945
shRNA_SOX6_1 bottom	AATTCAAAAACCAGCCCTGTAAGTCAAGTTACTCGAGTAACT TGAGTTACAGGGCTGG	
shRNA_SOX6_2 top	CCGGCCAGTGAAGTCTTGGAGAACTCGAGTTTCTCCAAGA AGTTCACTGGTTTTTG	0000017990
shRNA_SOX6_2 bottom	AATTCAAAAACCAGTGAAGTCTTGGAGAACTCGAGTTTCT CCAAGAAGTTCACTGG	
shRNA_SOX6_3 top	CCGGTGGTCTTAATTGTTTCGTAAACTCGAGTTTACGAAACA ATTAAGACCATTTTTG	0000430184
shRNA_SOX6_3 bottom	AATTCAAAAATGGTCTTAATTGTTTCGTAAACTCGAGTTTAC GAAACAATTAAGACCA	

### 3.1.12.2 Sequences for pCDH vector cloning

Oligoname	Sequence (5' → 3')
dsDNA	GCTAGCCCTAGGCCTGCAGGGAATTTAAATCGGATCCTTAATTAAGGATCTGCGAT CGC

### 3.1.12.3 Primer

Oligoname	Sequence (5' → 3')
RPLPO_FW	GAAACTCTGCATTCTCGCTTC
RPLPO_RV	GGTGTAAATCCGTCTCCACAG
SOX6_FW	TTCCCCGACATGCATAACTC
SOX6_RV	AAGTGGATCTTGCTTAGCCG
pGL3_mSat_FW	CTAGCCCGGGCTCGAGGAGATGTGTCAGCAGTCAATCCA
pGL3_mSat_RV	GATCGCAGATCTCGAGGGCAGTCCAGGATGTTCTGAATAA
E2F8_FW	ACAGAATGGAGAACGAAAAGGA
E2F8_RV	TTGGTAGGTGTGGTTAAAGGG
DEPDC1_FW	GGCCAATACAAGTAAACGTGG
DEPDC1_RV	CATCTCGTTCAAATCCAACATAAGT
CDCA3_FW	ACTGGAGGGTCTTAAACATGC
CDCA3_RV	ACTTCACTCAGCTGTTTCACC
Tet-pLKO_FW	GGCAGGGATATTCACCATTAT
Tet-pLKO_RV	CTATTCTTTCCCCTGCACTG
TXNIP_FW	GATCTGAACATCCCTGATACCC
TXNIP_RV	CATCCATGTCATCTAGCAGAGG
eGFP_FW	ATTAGAATTCATGGTGAGCAAGGGCGAG
eGFP_RV	ATTAGCGGCCGCTTACTTGTACAGCTCGTCCATGC
cDNA TXNIP_FW	ATTAGCTAGCGCCACCATGGTGATGTTCAAGAAGATCAAGTC
cDNA TXNIP_RV	GCGGCGTTAATTAATCACTGCACATTGTTGTTGAGG

### 3.1.12.4 Sequencing primer

Name	Sequence (5' → 3')
RVprimer3	CTAGCAAATAGGCTGTCCC
GLprimer2	CTTTATGTTTTGGCGTCTTCCA
pLKOseq_FW	GGCAGGGATATTCACCATTATCGTTTTCAGA
pLKOseq_RV	GACGTGAAGAATGTGCGAGA
pCDH_FW	ATGGTGATGTTCAAGAAGATCAAGTC
pCDH_RV	AAAGCCTTCACCCAGTAGTC

### 3.1.12.5 Sequences for small interfering RNAs (siRNA)

Name	Sequence (5' → 3')
siCtrl	No sequence given
siTXNIP (sense)	AAGCCGUUAGGAUCCUGGCdTdT
siTXNIP (antisense)	GCCAGGAUCCUACGGCUUdTdT

### 3.1.13 Vectors

Vector name	Number	Manufacturer
Tet-pLKO-puro	# 21915	Addgene
pGL3-Promotor Vector	# E1761	Promega
pRL Renilla Vector	# E2231	Promega
pCD/NL-BH*DDD ( <i>pol</i> , <i>gag</i> )	# 17531	Addgene
pCEF-VSV-G ( <i>env</i> )	# 41792	Addgene
cDNA TXNIP ORF clone (NM_006472.5)	# OHu20973	GenScript
pCAG-YFP	# 11180	Addgene
pCMV-GFP	# 11153	Addgene
pCDH-Cuo-MCS-EF1-CymR-T2A-Puro	# QM800A-1	System Biosciences

### 3.1.14 Software

Software	Manufacturer
Bio Rad CFX Manager 3.1	Biorad
GraphPad PRISM 5	GraphPad
Image J	<a href="http://www.rsbweb.nih.gov/ij/">www.rsbweb.nih.gov/ij/</a>
Image Studio Lite	LI-COR
BD Accuri C6 Software	BD Biosciences
GSEA	Broad Institute

## 3.2 Methods

### 3.2.1 Microbiology

#### 3.2.1.1 Cloning with the pGL3-Promotor vector

In order to verify if EWSR1-FLI is binding GGAA-mSats in the intron 1 of the *SOX6* gene and thereby using these GGAA-mSats as enhancer to trigger *SOX6* expression, a 1-kb fragment including the mSat and its flanking regions ( $-/+$  500 bp) were investigated more closely.

For this experiment the “In-Fusion HD cloning” method was used according to the manufacturer’s protocol. In contrast to a classical ligation method, this method is based on recombination of the insert with the linearized backbone.

Primers were specifically designed according to the manufacturer’s protocol including 15 bp-overhangs that are homologous to the backbone containing the desired insert. Once the inserts were amplified with the specific overhangs, recombinase enzymes enable the fusion of the insert into the backbone. The pGL3-Promotor vector was used as a backbone that is suitable for cloning and testing putative enhancer regions like the GGAA-mSats and its flanking regions.

The pGL3-Promotor vector (1  $\mu$ g) was linearized with the restriction enzyme XhoI (1  $\mu$ l) overnight at 37°C as given in **Table 3**. The genomic DNA (gDNA) was extracted from three EwS cell lines with high- (RDES, TC-32 and POE), three with intermediate- (EW17, ORS and SK-N-MC), and two with low-*SOX6* expression (A673 and EW7) using the NucleoSpin Tissue Kit. Afterwards, 5  $\mu$ g of gDNA were digested to smaller fragments of  $\sim$  1-kb including the desired GGAA-mSat of the *SOX6* gene to facilitate subsequent amplification using the restriction enzymes EcoRV (2.5  $\mu$ l) and HindIII (2.5  $\mu$ l) as shown in **Table 3**. Here, it was important to choose restriction enzymes that do not cut in the region where the GGAA-mSat is supposed to be. Both, the linearized pGL3-Promotor vector and the mSat-amplicon were cleaned with the NucleoSpin PCR and Gel clean up kit.

Components	Amount ( $\mu$ l)
1 $\mu$ g pGL3-Promotor vector/ 5 $\mu$ g gDNA	x
10 $\times$ CutSmart buffer	10
Restriction enzyme 1	1
(Restriction enzyme 2)	(1)
dH <sub>2</sub> O	Up to 50 $\mu$ l

**Table 3:** Digestion protocol of pGL3-Promotor vector and gDNA.

Specific primers were designed for “In-Fusion HD cloning” including following characteristics:

1) The 5’-end of the primer must contain 15 bases that are homologous to 15 bases of the pGL3-Promotor vector linearized with XhoI to which it will be joined afterwards. The primers were designed to include the restriction site for XhoI.

2) The 3’-end of the primer must contain the sequence that is specific to the genomic GGAA-mSat region (see below).

3) The melting temperature ( $T_m$ ) of the primer that contains XhoI-site and the beginning of the GGAA-mSat region need to be between 57–65°C. If not the  $T_m$  is considered as 58°C.

4) The last five nucleotides at the 3’-end of each primer should not contain more than two guanines or cytosines. Therefore, the primers were designed based on the sequence for GGAA-mSat region that was extracted from the reference genome (see list 8.1).

The desired mSat-amplicon was amplified from pre-digested gDNA with the corresponding primer (see 3.1.12.3) as described in Table 4.

Components	Amount ( $\mu$ l)
5 $\times$ Gotaq colorless buffer	10
10 mM dNTPs	1
25 mM MgCl <sub>2</sub>	6
10 $\mu$ M pGL3_mSat-FW	2.5
10 $\mu$ M pGL3_mSat-RV	2.5
Gotaq polymerase	0.25
200 ng gDNA	x
dH <sub>2</sub> O	= up to 50

**Table 4:** Protocol for Gotaq PCR-amplification from gDNA.

The PCR program (**Table 5**) included a touch-down (TD) PCR to avoid amplifying non-specific sequences. The corresponding  $T_m$  for the TD-PCR was calculated as follows:

1)  $T_m$  of primer mix – 5°C (GoTaq Polymerase requirements) – 10°C (decrease of 0.5°C for the 1<sup>st</sup> 20 cycles):

$$62^\circ\text{C} (T_m) - 5^\circ\text{C} = 57^\circ\text{C} - 10^\circ\text{C} (20 \text{ cycles with a decrease of } 0.5^\circ\text{C}) = 47^\circ\text{C}^*$$

2) The annealing temperature in the 2<sup>nd</sup> 20 cycles was chosen based on the actual  $T_m$  of the primer (57°C) \*\*.

Step	°C	Time	Cycles
Initialization	95	2 min	1
Denaturation	98	10 sec	1 <sup>st</sup> 20
Annealing	57 – 47*	30 sec	
Elongation	72	1 min	
Denaturation	98	10 sec	2 <sup>nd</sup> 20
Annealing	57**	30 sec	
Extension	72	1 min	
Final Extension	72	∞	

**Table 5:** Thermal cycling conditions for Gotaq-mediated mSat-PCR-amplification.

The mSat-amplicon was purified with the NucleoSpin PCR and Gel clean up kit. According to the manufacturer's protocol of the In-Fusion HD cloning, 20 ng of the mSat-fragment and 10 ng of the linearized pGL3-Promotor vector were incubated for 15 min at 50°C. Further controls were also included (**Table 6**).

Components	Sample	Pos. Ctrl	Neg. Ctrl
20 ng DNA	x µl mSat-fragment	2 µl control insert	-
pGL3 backbone	1 µl (10 ng) linearized pGL3 vector	1 µl PUC19 linearized vector	1 µl (10 ng) linearized pGL3 vector
Premix	2 µl	2 µl	2 µl
dH <sub>2</sub> O	x µl	5 µl	7 µl

**Table 6:** "In-Fusion HD cloning" reactions according to manufacturer's protocol.

The reaction was stopped by incubation on ice for 5 min. For amplification of the plasmid see section 3.2.1.4. The cloned pGL3-mSat vector with a representative mSat is depicted in **Figure 2**.

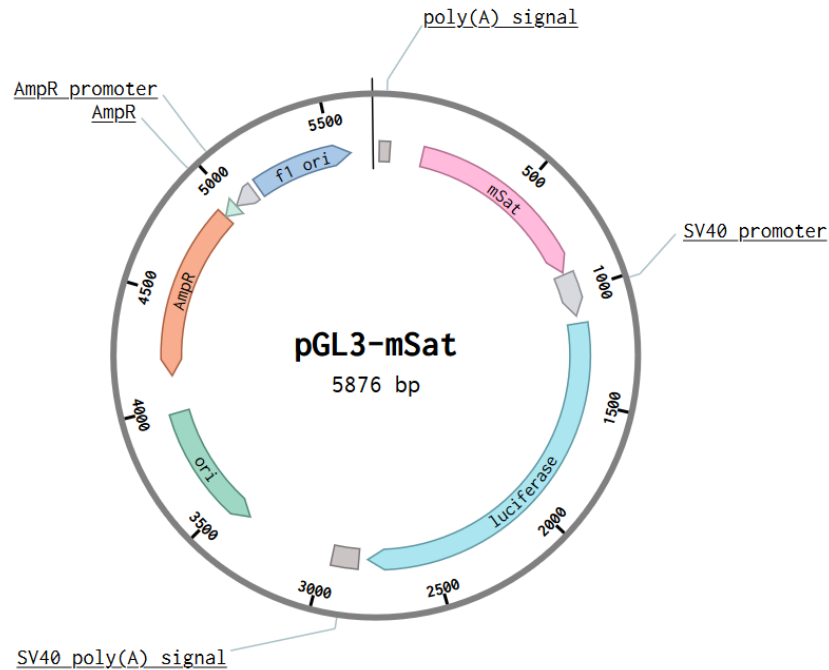


**Figure 2: The pGL3-mSat plasmid with the pGL3-Promoter vector as backbone and the microsatellite (mSat).**

AmpR promoter: expression of the ampicillin resistance; AmpR: ampicillin resistance in *E.coli*; ori: origin of plasmid replication in *E.coli*; f1 ori: origin of replication derived from filamentous phage; poly (A) signal: stabilization of mRNA; mSat: cloned GGAA-mSat region; SV40 promoter: expression of cloned DNA in mammalian cells; luciferase: cDNA encoding firefly luciferase; SV40 poly (A) signal: terminator sequence.

### 3.2.1.2 Cloning with the pLKO-Tet-On system

In order to perform long-term analyses, EwS cell lines were transduced with the lentiviral Tet-pLKO-puro vector containing the pLKO-Tet-On system as described and reviewed in (Das et al., 2016).

The Tet-ON system is under control of the tetracycline analog Doxycycline (Dox) that induces the transcription of small hairpin RNA (shRNA) against the *SOX6* gene in order to silence gene expression through RNA-interference. The cloning with the Tet-pLKO-puro vector was performed according to Wiederschain's protocol (Wiederschain et al., 2009) deposited at Addgene (Plasmid # 21915).

The shRNA of the Tet-pLKO-puro vector was designed as described in **Table 7** including the restrictions sites *AgeI*, *XhoI* and *EcoRI*. The sequences for the shRNA against *SOX6* were taken from the "Genetic Perturbation Platform (GPP) Web Portal" from the Broad institute. They were designed to form a hairpin with top and bottom strand. The shControl, in contrast, was randomly generated (**Table 7**).

	<b>AgeI</b>	<b>Target sequence</b>	<b>XhoI</b>	<b>Target sequence</b>	<b>Term. signal</b>	<b>EcoRI</b>	
<b>shSOX6_1:</b>							
Top	CCGG	CCAGCCCTGTAAC TCAAGTTA	CTCGAG	TAAGTTGAGTTAC AGGGCTGG	TTTTTG		
		TAAGTTGAGTTAC AGGGCTGG	CTCGAG	CCAGCCCTGTAAC TCAAGTTA	CAAAAA	AATT	bottom
<b>shSOX6_2:</b>							
Top	CCGG	CCAGTGAAGTTCT TGGAGAAA	CTCGAG	TTTCTCCAAGAAG TTCAGTGG	TTTTTG		
		TTTCTCCAAGAAG TTCAGTGG	CTCGAG	CCAGTGAAGTTCT TGGAGAAA	CAAAAA	AATT	bottom
<b>shSOX6_3:</b>							
Top	CCGG	TGGTCTTAATTGT TTCGTAAA	CTCGAG	TTTACGAAACAAT TAAGACCA	TTTTTG		
		TTTACGAAACAAT TAAGACCA	CTCGAG	TGGTCTTAATTGT TTCGTAAA	CAAAAA	AATT	bottom
<b>shControl:</b>							
Top	CCGG	CAACAAGATGAA GAGCACCAA	CTCGAG	TTGGTGCTCTTCA TCTTGTTG	TTTTTG		
		TTGGTGCTCTTCA TCTTGTTG	CTCGAG	CAACAAGATGAA GAGCACCAA	CAAAAA	AATT	bottom

**Table 7:** Design of shRNAs against *SOX6* or control.

The Tet-pLKO-puro vector was double digested with the corresponding *AgeI* and *EcoRI* restriction enzymes according to **Table 8**:

Components	Amount ( $\mu$ l)
10 $\times$ CutSmart buffer	2
Restriction enzyme 1	2
Restriction enzyme 2	2
4 $\mu$ g Tet-pLKO-puro vector	x
dH <sub>2</sub> O	Up to 20

**Table 8:** Double digestion protocol.

First, the reaction was incubated for 15 min at 37°C and deactivated at 65°C for 20 min. Both digestions were pooled to increase the yield. The linearized vector backbone (= 20  $\mu$ l) was precipitated by adding 180  $\mu$ l of water and 20  $\mu$ l of 3 M sodium acetate (corresponding 1/10 from total volume of 200  $\mu$ l). The mixture was incubated for 45 min at -80°C and afterwards centrifuged at 4°C for 30 min at 13,000 rpm. The pellet was washed with 70% ethanol and then centrifuged at 13,000 rpm for 15 min at 4°C. After drying the pellet for 2 min at 37°C it was reconstituted with 10  $\mu$ l dH<sub>2</sub>O. Verification of the linearized Tet-pLKO-puro vector occurred via gel (expected band at 1800 bp for the stuffer and ~8800 bp for linearized backbone).

In a second step, shRNA was annealed before ligation. Therefore, the designed top- and bottom-shRNAs were both reconstituted with dH<sub>2</sub>O to 100  $\mu$ M (0.1 nmol/ $\mu$ l) and 11.25  $\mu$ l of each oligo was mixed together with 2.5  $\mu$ l of 10 $\times$  annealing buffer to a final concentration of 0.8  $\mu$ g/ $\mu$ l each. The annealing program was set up as follows: The initial temperature was set to 95°C. Subsequently, the temperature was decreased by one degree/minute until 14°C was reached to ensure proper annealing of top- and bottom-strand. Afterwards, 1  $\mu$ l of the oligo mixture was diluted 1:400 with 0.5 $\times$  annealing buffer to a final concentration of 200 ng/ $\mu$ l.

In a third step, ligation of the 58 bp-annealed shRNA and double-digested and precipitated Tet-pLKO-puro vector was performed overnight at 16°C as described in **Table 9**:

Components	Amount (μl)
20 – 30 ng/μl linearized Tet-pLKO-puro	1
200 ng annealed shRNA	1
10× Ligase buffer	1.5
T4 DNA Ligase	1
dH <sub>2</sub> O	up to 15

**Table 9:** Ligation protocol of Tet-pLKO-puro with shRNAs.

The reaction was stopped by incubation on ice for 5 min. For amplification of the plasmid see section 3.2.1.4. The cloned pLKO-shSOX6/ (pLKO-shCtrl) vector is depicted in **Figure 3**.

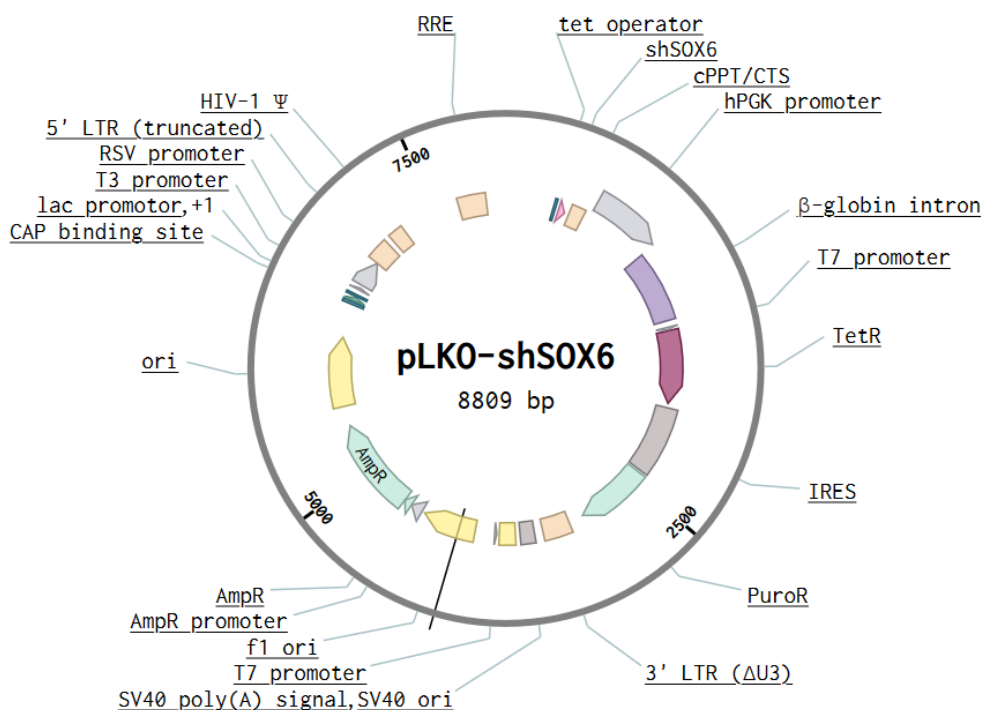


**Figure 3:** The pLKO-shSOX6 plasmid with the Tet-pLKO-puro vector as backbone with shRNA against SOX6 as insert.

hPGK promoter: eukaryotic promoter; β-globulin intron: enhancer of the T7 promoter; T7 promoter: prokaryotic promoter; TetR: tetracycline resistance; IRES: internal ribosome entry site (simultaneous expression of two proteins); PuroR: puromycin resistance; 3' LTR (ΔU3): lentivirus component; SV40 ori: SV40 promoter origin; SV40 poly (A) signal: terminator sequence; f1 ori: origin of replication derived from filamentous phage; AmpR promoter: expression of the ampicillin resistance; AmpR: ampicillin resistance in *E.coli*; ori: origin of plasmid replication in *E.coli*; CAP binding site: Catabolite Activator Protein binding site (facilitates the transcription activation of the lac promoter); lac promoter: prokaryotic promoter; lac operator (+1): lac operon; T3 promoter: prokaryotic promoter; RSV promoter: Rous Sarcoma Virus (HIV-based eukaryotic promoter); transfer plasmids: 5'LTR, HIV-1Ψ, RRE (Rev Response Element), 3' LTR (ΔU3); tet operator: tetracycline-controlled transcriptional activation; shSOX6: shRNA against SOX6; cPPT/CTS: increases the viral infectivity in non-dividing cells.

### 3.2.1.3 Cumate-inducible pCDH-CuO-MCS-EF1 $\alpha$ -CymR-T2A-Puro

For TXNIP rescue experiments with cumate-inducible *TXNIP* re-expression in *SOX6*-silenced TC-32 EwS cell lines (Tc-32/TR/shSOX6\_2), following cloning strategies were carried out. The "Cumate-Switch System Vector" constitutively co-expresses CymR, a repressor that binds a cumate operator sequence in absence of cumate. The "Cumate-Switch System Vector" is able to co-express both the cDNA of *TXNIP* and the eGFP marker combined with a T2A element from the cumate switch promoter. The *TXNIP* expression can be controlled by adding cumate to the cells as the cumate repressor (CymR) has a higher binding affinity for cumate (Mullick et al., 2006). The cumate-inducible *TXNIP* re-expression plasmid is based on the pCDH-CuO-MCS-EF1 $\alpha$ -CymR-T2A-Puro SparQ™ All-in-one Cloning and Expression Lentivector.

In a first step, the multiple cloning site (MCS) was modified as it was necessary to eliminate the EcoRI and NotI restriction sites. Therefore, a customized dsDNA oligonucleotide sequence (**Table 10**) was created, including AvrII, SbfI, BamHI and PacI restriction sites:

NheI	AvrII	SbfI	Random sequence	PacI	BamHI	AsiSI
GCTAGC	CCTAGG	CCTGCAGG	GAATTTAAATCGG ATCC	TTAATTAA	GGATCC	GCGATCGC

**Table 10:** Customized dsDNA (5'  $\rightarrow$  3').

Both, 1  $\mu$ g of the dsDNA oligonucleotide sequence and 1  $\mu$ g of the pCDH vector were double digested with NheI and AsiSI overnight at 37°C according to **Table 3**, and cleaned with the NucleoSpin PCR and Gel clean up kit. Subsequently, both the digested pCDH and the dsDNA were ligated by T4 Ligase (**Table 11**). The reaction was stopped by incubation on ice for 5 min.

Components	Amount ( $\mu$ l)
25 ng pCDH vector	x
Insert (dsDNA) – 6:1 ratio	x
10 $\times$ Ligase buffer	2
T4 DNA Ligase	1
dH <sub>2</sub> O	up to 20

**Table 11:** Ligation protocol of pCDH vector with dsDNA oligonucleotide sequence.

Secondly, as the TC-32/TR/shSOX6\_2 cell already contained a puromycin-resistance cassette, the puromycin-resistance gene within the pCDH vector was removed by double digestion (**Table 8**) of the pCDH vector with EcoRI and NotI. In order to be able to select the cells that express the cDNA of *TXNIP*, an eGFP reporter protein for co-expression was included. The eGFP sequence was PCR-amplified using a pCMV-GFP vector as a template (**Table 15**) with the following primers (**Table 12**):

	Start	EcoRI	Primer sequence (5'→3')
<b>eGFP_FW:</b>	ATTA	GAATTC	GCCACCATGGTGATGTTCAAGAAGATCAAGTC

	Start	PacI	Primer sequence (5'→3')
<b>eGFP_RV:</b>	ATTA	GCGGCCGC	TTACTTGACAGCTCGTCCATGC

**Table 12:** Primer for eGFP amplification from pCMV-GFP vector.

The amplicon was purified with the NucleoSpin PCR and Gel clean up kit. In a last step, full-length cDNA of *TXNIP* was PCR-amplified (**Table 13** and **Table 15**) from a cDNA *TXNIP* ORF clone (see **3.1.13**) and modified in order to be ligated into the customized MCS.

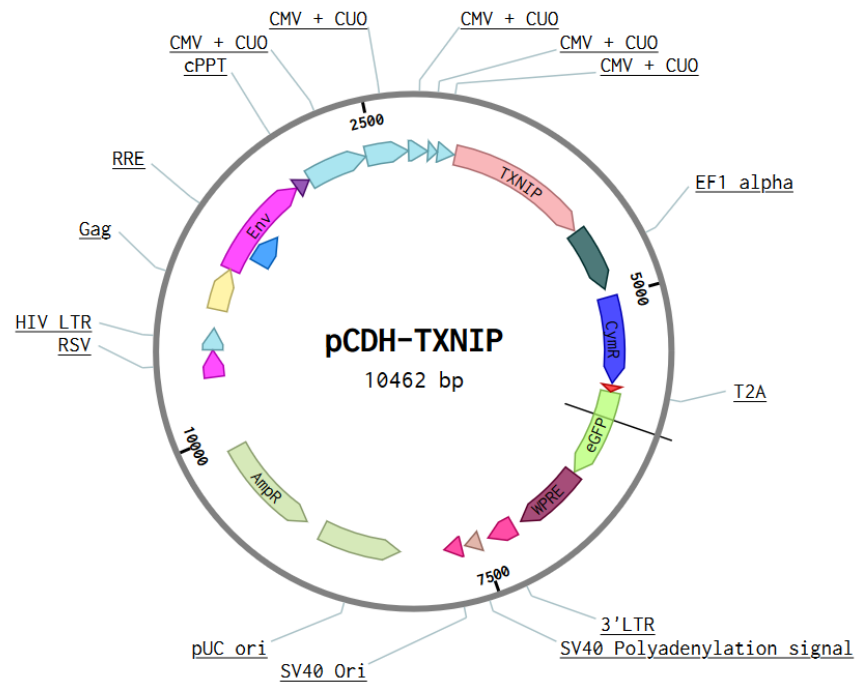
	Start	NheI	Primer sequence (5'→3')
<b>cDNA TXNIP_FW:</b>	ATTA	GCTAGC	GCCACCATGGTGATGTTCAAGAAGATCAAGTC

	Start	PacI	Primer sequence (5'→3')
<b>cDNA TXNIP_RV:</b>	GCGGCG	TTAATTAA	TCACTGCACATTGTTGTTGAGG

**Table 13:** Primer for cDNA *TXNIP* amplification.

The transgene was then inserted by NheI-PacI double digestion (**Table 8**), and cleaned with the NucleoSpin PCR and Gel clean up kit. For amplification of the plasmid see section **3.2.1.4**. The cloned cumate-inducible pCDH-TXNIP vector is depicted in **Figure 4**.



**Figure 4: Cumate-inducible pCDH-TXNIP vector.**

Lentivirus components: RSV promoter: eukaryotic promoter, transfer plasmids: 5'LTR, HIV-1 $\Psi$ , RRE, 3' LTR ( $\Delta$ U3); packaging plasmids: *gag*, *pol* and RRE; envelope plasmid: *env*; cPPT: increases the viral infectivity in non-dividing cells; CMV promoter: eukaryotic promoter; CUO: cumate operator sequence; TXNIP: cDNA of TXNIP; EF1 alpha promoter: eukaryotic promoter with constitutive expression; CymR: repressor that binds CUO; T2A: enables the simultaneous expression of two proteins; WPRE element: enhances stability and translation of the CMV-driven transcript; SV40 ori: SV40 promoter origin; SV40 poly(A) signal: termination and processing of the recombinant transcript; pUC origin: replication and maintenance of the plasmid in *E.coli* cells; AmpR promoter: expression of the ampicillin resistance; AmpR: ampicillin resistance in *E.coli*.

### 3.2.1.4 Transformation of *E.coli* and colony PCR

After the cloning strategy of the pGL3-mSat, pLKO-shSOX6 and pCDH-TXNIP vectors, the plasmids were transformed into Stellar Competent cells. Therefore, 50  $\mu$ l of competent cells were quickly thawed on ice for 5 min, directly mixed with 5 ng ( $\sim$  2.5  $\mu$ l) of ligation-mixture and incubated for 30 min on ice. A heat shock occurred for exactly 45 seconds at 42°C with subsequent 2 min incubation on ice. The competent cells were reconstituted with 500  $\mu$ l of pre-warmed SOC-medium and incubated while shaking for 1 h at 37°C. An appropriate amount of transformed bacteria were plated out on ampicillin plates (50 – 100  $\mu$ g/ml) and incubated overnight at 37°C for further selection.

The transformation success was verified through the colony touch-down (TD) PCR. At least 20 colonies were picked and each incubated in 100  $\mu$ l LB-Medium containing 100  $\mu$ g/ml ampicillin for 1h at 37°C.

The PCR mix was prepared as follows (**Table 14**):

Components	Amount ( $\mu$ l)
5 $\times$ Gotaq colorless buffer	10
10 mM dNTPs	1
25 mM MgCl <sub>2</sub>	6
10 $\mu$ M Forward primer <sup>*/#</sup>	2.5
10 $\mu$ M Reverse primer <sup>*/#</sup>	2.5
Gotaq polymerase	0.25
Colony solution	2
dH <sub>2</sub> O	x
Total volume	up to 50

**Table 14:** Protocol for colony-PCR of pGL3-mSat (\*)– and pLKO-shSOX6/shCtrl (#)-insert amplification.

Components	Amount ( $\mu$ l)
5 $\times$ HiFi buffer	5
10 Mm dNTPs	1
100% DMSO	1.5
10 $\mu$ M primer mix <sup>**/#</sup>	2.5
10 $\mu$ M primer mix <sup>**/###</sup>	2.5
Phusion polymerase	0.5
100 ng DNA	x
dH <sub>2</sub> O	up to 50

**Table 15:** Protocol for PCR-amplification of eGFP (\*\*\*) or cDNA *TXNIP* (###) from pCMV-GFP or TXNIP ORF vector, respectively and protocol for colony-PCR of pCDH-TXNIP-insert (###) amplification.

For pGL3-mSat, pLKO-shSOX6/shCtrl, pCMV-GFP or TXNIP ORF vectors the following primers were included:

- pGL3-specific primers\*:

pGL3\_mSat\_FW: 5'-CTAGCCCGGGCTCGAGGAGATGTGTCAGCAGTCAATCCA-3';

pGL3\_mSat\_RV: 5'-GATCGCAGATCTCGAGGGCAGTCCAGGATGTTCTGAATAA-3',

- pLKO-specific primers#:

Tet-pLKO\_FW: 5'-GGCAGGGATATTCACCATTAT-3';

Tet-pLKO\_RV: 5'-CTATTCTTCCCCTGCACTG-3'.

- pCMV-GFP-specific primers\*\*:

eGFP\_FW: 5'-ATTAGAATTCATGGTGAGCAAGGGCGAG-3';

eGFP\_RV: 5'-ATTAGCGGCCGCTTACTTGTACAGCTCGTCCATGC-3'.

- cDNA TXNIP ORF/pCDH-specific primers###:

cDNA TXNIP\_FW: 5'-ATTAGCTAGCGCCACCATGGTGATGTTCAAGAAGATCAAGTC-3';

cDNA TXNIP\_RV: 5'-GCGGCGTTAATTAATCACTGCACATTGTTGTTGAGG-3'.

The colony-PCR included a touch-down (TD)-PCR (colony-TD-PCR) to increase specificity. This possesses a higher initialization time, as it first needs to disrupt the bacterial membrane (**Table 16** and

**Table 17**):

Step	°C	Time	Cycles
Initialization	95	10 min	1
Denaturation	98	10 sec	1 <sup>st</sup> 10
Annealing	X*	30 sec	
Elongation	72	1 min	
Denaturation	98	10 sec	2 <sup>nd</sup> 20
Annealing	X**	30 sec	
Extension	72	1 min	
Final Extension	72	∞	1

**Table 16:** Thermal cycling conditions for colony-TD-PCR of pLKO-Tet and pGL3 vectors.

X\*: The annealing temperature for the 1<sup>st</sup> 10 cycles needs to be adapted to the corresponding  $T_m$  of the constructs: For pGL3\_mSat vector:  $T_m = 57^\circ\text{C} - 47^\circ\text{C}$ ; for pLKO\_shSOX6/shCtrl vector:  $T_m = 67^\circ\text{C} - 57^\circ\text{C}$ .  
X\*\*: The annealing temperature for the 2<sup>nd</sup> 20 cycles is the actual  $T_m$  of the constructs: For pGL3\_mSat vector:  $T_m = 57^\circ\text{C}$ ; For pLKO\_shSOX6/shCtrl vector:  $T_m = 67^\circ\text{C}$ .

Step	°C	Time	Cycles
Initialization	98	3 min	1
Denaturation	98	10 sec	1-10
Annealing	69 – 0.5 per cycle	30 sec	
Elongation	72	25 sec/ 1kb	
Denaturation	98	10 sec	11-25
Annealing	64	30 sec	
Extension	72	25 sec/ 1kb	
Final Extension	72	5 min	1

**Table 17:** Thermal cycling conditions for (colony)-TD-PCR for pCMV-GFP/ TXNIP ORF vector and pCDH-TXNIP vectors.

The colony-PCR was loaded on an agarose gel to see if the picked colonies include the correct insert: mSat = 866 bp, shSOX6/shCtrl insert = 420 bp, eGFP = 720 bp, cDNA *TXNIP* = 1.2 kbp.

The selected candidates were cultivated in a 100 ml midi-culture (including 100 µg/ml ampicillin) at 37°C overnight. The plasmids were extracted with the PureYield Plasmid Midiprep System according to the manufacturer's protocol and re-suspended in 40 µl dH<sub>2</sub>O.

### 3.2.1.5 Sequencing of pGL3-mSat, pLKO-shSOX6/shCtrl and pCDH-TXNIP constructs

In order to exclude point mutations that could have occurred during transformation with *E.coli*, sequencing was performed. Thereby the sequencing-primers (see 3.1.12.4) were diluted to 10 µM and the plasmid to 50 ng – 100 ng in 30 µl total volume.

### 3.2.2 Cell culture

#### 3.2.2.1 Cell lines

In this thesis the following cell lines were used:

- EwS cell lines

A673, MHH-ES1, RDES, SK-N-MC, CHLA-10, CHLA-25, CHLA-32, CHLA-57, CHLA-99, COG-E-352, RH-1, TC-32, TC-71, TC-106, ES7, EW1, EW3, EW7, EW16, EW17, EW18, EW22, EW24, ORS, POE, SK-PN-DW, SK-PN-LI, SK-ES1, MIC and STA-ET1.

- Neuroblastoma cell lines

SK-N-AS and TGW.

- Rhabdomyosarcoma cell lines

Rh4 and Rh36.

- Osteosarcoma cell lines

SAOS-2 and U2OS.

- MSC-52 (From bone marrow of an EwS patient)
- HEK-293 (Human embryonic kidney cell line)

The A673/TR/shEF1 and SK-N-MC/TR/shEF1 cell lines used in this thesis were kindly provided from Dr. med. Martin Orth.

The following four cell lines were mainly used in this thesis (**Table 18**):

Cell line	Description
<b>A673</b>	EwS cell line (type 1 translocation) established from the primary tumor of a 15-year-old girl (Giard et al., 1973)
<b>RDES</b>	EwS cell line (type 2 translocation) established from the primary tumor (humerus) of a 19-year-old man
<b>TC-32</b>	EwS cell lines (type 1 translocation) isolated from the iliac bone and adjacent soft tissue of a 17 years old female before chemotherapy treatment (May et al., 2013)
<b>POE</b>	EwS cell lines (type 1 translocation) established at the Institute Curie, Paris.

**Table 18:** Origin of the mostly used EwS cell lines.

### 3.2.2.2 Cell culture methods

All EwS, neuroblastoma, rhabdomyosarcoma, osteosarcoma cell lines as well as the HEK-293 cell line were cultured in RPMI-1640 medium with stable glutamine supplemented with 10% tetracycline-free fetal calf serum (FCS) and 100 U/ml Penicillin and 100 µg/ml Streptomycin (P/S) at 37°C with 5% CO<sub>2</sub> in a humidified atmosphere. The patient-derived mesenchymal stem cell line (MSC-52) was cultivated in α-Medium supplemented with 100 U/ml penicillin and 100 µg/ml streptomycin (P/S), 10% FCS and 2 ng/ml β-FGF at 37°C with 5% CO<sub>2</sub>.

EwS cell lines were transduced with corresponding shRNA and selected with 1.5 µg/ml puromycin for a period of time.

About 1 × 10<sup>6</sup> cells/ml were frozen in liquid nitrogen for long-term storage by adding a freezing solution to the cell pellet. The cells were defrosted in a water bath at 37°C and re-suspended in 5 ml culture medium to eliminate DMSO. Subsequently, the cells were centrifuged at 1,200 rpm for 5 min and the supernatant was discarded. The pellet was re-suspended in an appropriate volume of medium and transferred to T<sub>75</sub> cm<sup>2</sup> flask. The splitting of the cells was carried out by previous washing of the cells with PBS and subsequent trypsinization to dissolve the adherence boundaries of the cells. The cell lines were routinely tested for mycoplasma contamination by nested PCR, and the cell line identity was regularly verified by Short Tandem Repeat (STR)-profiling.

### 3.2.2.3 Transduction of pLKO-shSOX6 and pLKO-shSOX6-pCDH-TXNIP in EwS cell lines

For long-term experiments RDES, POE and TC-32 cell lines were transduced with the Tet-pLKO-shSOX6 vector or additionally transduced with the pCDH-TXNIP vector.

For lentiviral transduction of EwS cell lines, 3 × 10<sup>5</sup> HEK-293 cells/T<sub>75</sub> flask were cultured with 10 ml RPMI medium containing 10% FCS and 1% P/S for 72h. In order to increase safety levels of lentiviruses, the packaging plasmids were added separately to the plasmids containing the DNA. Therefore, 10 µg DNA plasmid of pLKO\_shSOX6 or pCDH-TXNIP was added to 10 µg Δ8.9 (containing *gag* and *pol*) and 3 µg VSV-G (containing *env*) up to 4.6 ml of OptiMEM. Subsequently, 46 µl of Plus Reganet was added

to the mixture, incubated for 10 min at RT and then 60  $\mu$ l of Lipofectamine LTX were incubated for a further 25 min at RT. Thereafter, 4.4 ml of the transfection reaction were added to HEK-293 cells in 10 ml medium, that was replaced with a completely fresh medium after 4h of incubation in order to reduce toxicity. 24h after transfection, the medium was replaced with 30% FCS-containing medium to accelerate virus production.

At the same time  $2 \times 10^5$  cells/ 6-well were pre-cultured in a total volume of 1.7 ml RPMI medium. 48h after transfection, the virus-containing supernatant was filtered through a 0.45  $\mu$ m filter in order to exclude cell contamination with HEK-293 cells. Depending on the construct, 500  $\mu$ l of the virus-containing supernatant was added to the pre-cultured cells for 72h. Subsequently, EwS cells transduced with pLKO\_shSOX6 or pLKO-shSOX6-pCDH-TXNIP respectively, were washed twice with PBS and further selected with medium containing 1  $\mu$ g/ml puromycin for at least 1 week. Additionally, pLKO-shSOX6-pCDH-TXNIP vectors were sorted by eGFP-positive cells.

The resulting EwS cell lines were called: TC-32\_shCtrl, TC-32\_shSOX6\_2, TC-32\_shSOX6\_3, RDES\_shCtrl, RDES\_shSOX6\_2, RDES\_shSOX6\_3, POE\_shCtrl, POE\_shSOX6\_1, POE\_shSOX6\_3 or TC-32\_shSOX6\_2\_pCDH-TXNIP.

#### **3.2.2.4 Transfection**

For RNA interference experiments A673, EW7, RDES, TC-32 and POE cell lines were transiently transfected with Lipofectamine RNAiMAX (see 3.2.5.1). Transfection of the pGL3\_mSat vector into A673/TR/shEF1 cells as well as the pLKO\_shSOX6 vector and the pCDH-TXNIP vector into HEK-293 cells was performed with Lipofectamine LTX with Plus Reagent according to the manufacturer's protocol if not otherwise specified.

### 3.2.3 Molecular biology

#### 3.2.3.1 Isolation of total RNA, cDNA synthesis and quantitative real time PCR (qRT-PCR)

The total RNA was isolated from cell lines and tumor tissue using the NucleoSpin RNA kit. Afterwards, 1 µg of total RNA was reverse-transcribed using High-Capacity cDNA Reverse Transcription Kit as follows (**Table 19**):

Components	Amount (µl)
10× RT buffer	2
10× RT random primers	2
25× dNTP Mix (100 mM)	0.8
Reverse Transcriptase (50 U/µl)	0.8
1 µg RNA diluted with dH <sub>2</sub> O	14.4

**Table 19:** Reverse transcription protocol for EwS cells.

The qRT-PCR reactions were performed using ‘*SYBR green master mix*’ that was mixed with diluted cDNA (1:10) and 10 µM forward/ reverse primer mix (**Table 20**) on a Bio-Rad CFX Connect instrument and analyzed using Bio Rad CFX Manager 3.1 software.

Components	Amount (µl)
SYBR green master mix	7.4
10 µM FW/RV primer mix	0.9
cDNA (1:10 diluted in dH <sub>2</sub> O)	6.7

**Table 20:** qRT-PCR protocol with SYBR green master mix.

Gene expression values were calculated using the “ $2^{-\Delta\Delta Ct}$  method” (Livak and Schmittgen, 2001) relative to the housekeeping gene *RPLP0* as internal control. Thereby  $\Delta Ct$  values of “*RPLP0*-Target” were calculated and the  $\Delta\Delta Ct$  value of each sample was calculated relative to the internal control (Sample X – control) and  $\log_2$ -transformed. Primers were purchased from MWG Eurofins Genomics and listed in the section **3.1.12.3**.

The thermal conditions for qRT-PCR were as follows (**Table 21**):

Step	°C	Time	Cycles
Heat activation	95	2 min	1
Denaturation	95	10 sec	50
Annealing	60	20 sec	
Extension	60	20 sec	
Final denaturation	95	30 sec	1

**Table 21:** Thermal cycling conditions for qRT-PCR.

### 3.2.3.2 DNA extraction

For genomic DNA extraction, about  $1 \times 10^7$  cells were collected and genomic DNA was extracted with the NucleoSpin Tissue/DNA kit according to manufacturer's protocol. DNA concentration was measured by Nanodrop.

## 3.2.4 Biochemistry

### 3.2.4.1 Generation of cell lysates and Bradford assay

RDES\_shCtrl, RDES\_shSOX6\_2, RDES\_shSOX6\_3, TC-32\_shCtrl, TC-32\_shSOX6\_2 and TC-32\_shSOX6\_3 EwS cell lines were treated for 96h with Dox to induce *SOX6* knockdown. To this end,  $2 \times 10^5$  cells were seeded out and after 96h whole cellular proteins were extracted with 100  $\mu$ l/ 6-well RIPA buffer containing 1 mM  $\text{Na}_3\text{VO}_4$  and 100  $\mu$ l/ml protease inhibitor cocktail.

The total protein concentration of cell lysates was determined by Bradford protein assay (Bradford, 1976). The standard curve was determined by diluting Bovine Serum Albumin Standard (0.125  $\mu$ g, 0.25  $\mu$ g, 0.5  $\mu$ g, 0.75  $\mu$ g, 1  $\mu$ g and 2  $\mu$ g) and the Bradford reagent 1:5 with  $\text{dH}_2\text{O}$ . The standard curve was measured and later used for calculation of the relative protein concentrations of the samples. The protein concentration was determined by diluting 1  $\mu$ l of cell lysate in 99  $\mu$ l of diluted (1:5) Bradford reagent. The protein absorption was measured at 595 nm with the spectrophotometer.

### 3.2.4.2 SDS-PAGE and Western Blot

For Western blot analyses the lysates were mixed in 4× loading dye containing DDT and denatured at 95°C for 5 min. Lysates were stored at –80 °C. The separation of proteins was done by SDS-polyacrylamide-gelelectrophoresis (SDS-PAGE). Therefore, the stacking and the running gel were prepared according to section 3.1.11.

The nitrocellulose membranes were incubated with a primary mouse monoclonal anti-SOX6 antibody (1:1000) diluted in 5% BSA-TBST, and mouse monoclonal anti-GAPDH (1:800) and rabbit monoclonal anti-TXNIP (1:1000) diluted in 5%-milk-TBST. The nitrocellulose membranes were secondarily incubated with anti-mouse IgG (H+L) HRP-coupled (1:3000) or anti-rabbit IgG-HRP (1:5000) in 5%-milk-TBST. Proteins were detected using chemiluminescence HRP substrate and a densitometric protein quantification was carried out by ImageJ.

### 3.2.5 Cell-based assays

#### 3.2.5.1 Cell proliferation

For proliferation assays with **sipool-mediated** knockdown of SOX6 and cell-cycle related genes (*CDCA3*, *DEPDC1* and *E2F8*) reverse transfection with Lipofectamine RNAiMAX was performed according to siTOOL's protocol. All sipools consist of 30 different short interfering RNAs (siRNAs) directed against the target transcript, which largely eliminate off-target effects (Hannus et al., 2014).

For this purpose,  $7.5 \times 10^4$  cells/12-well for RDES, TC-32 and POE were seeded out in serum-free medium on the same day as the transfection with a sipool specifically directed against *SOX6*, *CDCA3*, *DEPDC1* and *E2F8* (Table 22) or a corresponding non-targeting sipool Control (sipControl) at a final concentration of 5 – 15 nM, respectively.

sipool	Pre-dilution stock	Final concentration
<i>CDCA3</i>	0.25 $\mu$ M	5 nM
<i>DEPDC1</i>	0.5 $\mu$ M	10 nM
<i>SOX6</i>	0.5 $\mu$ M	10 nM
<i>E2F8</i>	0.75 $\mu$ M	15 nM

**Table 22:** Pre-dilutions and final concentration of sipool-mediated transfection.

OptiMEM for sipool as well as sipool pre-dilution stocks (1) and OptiMEM for RNAiMax as well as RNAiMax (2) were mixed simultaneously. Subsequently, both mixes ((1) + (2)) were mixed, vortexed in a 1:1 ratio (3) and incubated for 5 min at RT. Thereafter, 250  $\mu$ l of this transfection-mix (3) was given to 750  $\mu$ l of cell suspension (4) in a 12-well and mixed well (**Table 23**):

Final volume/well	OptiMEM for sipool dilution	Sipool pre-dilution	OptiMEM for RNAiMax	RNAiMax	Transfection mix/well	Cell seeding density (cells/ml)	Cell suspension volume
	(1)		(2)		(3)	(4)	
1 ml	105 $\mu$ l	20 $\mu$ l	123 $\mu$ l	2 $\mu$ l	250 $\mu$ l	75.000	750 $\mu$ l

**Table 23:** Transfection protocol for sipool-mediated knockdown.

For proliferation assays with **siRNA-mediated** knockdown of *TXNIP*, reverse transfection with Lipofectamine RNAiMAX was performed. To this end,  $2.5 \times 10^5$  cells/6-well were seeded out in serum-free medium the same day as the transfection with a siRNA specifically directed against *TXNIP* or a corresponding non-targeting siRNA (siCtrl), at a concentration of 25 nM, respectively. The transfection was performed according to the manufacturer's protocol with a final concentration of 10 nM.

For proliferation assays with **shRNA-mediated** *SOX6* knockdown,  $2 \times 10^5$  EwS cells were seeded in a 6-well plate and treated with 0.1  $\mu$ g/ml Dox every 48h for transient knockdown for a total period of 96h.

The knockdown efficacy of all knockdown-variants, was validated by qRT-PCR and/or Western blot. 48h after transfection cells were re-transfected or Dox was re-freshed. The cell viability was

determined 96h after the initial transfection, including the supernatant, by counting the cells with Trypan-Blue using standardized hemocytometers.

### 3.2.5.2 Clonogenic (2D) and sphere (3D) assay

For clonogenic growth assays, EwS cell lines, harboring a shRNA against *SOX6* or Ctrl, were seeded at low density (200 cells) in a 12-well plate and grown for 21 days. Thereby Dox was renewed every 48h to maintain *SOX6* knockdown. Three technical replicates per biological replicate were counted independently and the colony area was measured with the ImageJ Plugin *Colony area*. The clonogenicity index was calculated by multiplying the counted colonies with the corresponding colony area.

For the sphere formation assay (anchorage-independent growth), EwS cell lines, harboring a shRNA against *SOX6*, were pre-treated with Dox 48h before seeding to induce the knockdown of *SOX6*. Consequently,  $1 \times 10^3$  cells/96-well were seeded in 200  $\mu$ l total volume in ultra-low attachment plates for 12 days. Assays with A673 EwS cell lines with siRNA against *SOX6* were performed as described in **section 3.2.5.1**. Thereby, the transfection was repeated every 48h. Subsequently, low attachment wells were photographed and only spheres larger than 500  $\mu$ m in diameter were counted. The area was measured using ImageJ and the sphere volumes were calculated as follows:  $V = 4/3 \times \pi \times r^3$ . The sphere index was calculated by multiplying the counted colonies with the corresponding colony volume.

### 3.2.5.3 Cell cycle analysis with propidium iodide

For cell cycle analysis, EwS cell lines harboring a shRNA against *SOX6*, were seeded at  $4 \times 10^5$  cells per 10 cm dish and subsequently starved for 56h. Stimulation of the cells occurred with 10% FCS for 20h. On the day of analysis, the cells were fixed with ice-cold 70% ethanol, treated with 100  $\mu$ g/ml RNase and stained with 50  $\mu$ g/ml propidium iodide (PI) for 45 min in the dark. The analysis of the cell cycle

was performed within 2 – 3 hours in time with BD Accuri C6 Cytometer by counting at least  $1 \times 10^5$  events. An example for the gating strategy is provided in **Figure 5**.

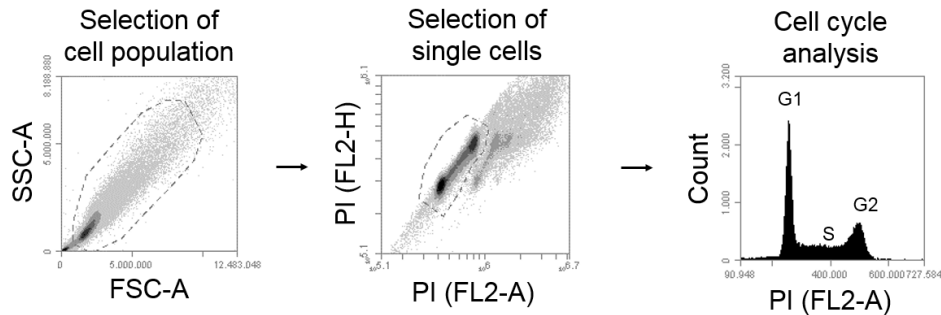


**Figure 5: Gating strategy for cell cycle analysis with propidium iodide.**

### 3.2.5.4 Determination of apoptosis with Annexin V staining

For determination of apoptosis with Annexin V staining, EwS cell lines harboring a shRNA against *SOX6* were seeded at  $3 \times 10^5$  cells per 10 cm dish and treated with 0.1  $\mu\text{g}/\text{ml}$  Dox every 48h to ensure *SOX6* knockdown. After 96h, cells were washed with PBS and the cells were re-suspended in 500  $\mu\text{l}$  1x Annexin V buffer containing 5  $\mu\text{l}$  of Annexin V and 5  $\mu\text{l}$  PI solution for 15 min. Analysis of Annexin V positivity was performed within 1h with BD Accuri C6 Cytometer by counting at least  $1 \times 10^5$  events. An example for the gating strategy is provided in **Figure 6**.

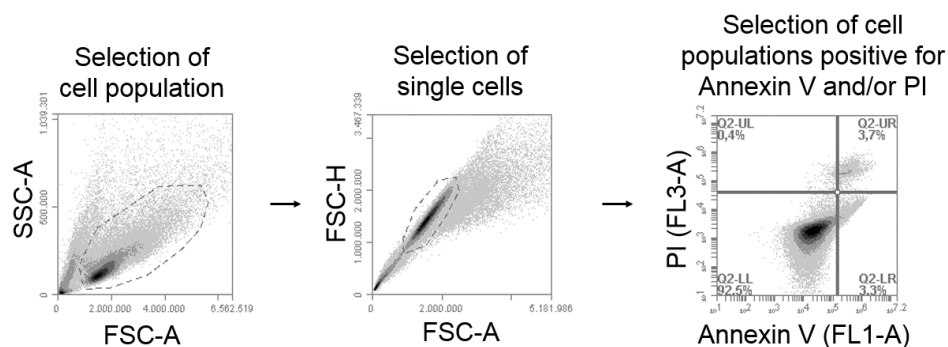


**Figure 6: Gating strategy for apoptosis analysis with Annexin V staining.**

### 3.2.5.5 Drug-response assay

For drug-response assays with **Elesclomol** and **Menadione**,  $1.5 \times 10^3$  cells of RDES and TC-32 with Dox-inducible *SOX6* knockdown as well as  $2.5 \times 10^3$  cells of MSC-52 and SAOS-2 were seeded in 96-well plates. Therefore, EwS cell lines harboring shRNA against *SOX6* were pre-treated for 48h with Dox to induce *SOX6* knockdown whereas MSC-52 and SAOS-2 cells were not pre-treated before the addition of Elesclomol (STA-4783) and Menadione. The pre-treatment medium was discarded prior to the addition of different concentrations of Elesclomol or Menadione ranging from 0.1 nM to 10  $\mu$ M or 0.1  $\mu$ M – 25  $\mu$ M, respectively with/without Dox to the cells in a total volume of 100  $\mu$ l per technical replicate for a further 72h.

In order to measure drug-response in **siRNA-mediated *TXNIP* knockdown** cells with Elesclomol,  $3.5 \times 10^3$  TC-32 cells were seeded in a 96-well plate for 48h and subsequently pre-treated with siRNA against *TXNIP* (final concentration 10 nM). After 48h, the 96-well plate was again transfected with siRNA against *TXNIP* but simultaneously also treated with different concentrations of Elesclomol, ranging from 0.1 nM to 10  $\mu$ M for further 72h.

For oxidative stress **scavenging experiments** with **N-acetylcysteine (Nac)** and **Tiron**, EwS cell lines, harboring a shRNA construct against *SOX6*, were additionally treated with 0.01 mM Nac or 0.1 mM Tiron, respectively for 72h.

For ***TXNIP*-rescue experiments** in Dox-inducible shRNA-mediated *SOX6* knockdown cells by a cumate-inducible *TXNIP* re-expression, TC-32 EwS cells were pre-treated with 0.1  $\mu$ g/ml Dox and 5  $\mu$ g/ml cumate for 48h to induce *SOX6* knockdown and simultaneously re-induce *TXNIP* expression in these cells to physiological levels. Subsequently, the cells were also treated with 0.1 nM to 10  $\mu$ M Elesclomol with/without Dox and cumate, respectively for further 72h.

For **rescue experiments** with **H<sub>2</sub>O<sub>2</sub>**,  $1.5 \times 10^3$  the EwS cells were seeded in 96-well plates and pre-treated for 48h with Dox to induce *SOX6* knockdown. After 48h, the cells were either further subjected to Elesclomol (10 nM) or vehicle (DMSO) and additionally treated with 30 mM H<sub>2</sub>O<sub>2</sub>.

After 72h, Resazurin (16  $\mu\text{g/ml}$ ) was added to the cells in order to measure cell viability. The relative IC50 concentrations were calculated using PRISM 5 and normalized to the respective controls.

### 3.2.5.6 Detection of oxidative stress by DCF-DA fluorescence

For detection of oxidative stress changes, EwS cells were seeded at a density of  $5 \times 10^4$  cells/2 ml per 6-well and either 1) directly treated for 96h with Dox to induce the knockdown, 2) directly treated for 48h with 0.01 mM Nac or 0.1 mM Tiron or 3) treated for 24h with 10 nM Elesclomol. For detection of oxidative stress changes after *TXNIP* knockdown, TC-32 cells were seeded at a density of  $7 \times 10^4$  cells/2 ml per 6-well and reversely transfected with siRNA against *TXNIP*.

After 96h, 2.5  $\mu\text{M}$  2',7'-dichlorodihydrofluorescein diacetate (DCF-DA) was added to the medium containing the cells for 30 min at 37°C. Subsequently, the cells were harvested and re-suspended in PBS and further incubated for 40 min, in the dark to recover. Flow cytometry analysis with Accuri C6 Cytometer was carried out by measuring at least  $1 \times 10^5$  events. This gating strategy is provided in

**Figure 7.**

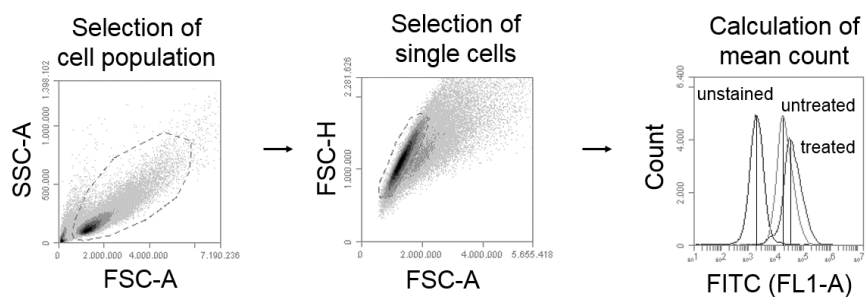


**Figure 7: Gating strategy for oxidative stress analysis with DCF-DA staining.**

### 3.2.5.7 Detection of mitochondrial ROS (mito-ROS) by MitoSOX Red fluorescence

For the detection of specific mitochondrial reactive oxygen species, so-called mito-ROS, cells were incubated after Elesclomol treatment with MitoSOX Red, which can detect mitochondrial superoxide anions. The resulting MitoSOX Red fluorescence signal was normalized to the mitochondrial mass

determined by the MitoTracker Green fluorescent signal (De Biasi et al., 2016; Ikeda et al., 2019). To this end,  $1.5 \times 10^5$  cells/6-well were seeded in an appropriate amount of medium and directly treated for 96h with Dox to induce *SOX6* knockdown or directly treated for 24h with 10 nM Elesclomol, or 24h with 0.1 mM Tiron. The cells were first incubated with 200 nM MitoTracker Green within the 6-well in PBS for 30 min and subsequently simultaneously incubated with 5  $\mu$ M MitoSOX Red for further 15 min. The cells were washed twice with PBS, trypsinized and re-suspended in PBS for flow cytometry analysis with BD Accuri C6 Cytometer thereby measuring at least  $1 \times 10^5$  events. MitoTracker Green was used as mitochondrial mass for internal control. This gating strategy is explained in **Figure 8**.

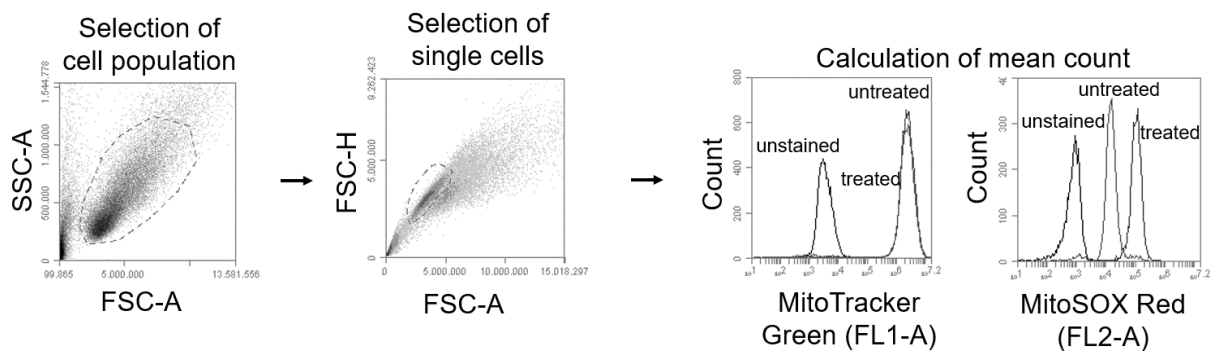


**Figure 8: Gating strategy for mito-ROS by MitoSOX Red and MitoTracker Green staining.**

### 3.2.5.8 Luciferase assay

The enhancer activity of the microsatellite was measured through the cloning of the GGAA-mSat into the pGL3-Promotor vector. The forward transfection was performed with the Lipofectamine LTX with Plus Reagent. To this end,  $3 \times 10^5$  A673/TR/shEF1 cells for each 6-well were seeded out one day before. A673/TR/shEF1 cells were simultaneously and transiently transfected with control plasmid (pRL Renilla) and pGL3\_mSat\_alleleA or pGL3\_mSat\_alleleB respectively or pGL3\_empty (**Table 24**). For verification of the transfection procedure and also for the quantification of the knockdown efficacy of shRNA-mediated *EWSR1-FLI1* knockdown in Dox-inducible A673 EwS cells, those cells were additionally transfected with a pCAG-YFP vector for knockdown efficiency.

	Number of well	Amount
(1)	Amount of DNA*	1 µg
(2)	OptiMEM + 10 ng pRL Renilla	200 µl
(3)	Plus reagent	
(4)	Incubate for 10 min at RT	
(5)	Lipofectamine LTX	2.5 µl
(6)	Incubate for 25 min at RT	
(7)	Add on each well	191 µl
(8)	Medium in well	1.8 ml

**Table 24:** Transient transfection protocol of pGL3-mSat\* or pCAG-YFP\* in A673/TR/shEF1 cells for luciferase assay.

On the second day of seeding 2 µg of pGL3\_empty, pGL3-mSat\_alleleA, pGL3-mSat\_alleleB or pCAG-YFP vector (1) were mixed with OptiMEM containing 10 ng pRL Renilla plasmid (2) per 6-well as a house keeping control. The Plus reagent (3) was gently mixed with diluted DNA and incubated for 10 min at RT (4). The Lipofectamine LTX was added directly to the diluted DNA and incubated further 25 min at RT (6). An appropriate amount (7) of diluted DNA mixture was added to the serum-containing medium of the cells (8). The medium was changed 4h later and replaced by Dox-containing RPMI medium to induce *EWSR1-FLI1* knockdown in A673 cells (**Table 24**). After 48h, transfection efficacy was evaluated by fluorescence microscopy of pCAG-YFP-transfected cells. Subsequently, cell lysates were extracted and measured with Beetle and Renilla juice according to manufacturer's protocol using a Luminometer device. The *EWSR1-FLI1* knockdown efficacy was measured by extracting the RNA out of the YFP-transfected cells and subsequently performing qRT-PCR analysis with *EWSR1-FLI1* primers.

### 3.2.6 Histology

#### 3.2.6.1 Immunohistochemistry of cleaved caspase 3, SOX6, Ki67, 8-OHG and TXNIP

Mice xenografts were cut in 4-µm sections for immunohistochemistry and antigen retrieval was carried out by heat treatment with Target Retrieval Solution Citrate pH6 for **SOX6, cleaved caspase 3, Ki67** or with Epitope Retrieval Solution pH6 for **TXNIP**. Subsequently, the slides were stained with either polyclonal anti-SOX6 antibody raised in rabbit (1:1600) or with monoclonal anti-Ki67 raised in rabbit (1:200) for 60 min at RT, followed by a monoclonal secondary horseradish peroxidase (HRP)-coupled

horse-anti-rabbit antibody of the *ImmPRESS Reagent Kit*. Thereby, AEC-Plus was used as chromogen and slides were counterstained with Hematoxylin Gill's Formula.

For **8-OHG** staining, the slides were pre-treated with proteinase K for 15 min at 37°C. The slides were incubated with the polyclonal cleaved caspase 3 primary rabbit antibody (1:100) or with a polyclonal anti-TXNIP rabbit antibody (1:250) or a monoclonal anti-8-OHG antibody raised in mouse (1:2500) for 60 min at RT followed by a monoclonal secondary horseradish peroxidase (HRP)-coupled horse-anti-rabbit or horse-anti-mouse antibody of the *ImmPRESS Reagent Kit*. Thereby, DAB+ was used as chromogen and Hematoxylin Gill's Formula for counterstaining. All the stainings were performed by Andrea Sendelhofert and Anja Heier.

### **3.2.6.2 Quantification of immunohistological stainings**

An evaluation of the immunoreactivity of SOX6, TXNIP and 8-OHG was carried out in analogy to the scoring of the hormone receptor Immune Reactive Score (IRS) from Remmele and Stegner (Remmele and Stegner, 1987) ranging from 0 – 12 as previously described (Baldauf et al., 2018a). The percentage of positive cells was scored and classified in five grades (grade 0 = 0 – 19%, grade 1 = 20 – 39%, grade 2 = 40 – 59%, grade 3 = 60 – 79% and grade 4 = 80 – 100%). In addition, the intensity of the marker immunoreactivity was determined (grade 0 = none, grade 1 = low, grade 2 = moderate and grade 3 = strong). The final IRS was calculated by multiplying the grade by the intensity.

To evaluate the immunohistological staining of cleaved caspase 3 and Ki67, six high power field (HPF) of 20× magnification pictures were analyzed through an estimation of the stained areas compared to the whole area.

For a quantification of necrosis, the slides were stained with H&E and the necrotic area was compared to normal tissues by four different observers. For mitoses quantification, six HPF areas of H&E-stained slides with 20× magnification were count by three different observers.

The quantifications was carried out by Dr. Fabienne Wehweck, Dr. Thomas Grünewald Ph.D., Maximilian Knott and Jing Li.

### **3.2.6.3 Human samples and ethics approval**

Human tissue samples were retrieved from the archives of the Institute of Pathology of the Ludwig-Maximilians University (LMU) Munich (Germany) following approval by the institutional review board. The current study (approval no. 550-16 UE) was approved by the ethics committee of the LMU Munich.

### **3.2.7 Survival analysis**

To test for association of SOX6 protein expression with EwS patients' survival, a validation-cohort comprising tumor specimens of 161 EwS patients with clinical annotations, treated with first-line therapy, were analyzed. Tumor specimens were immunohistochemically stained for SOX6 (see 3.2.6.1) and staining intensity was quantified according to the immunoreactivity score (IRS). Patients were stratified by different IRS values in those with lower and higher SOX6 expression. Differences in overall survival (OS) between the resulting patients groups was assessed by the Kaplan-Meier method (Log-rank Mantel-Cox test).

### **3.2.8 *In vivo* models**

#### **3.2.8.1 Xenograft subcutaneous murine model**

For long-term *in vivo* analysis of SOX6 functionality,  $3 \times 10^6$  EwS cells harboring a shRNA against *SOX6* were injected with Geltrex Basement Membrane Mix 1:1 in the right flank of 10 to 12 weeks old NOD/Scid/gamma (NSG) mice. Tumor volume was measured and monitored every second day with a caliper and calculated with the standard formula  $(L \times l^2) / 2$ . The mice were separated into two groups at the moment when the tumor reached an average volume of  $80 \text{ mm}^3$ . For the analysis of the tumor growth one group of mice was treated with 2 mg/ml BelaDox dissolved in drinking water containing

5% sucrose to induce an *in vivo* knockdown, whereas the control group of mice only received 5% sucrose. Once the tumors of the control group of mice reached an average volume of 1,500 mm<sup>3</sup>, all the mice of the same experiment were sacrificed by cervical dislocation.

### 3.2.8.2 Intravenous injection of Elesclomol

For the *in vivo* drug assay with Elesclomol,  $3 \times 10^6$  EwS cells were subcutaneously injected with Geltrex basement Membrane Mix in mice as described above. Whenever the tumors reached an average volume of 80 mm<sup>3</sup>, the mice were randomly separated into two groups and subsequently either treated intravenously (i.v.) with 5 mg/kg Elesclomol, or vehicle (DMSO) for 5 days/week, for the subsequent 2.5 weeks.

Once the tumors of the control group of mice (vehicle) reached an average volume of 1,500 mm<sup>3</sup> or the experimental end-point was reached, all the mice were sacrificed by cervical dislocation. Thereby, tumors were extracted and a small sample was snap frozen in liquid nitrogen for RNA extraction. The remaining tumor tissue was fixed in 4%-formalin and paraffin-embedded for further immunohistological analysis.

Animal experiments were approved by local authorities and conducted in accordance with the recommendations of the European Community (86/609/EEC) and UKCCCR (guidelines for the welfare and use of animals in cancer research). The sample size was not predetermined. The above mentioned experiments were performed by Dr. med. vet. Shunya Ohmura.

### 3.2.8.3 Orthotopic bone injection model

As EwS is a bone-related disease, analysis of tumor growth in bone was performed. Orthotopic bone injection models have already been described for EwS (Hauer et al., 2013; Stewart et al., 2014, 2017). For orthotopic mouse experiments, mice were first analgo-anesthetized by intra-peritoneal injection (i.p.) of 0.5 mg/kg Medetomidin, 5 mg/kg Midazolam and 0.05 mg/kg Fentanyl (per body weight). Only

when mice did not show any reflexes, the joint was disinfected with iodide tincture before pre-puncturing the tibia with a 26 Gauge needle. Subsequently, using a 28 Gauge needle,  $2 \times 10^5/20 \mu\text{l}$  of EwS cells harboring a shRNA against *SOX6* were injected intraosseously in the right tibia of 10 to 12 week old NOD/Scid/gamma (NSG) mice. To prevent bleeding at the injection side, a pad was tightly pressed against the puncture. For durable pain prophylaxis, mice were treated with 0.05 mg/kg Buprenorphin i.p. and analgo-anesthetics were antagonized with 1.2 mg/kg Naloxon and 2.5 mg/kg Atipamezol subcutaneously. The mice were tightly monitored until they had fully recovered from anesthesia. The following day, mice were randomized into two groups and either treated with 2 mg/ml BelaDox dissolved in drinking water containing 5% sucrose to induce an *in vivo* knockdown, or only received 5% sucrose for the control group. Osseous tumor growth was monitored every two days. Once the tumor growth provoked an obvious limping in individuals, they were sacrificed by cervical dislocation. These experiments were performed by Florencia Cidre Aranaz, PhD and Dr. med. vet. Shunya Ohmura.

#### **3.2.8.4 Patient-derived xenograft (PDX) model**

For the establishment of xenografts, EwS tumor tissue was surgically removed from EwS patients and small pieces (3 to 4 mm in width) were subcutaneously transplanted into immunodeficient NOD/SCID mice. The gender of the mice was chosen accordingly to the gender of the patient. The PDX tumor diameters were measured every second day with a caliper and the PDX tumor volume were calculated by the formula  $L \times l^2/2$ . When the PDXs had reached an average volume of  $1.5 \text{ cm}^3$  (defined end-point), the mice were sacrificed by cervical dislocation. Thereby, the PDX tumors were extracted, fixed in 4%-formalin and subsequently paraffin-embedded for immunohistology as described above (**see 3.2.6.1**).

All animal experiments were conducted in collaboration with Experimental Pharmacology and Oncology GmbH, Berlin Buch in accordance with the UKCCR for the welfare and use of animals in cancer research, German Animal Protection Law and had been approved by local authorities (LaGeSo, Berlin, Germany).

### 3.2.9 Bioinformatic data analyses

#### 3.2.9.1 Analysis of published DNase sequencing (DNase-Seq) and chromatin immuno-precipitation

##### DNA sequencing (ChIP-Seq) data

ENCODE SK-N-MC DNase-Seq (GSM736570) and ChIP-Seq data (GSE61944) were downloaded from the Gene Expression Omnibus (GEO) and processed as previously described (Grünewald et al., 2015). The following samples were loaded into the UCSC genome browser:

ENCODE\_SKNMC\_hg19\_DNaseHS\_rep1

GSM1517546\_SKNMC.shGFP96.FLI1

GSM1517555\_SKNMC.shFLI196.FLI1

GSM1517547\_SKNMC.shGFP96.H3K27ac

GSM1517556\_SKNMC.shFLI196.H3K27ac

GSM1517569\_A673.shGFP48.FLI1

GSM1517572\_A673.shFLI148.FLI1

GSM1517570\_A673.shGFP48.H3K27ac

GSM1517573\_A673.shFLI148.H3K27ac

#### 3.2.9.2 Analysis of *SOX6* expression levels in human embryoid bodies

Publicly available gene expression microarray data of ectopically expressed *EWSR1-FLI1* in human embryoid bodies (generated on the Affymetrix HG-U133Plus2.0 array (GSE64686) (Gordon et al., 2016)), were normalized by Robust Multiarray Average (RMA) (Irizarry et al., 2003) using custom brainarray chip description files (CDF; ENTREZG, v19) yielding one optimized probe-set per gene (Dai et al., 2005).

### 3.2.9.3 Analysis of copy-number-variation and promoter methylation in primary EwS

For the analysis of possible copy-number-variations (CNV), publicly available DNA copy number data for EwS tumors (Tirode et al., 2014) with corresponding RNA expression data (GSE34620 and GSE37371,  $n = 32$ ), were downloaded from the 'soft tissue cancer – Ewing sarcoma – FR' project from the International Cancer Genome Consortium (ICGC) Data Portal and from GEO of the NCBI, respectively. For the analysis of the *SOX6* locus, segment mean values were extracted from these data using Visual Basic for Applications (VBA). The log<sub>2</sub>-transformed expression of the *SOX6* gene was correlated with the aforementioned and generated segment mean.

For the analysis of CpG methylation, publicly available data on CpG methylation in 40 EwS tumors (GSE88826) (Sheffield et al., 2017) and the corresponding RNA expression data (GSE34620) were downloaded from GEO. For the analysis of the *SOX6* locus, the ratio of methylated versus unmethylated reads was calculated for two CpG sites (CpG1 hg19: chr11:15994482; CpG2 hg19: chr11:15994519) in each sample ( $n = 40$ ) using VBA, covering at least four reads. The bioinformatic analyses were performed by Dr. med. Martin Orth.

### 3.2.9.4 Transcriptome and splicing analyses

Microarray analyses were performed in order to assess the impact of *SOX6* on gene expression and alternative splicing in EwS. Herefore,  $1.2 \times 10^4$  cells were seeded in 6-well plates and treated with Dox (refreshing Dox every 48h) for 96h. Total RNA was extracted with the ReliaPrep miRNA Cell and Tissue Miniprep System and the transcriptome analysis was profiled at IMGM laboratories. The RNA quality was measured with a Bioanalyzer and samples with RNA integrity numbers (RIN) > 9 were hybridized to Human Affymetrix Clariom D microarrays. The generated data were quantile normalized with Transcriptome Analysis Console (V4.0) using the SST-RMA algorithm as previously described (Machiela et al., 2018). The annotation of the data, on gene and exon level, was performed using the Affymetrix library for Clariom D Array (version 2, human). Differentially expressed genes (DEGs) with consistent and significant fold changes (FCs) across shRNAs and cell lines were identified as follows:

First, data were log<sub>2</sub> transformed and subsequently minimally expressed genes were excluded. This step was crucial to avoid false discovery artifacts due to minimally expressed genes. Therefore, the expression of *ERG* (mean log<sub>2</sub> expression signal of 6.05) was declared as minimal cut-off as this gene is not expressed in *EWSR1-FLI1* positive EwS cell lines (Crompton et al., 2014). Accordingly, only genes with mean log<sub>2</sub> expression signal of at least 7 were considered for further analysis. The FCs of the shControl samples (Dox -/+ ) and both specific shRNAs (Dox -/+ ) were calculated for each cell line separately. In order to clean the FC from the shControl, the FCs observed in the respective shControl samples were subtracted from those seen in both shSOX6 samples and resulted in the final FCs for each specific shRNAs in each cell line. These final FCs for both specific shRNAs were averaged across cell lines to obtain the final mean-FC per gene across shRNAs and cell lines. As the FC for SOX6 was -1.486, only those genes that had a minimum absolute log<sub>2</sub> FC of 1 were considered strongly regulated and thus, DEGs.

Additionally, the false discovery rate (FDR) was estimated for each gene using the R package 'qvalue' from Bioconductor (Storey et al., 2019). To identify enriched gene sets, a GSEA was carried out with all genes that comply with the minimum expression criteria of log<sub>2</sub> FC of 1. In this regard, the genes were ranked by their expression FC between the groups Dox (-/+), and a pre-ranked GSEA (MSigDB v5.2, c2.cpg.all) with 1,000 permutations was performed (Subramanian et al., 2005).

To assess the potential role of SOX6 on alternative splicing, probe selection region (PSR) expression on Affymetrix microarray was analyzed more closely. In case the RNA was not alternatively spliced, the ratio of each probe selection region (PSR) expression with and without *SOX6* knockdown remains unaltered irrespective of up- or downregulation of the *SOX6* gene. The additional FC between the expression value of each PSR before and after SOX6 knockdown to the expected FC, was calculated by expression regulation assessed on the gene level. Out of 539,385 PSRs with 47,851 matched genes in this analysis, 22,155 PSRs (10,754 genes) showed a consistently positive or negative additional log<sub>2</sub> transformed expression FC of  $\geq 0.3$ . For 20,050 PSRs, thus 10,179 genes, the expression differences were significant ( $P < 0.05$ ) when corrected for the FC on gene level.

However, after Bonferroni correction for multiple testing none of the PSRs remained significant. The generated gene expression data were deposited at the GEO (accession code GSE120576). The normalization of the data was done by Julia S. Gerke and the bioinformatical data analysis was performed by Dr. med. Martin Orth.

### 3.2.9.5 Gene expression and drug response correlation

Publicly available EwS cell line gene expression microarray data and matched drug-response values were obtained from the EBI (E-MTAB-3610) and from [www.cancerrxgene.org](http://www.cancerrxgene.org) (Iorio et al., 2016) in order to identify drugs whose efficacy correlates with *SOX6* expression in EwS cells. All CEL-files generated on Affymetrix Human Genome U219 arrays were simultaneously normalized using RMA (Irizarry et al., 2003) and a custom brainarray chip description file (v20, ENTREZG) yielding one optimized probe set for each gene (Dai et al., 2005). The Pearson correlation coefficient ( $r_{\text{Pearson}}$ ) for all tested drugs in EwS cell lines and its significance between *SOX6* expression and the IC50 values were calculated.

### 3.2.10 Statistical analysis

Statistical data analysis was performed using PRISM 5 (GraphPad Software Inc.) on the raw data. Comparison of two groups in functional *in vitro* experiments was carried out using a two-sided Mann-Whitney test if not otherwise specified. Data are displayed as dot plots with horizontal bars representing means and whiskers representing the standard error of the mean (SEM). Sample size for all *in vitro* experiments were chosen empirically.

## 4. Results

EwS predominantly occurs in bone or soft tissues and displays a highly proliferative, undifferentiated and embryonal phenotype. The transcription factor *SOX6* is mainly involved in the cell cycle regulation during endochondral ossification, where it regulates chondrocyte proliferation. As EwS cells seems to arise from osteo-/chondrogenic progenitors, a closer insight into the expression of the bone-associated transcription factor *SOX6* in EwS appeared promising.

### 4.1 *SOX6* is highly expressed in EwS compared to other sarcomas

In order to validate the hypothesis-driven assumption of *SOX6* being part of the typical undifferentiated but highly proliferative phenotype of EwS, an expression pattern of *SOX6*, from a previously established DNA microarray set (> 750) (Baldauf et al., 2018a, 2018b) comprising 18 representative normal tissues types and 10 cancer entities, was analyzed. Indeed, comparative analyses revealed a *SOX6* overexpression in EwS in contrast to other cancers and normal tissue (**Figure 9A, B**). The depicted mRNA expression levels (**Figure 9A**) were also validated at the protein level (**Figure 9B**) in the same comprehensive tissue microarray (Baldauf et al., 2018a, 2018b). Both analyses showed that *SOX6* is highly expressed in EwS tumors, but with inter-tumor heterogeneity (**Figure 9 A, B, C**).

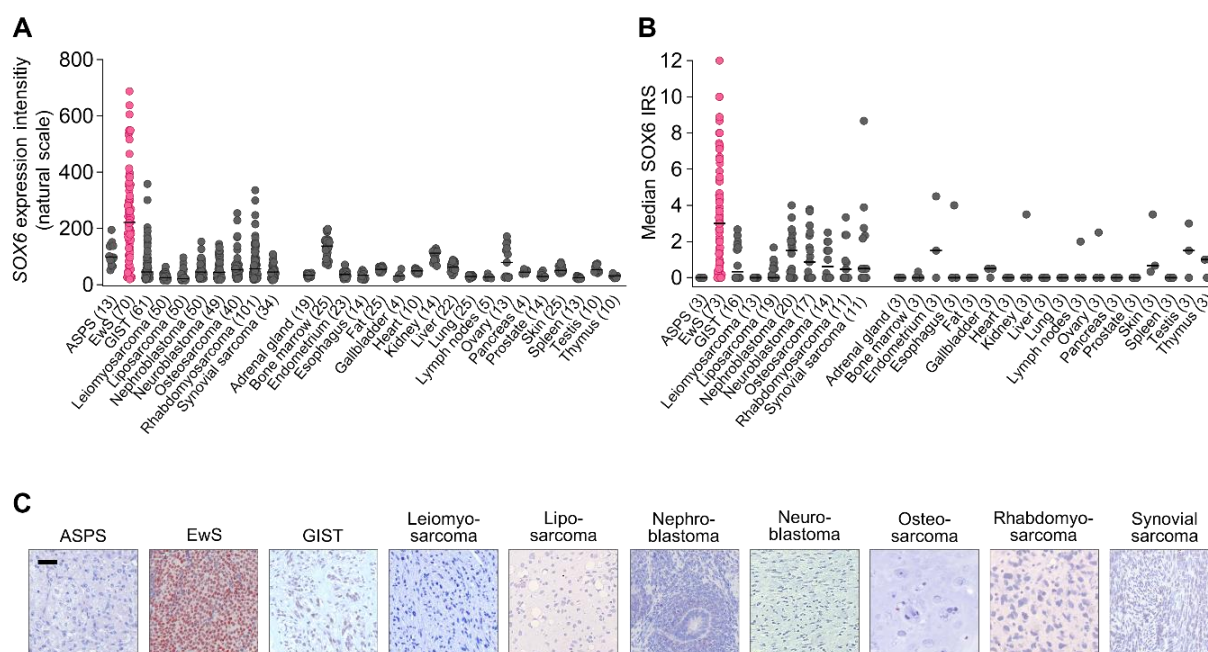


**Figure 9: SOX6 is highly but variably expressed in EwS**

**A)** Analysis of *SOX6* expression at the mRNA level in EwS tumors, sarcomas/pediatric tumors compared to normal tissue types. The number of samples is indicated in parentheses. Data represent medians. **B)** Validation of *SOX6* expression at the protein level by IHC in EwS tumors and other sarcomas/pediatric tumors compared to normal tissue types. Data represent median IRS. The number of samples is given in parentheses. **C)** Representative pictures of *SOX6* staining by IHC of EwS tumors, sarcomas and normal tissues from **(B)**. Scale bar = 20  $\mu$ m. **ASPS** = alveolar soft part sarcoma; **GIST** = gastrointestinal stromal tumor.

The higher, yet heterogeneous mRNA expression of *SOX6* was also observed in 27 EwS cell lines compared to cell lines of three other pediatric cancer types including osteosarcoma (U2OS and SAOS-2), neuroblastoma (TGW and SK-N-AS) and rhabdomyosarcoma (Rh36 and Rh4) (**Figure 10**). Based on this *SOX6* expression pattern TC-32, RDES and POE cell lines were selected to perform *in vitro* and *in vivo* experiments in this thesis.

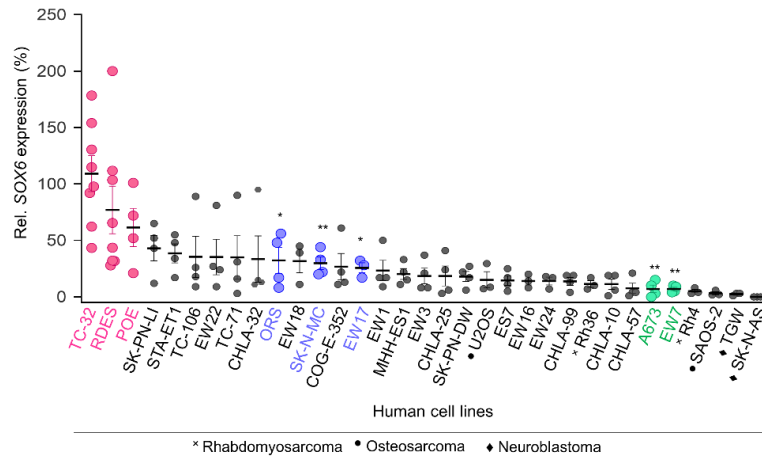


### Figure 10: SOX6 is heterogeneously expressed in EwS cell lines

Analysis of relative SOX6 mRNA levels of different EwS, rhabdomyosarcoma, neuroblastoma and osteosarcoma cell lines to that of TC-32 by qRT-PCR. Pink color: highest SOX6 expression (TC-32, RDES and POE), blue color: intermediate SOX6 expression (ORS, EW17 and SK-N-MC), green color: low SOX6 expression (A673, EW7). Means and SEM,  $n \geq 3$ . \*\* $P < 0.01$ , \* $P < 0.05$ .

## 4.2 SOX6 does not correlate with EwS patient survival

To investigate if SOX6 expression correlates with patients' overall survival (OS) in EwS, a validation cohort comprising 161 EwS tumor specimens, for which matched clinical data were available, was performed.

Stratifying SOX6 protein by different cut-offs such as no (IRS = 0), intermediate (IRS = 1 – 4) or high (IRS  $\geq$  4) SOX6 expression revealed that survival is independent of SOX6 ( $P$  value = 0.667) (**Figure 11**).

$P$  values were corrected for multiple testing by Bonferroni correction.

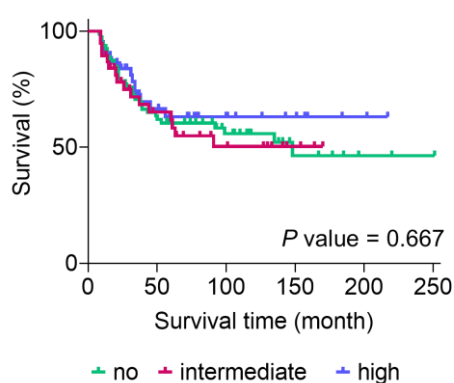


**Figure 11: Kaplan-Maier curves comprising 161 primary tumors of EwS patients.**

Depicted are data of primary tumors of EwS patients categorized in no SOX6 expression (green), intermediate SOX6 expression (pink) and high SOX6 expression (blue);  $P$  value = 0.669. High SOX6 expression is referred to IRS  $\geq$  4.

### 4.3 Functional analysis of *SOX6* *in vitro* and *in vivo*

In the following part of this thesis, the functional role of *SOX6* *in vitro* and *in vivo* regarding proliferation and tumorigenesis was investigated more closely. As described in the methods part, EwS cell lines harboring a Dox-inducible shRNA against *SOX6* were generated for long-term analysis.

#### 4.3.1 *SOX6* is induced by *EWSR1-FLI1* via an intronic enhancer-like GGAA-mSat

As *SOX6* was previously shown to be highly expressed in EwS compared to other sarcomas and cancers (**Figure 1**), the assumption that can be made is that *SOX6* might be regulated by the fusion protein EWSR1-FLI1.

To further investigate the interaction between *SOX6* and EWSR1-FLI1, the EwS cell lines A673 and SK-N-MC were transduced with a Dox-inducible shRNA against the fusion *EWSR1-FLI1*. The fusion oncogene knockdown reduced *SOX6* expression in a time-dependent manner *in vitro* (**Figure 12A**) and *in vivo* (**Figure 12B**). The analysis of gene expression microarray data of human embryoid bodies upon ectopical expression of the *EWSR1-FLI1* fusion oncogene revealed a strong *SOX6* induction (**Figure 12C**).

Publicly available DNase-Seq data from SK-N-MC EwS cell lines, as well as ChIP-Seq data of EWSR1-FLI1 from A673 and SK-N-MC EwS cell lines were investigated in order to understand the underlying regulatory mechanism between *SOX6* and EWSR1-FLI1. Indeed, a prominent EWSR1-FLI1 ChIP-Seq peak mapped to a GGAA-mSat within intron 1 of the *SOX6* gene that was reduced upon *EWSR1-FLI1* knockdown. Interestingly, this EWSR1-FLI1 peak overlapped with a DNase I hypersensitivity site, indicating open chromatin, and showed *EWSR1-FLI1*-dependent acetylation of H3K27, standing for active enhancers (**Figure 12D**).

To confirm the EWSR1-FLI1-dependent enhancer activity of this GGAA-mSat, a luciferase reporter assay was carried out. To this end, A673/TR/shEF1 cells were transfected with the pGL3 reporter

plasmid that contained a 1-kb fragment of the afore-mentioned *SOX6*-associated GGAA-mSat from the human reference genome (**Figure 12E**).

The author of this thesis hypothesized that the observed variability in *SOX6* expression might be caused by differences in repeat numbers at the *SOX6*-associated GGAA-mSat. This hypothesis is supported by prior studies that already showed that the enhancer activity at *EWSR1-FLI1*-bound GGAA-mSats positively correlates with the number of consecutive GGAA-repeats (Gangwal et al., 2008; Grünewald et al., 2015).

To test this, paternal and maternal alleles for this GGAA-mSat (referred to as allele A and B) from eight EwS cell lines with largely different *SOX6* expression levels (**Figure 10**) were analyzed and the amount of their consecutive GGAA-repeats were determined by Sanger Sequencing. The corresponding enhancer activity was measured in a luciferase reporter assay by cloning both alleles, separately into a reporter vector. A positive correlation ( $P = 0.016$ ) of the average *SOX6* expression levels with the average enhancer activity across cell lines was observed. This correlation was in line with the increasing average amount of consecutive GGAA-repeats of both alleles (**Figure 12F, see list 8.2**). Furthermore, all parental cell lines were subjected to whole-genome sequencing, which revealed that the cloned flanking regions adjacent to the *SOX6*-associated GGAA-mSat were entirely identical in all cell lines, thus excluding genetic variations and additional regulatory factors nearby the microsatellite.

Of note, the observed heterogeneous *SOX6* expression levels did neither correlate with alteration in the *SOX6* promoter methylation (**Figure 12G**) nor with CNV (**Figure 12H**) at the *SOX6* locus in primary EwS tumors.

Collectively, these results indicate a possible interaction between *EWSR1-FLI1* and *SOX6* in EwS. *SOX6* expression appeared to be induced by the fusion protein binding to an intronic GGAA-mSat of *SOX6* that has been shown to exhibit length-dependent enhancer activity in EwS. The *SOX6* regulation appears to be independent of the flanking regions nearby the GGAA-mSat.

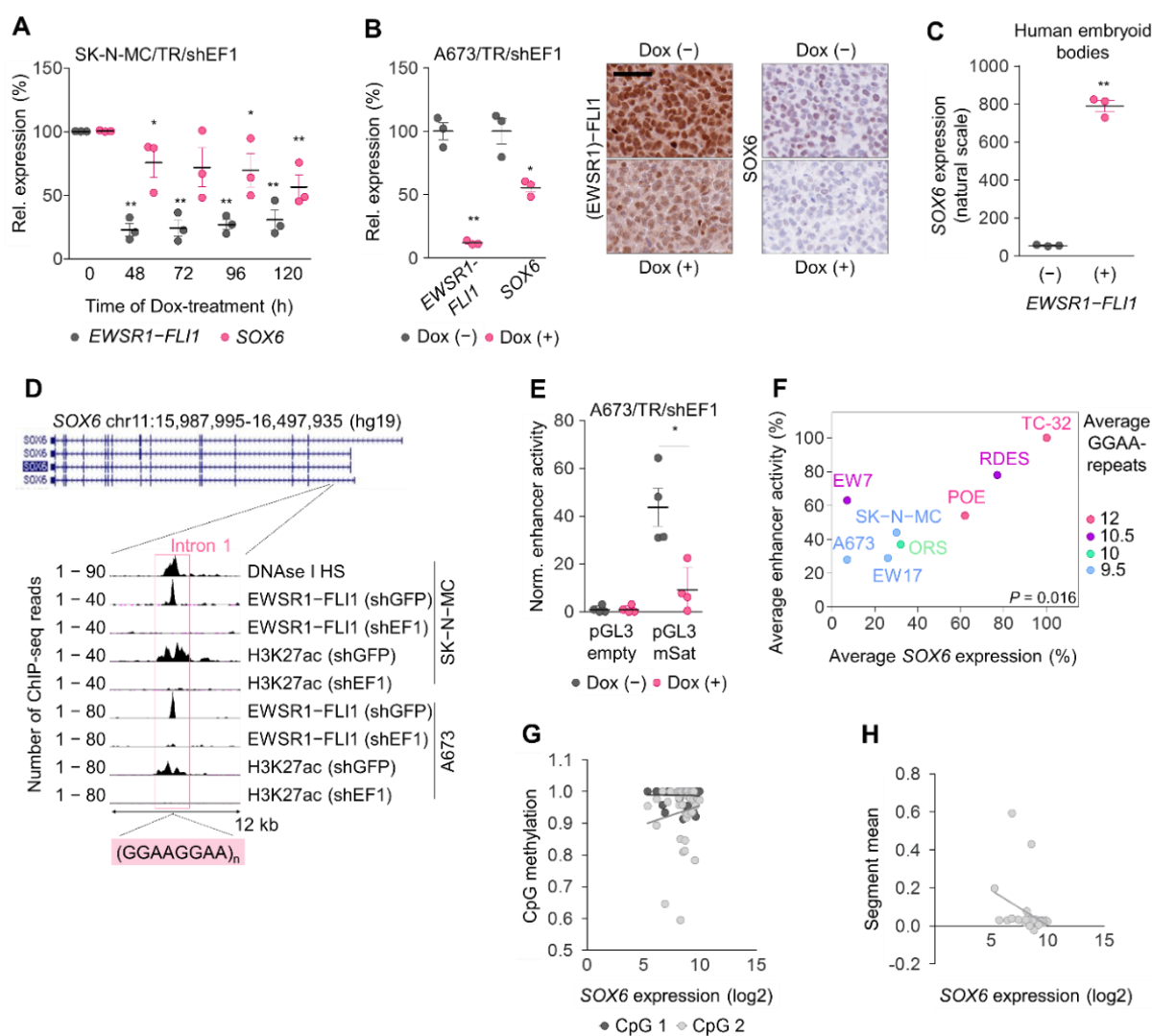


**Figure 12: EWSR1-FLI1 induces SOX6 expression via an intronic enhancer-like GGAA-mSat.**

**A**) Analysis of *EWSR1-FLI1* and *SOX6* expression by qRT-PCR in SK-N-MC/TR/shEF1 cells at different time points after Dox-inducible knockdown. Means and SEM,  $n = 3$ . **B**) **Left:** Analysis of *EWSR1-FLI1* and *SOX6* mRNA expression by microarrays in xenografts from A673/TR/shEF1 cells 96h after Dox-inducible knockdown. Means and SEM,  $n = 3$ . *P* values were determined via independent one-sample *t*-test. **Right:** Representative IHC-stainings of the same xenografted cells in mice, for (EWSR1)-FLI1 and SOX6. Scale bar = 20  $\mu$ m. **C**) Analysis of *SOX6* expression by microarrays in human embryoid bodies after ectopic *EWSR1-FLI1* expression. Means and SEM,  $n = 3$ . *P* values were determined via unpaired two-sided *t*-test with Welch's correction. **D**) Genomic overview of the *SOX6* gene and its isoforms displaying tracks for DNase I hypersensitivity (HS) and ChIP-Seq data for *EWSR1-FLI1* and H3K27ac in A673 and SK-N-MC EwS cells transduced with a shRNA against *EWSR1-FLI1* (shEF1) or control shRNA (shGFP). **E**) Analysis of the relative enhancer activity of the *SOX6*-associated GGAA-mSat (from human reference genome) by luciferase reporter assays in A673/TR/shEF1 cells with and without *EWSR1-FLI1* knockdown. Means and SEM,  $n = 4$ . **F**) Correlation of the average enhancer activity of both alleles of the *SOX6*-associated GGAA-mSat and the average *SOX6* mRNA expression levels of the eight EwS cell lines. TC-32 cell lines was set as reference. **G**) Correlation analysis of the *SOX6* promoter with the CpG-methylation sites (CpG1 and CpG2) and the corresponding *SOX6* expression levels (log<sub>2</sub>) in primary EwS tumors,  $n = 40$ . Lines represents linear regression of the data. **H**) Correlation analysis of CNVs (represented by the segment mean) at the *SOX6* locus with the corresponding *SOX6* expression levels (log<sub>2</sub>) in primary EwS,  $n = 32$ . Lines represents linear regression of the data. \*\*\**P* < 0.001, \*\**P* < 0.01, \**P* < 0.05.

#### 4.3.2 SOX6 contributes to proliferation, cell-cycle progression and anchorage-independent colony-formation *in vitro*

To investigate the function of SOX6 in EwS, three cell lines (POE, RDES and TC-32) with two different Dox-inducible shRNAs against *SOX6* (shSOX6\_2 and shSOX6\_3) and a corresponding control with a Dox-inducible non-targeting control shRNA (shCtrl) were generated. The addition of Dox (0.1 µg/ml) to the culture medium of transduced cells for 96h significantly silenced *SOX6* expression at the mRNA and protein level (**Figure 13A**).

Depending on the cellular context, SOX6 can act as a splicing and/or transcription factor (Ohe et al., 2002, 2009). In order to get insight into the role of the versatile transcription factor SOX6 in EwS, *SOX6*-silenced RDES and TC-32 EwS cell lines were examined by using Affymetrix Clariom D array that enables the simultaneous transcriptome-wide analysis of splicing events and differential gene expression. The knockdown of *SOX6* for 96h revealed a small effect on splicing events as shown in **list 8.3**, whereas *SOX6* as a transcription factor had a strong effect on differential gene expression (**Figure 13B**). Indeed, **list 8.4** revealed that *SOX6*-silencing induced a corresponding up- or downregulation (absolute FC > 1; including minimal expression level of 7) of 54 and 499 genes respectively across both shRNAs and cell lines.

The **Figure 13C** shows the result of a Gene Set Enrichment Analysis (GSEA) with differentially expressed genes (DEGs) of *SOX6*-silenced EwS cells (including all minimally expressed genes > 7), showing a strong depletion of proliferation-related gene signatures (**see list 8.5**).

In order to validate the predicted role of SOX6 by GSEA in EwS cell lines, proliferation and knockdown experiments were performed using pooled short interfering RNAs (sipool) against *SOX6* in five EwS cell lines (A673, EW7, POE, RDES and TC-32). The usage of sipools induced a 60–80% *SOX6* knockdown compared to a non-targeting control sipool (sipCtrl) after 96h (**Figure 13D**). A sipool consists of 30 different siRNAs and eliminates off-target effects (Hannus et al., 2014). In these knockdown experiments, cell viability was significantly reduced in all three *SOX6*-high expressing EwS cell lines (POE, RDES and TC-32) that were counted (including the supernatant) with a hemocytometer (**Figure**

**13D).** Interestingly, sipool-mediated *SOX6*-silencing in *SOX6* low-expressing cell lines A673 and EW7 could indeed significantly reduce *SOX6* expression but the knockdown did not show an effect on the cell proliferation (**Figure 13D**). In accordance, long-term analysis of *SOX6* knockdown in Dox-inducible TC-32 and RDES EwS cell lines revealed a significantly reduced 2D clonogenic and 3D sphere formation capacity compared to their corresponding controls (shCtrl or Dox(-)), whereas the *SOX6*-low expressing A673 cell line did not reduce 3D sphere formation capacity (**Figure 13E, F**).

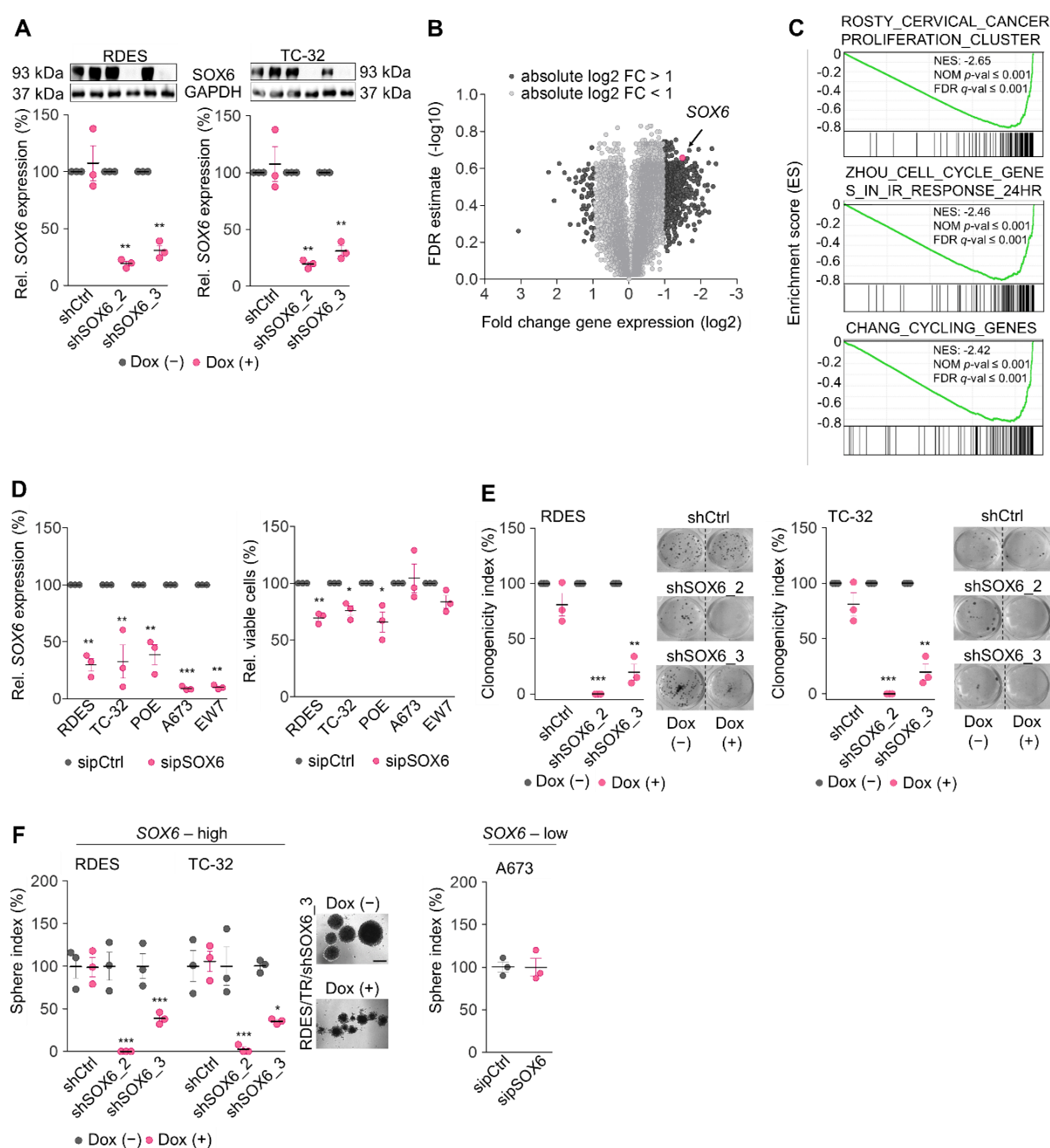


**Figure 13: *SOX6* promotes proliferation and anchorage-independent growth *in vitro* in EwS cells.**  
**A) Top:** Western blot analysis 96h after Dox-induced *SOX6* knockdown in RDES and TC-32 EwS cells. GAPDH was used as loading control. **Bottom:** Analysis of relative *SOX6* expression by qRT-PCR in RDES

and TC-32 EwS cell lines harboring a shRNA against *SOX6* or a non-targeting control shRNA (shCtrl) 96h after Dox-induced knockdown. Means and SEM,  $n = 3$ . **B)** Volcano plot of microarray data showing DEGs that are up- or downregulated after Dox-induced *SOX6* knockdown compared to a non-targeting shCtrl,  $n =$  two EwS cell lines. **C)** Representative enrichment plots from GSEA of DEGs from RDES and TC-32 EwS cells 96h after Dox-induced *SOX6* knockdown. NES: normalized enrichment score, NOM: nominal  $P$  value; FDR: false discovery rate. **D)** Analysis of relative *SOX6* expression in A673, EW7, POE, RDES and TC-32 cells 96h after transfection with a sipool against *SOX6* or a control sipool. Mean and SEM,  $n = 3$ . **Right:** Analysis of cell viability of the same cells depicted in **(D)**. Means and SEM,  $n = 3$ .  $P$  values were determined via an independent one-sample  $t$ -test. **E)** Quantification of the clonogenicity index after 12 days of dox-induced *SOX6* knockdown in RDES and TC-32 cells. Means and SEM,  $n = 3$ . Representative pictures of colony forming assays in a 12-well plate. **F)** Quantification of the sphere index after 12 days of shRNA-mediated (RDES and TC-32) or sipool-mediated (A673) *SOX6* knockdown. Means and SEM,  $n = 3$ . Representative pictures of spheres from RDES cells with a shRNA against *SOX6* (RDES/TR/shSOX6\_3). Scale bar = 1 mm. \*\*\* $P < 0.001$ , \*\* $P < 0.01$ , \* $P < 0.05$ .

As a reduction of cell viability was observed, flow cytometric assays with propidium iodide (PI) were carried out to test whether this effect was mediated via an alteration of the cell cycle or not. In this regard, serum-starved and thus  $G_0$ -synchronized cells showed a significant delay in cell cycle progression 20h after growth stimulation by re-addition of serum in *SOX6*-silenced cells. Interestingly, this delayed cell cycle transition was not accompanied by an increase in apoptotic death (**Figure 14A, B**).

As previously mentioned, *SOX6* knockdown had a strong effect on the transcriptome. A GSEA of those DEGs from the microarray data pointed to an important role of *SOX6* in proliferation of EwS cells (**see list 8.5**). Among the proliferation-associated genes (**Figure 13C**), three genes, *CDCA3*, *DEPDC1* and *E2F8*, appeared as plausible candidate genes to promote the observed pro-proliferative phenotype of *SOX6*. Indeed, in a validation assay with RDES and TC-32 cells upon sipool-mediated *SOX6* silencing, the mRNA levels of these pro-proliferative genes were downregulated (**Figure 14C**). These proliferation-associated genes were previously shown to be involved in cell cycle progression mostly during  $G_1 - S$  phase transition, an involvement that has also been observed in *SOX6*-mediated knockdown cells (Ayad et al., 2003; Christensen et al., 2005; Feng et al., 2017; Mi et al., 2015). In accordance, the knockdown of each pro-proliferative gene with a specific sipools against *CDCA3*, *E2F8*

or *DEPDC1* in RDES and TC-32 EwS cells phenocopied at least in part the observed anti-proliferative effect of *SOX6* knockdown (**Figure 14D**).

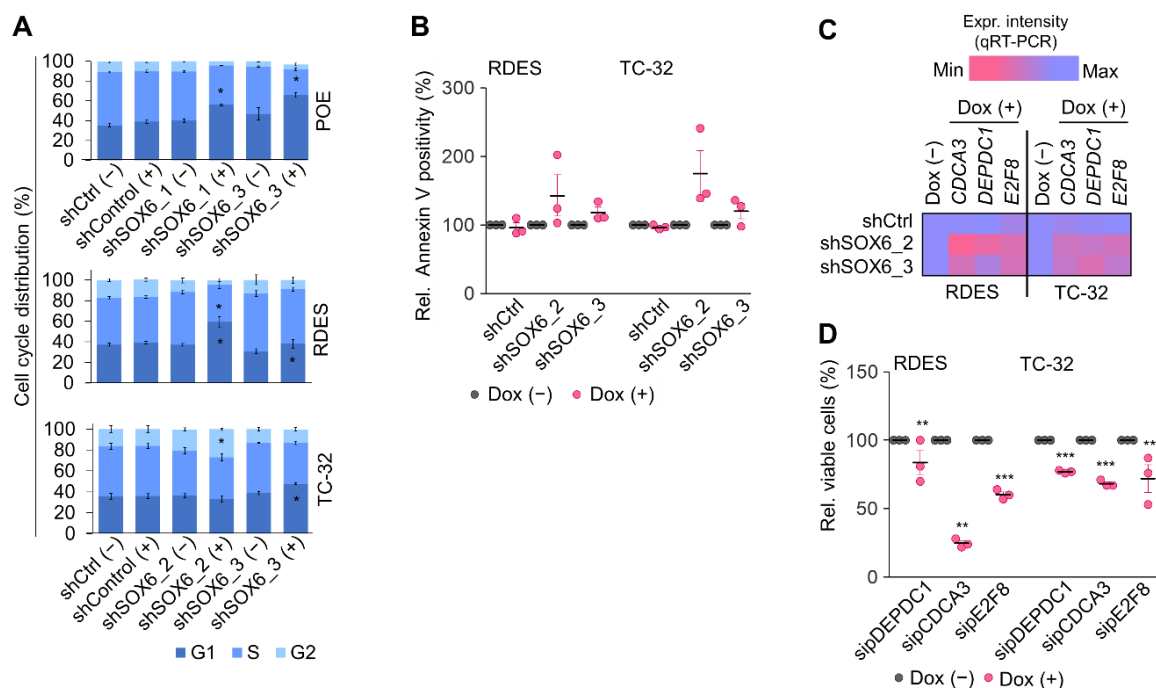


**Figure 14: SOX6 promotes cell cycle progression.**

**A)** Quantification of flow cytometric analysis with PI of the cell cycle distribution in POE, RDES and TC-32 EwS cells after dox-induced *SOX6* knockdown. Means and SEM,  $n \geq 3$ . **B)** Quantification of the relative Annexin V positivity of RDES and TC-32 cells 96h after *SOX6*-silencing. Means and SEM,  $n = 3$ . **C)** Heat-map showing relative expression levels of *CDCA3*, *DEPDC1* and *E2F8* in RDES and TC-32 cells 96h after *SOX6* withdrawal,  $n = 3$ . **D)** Analysis of cell viability of RDES and TC-32 cells after sipool-mediated knockdown of either *CDCA3*, *DEPDC1* or *E2F8* for 96h. Means and SEM,  $n = 3$ .  $P$  values were determined via an independent one-sample  $t$ -test. \*\*\* $P < 0.001$ , \*\* $P < 0.01$ , \* $P < 0.05$ .

Collectively, these results suggest an important contribution of *SOX6* to cell cycle-related genes, cell-cycle progression and proliferation as well as to clonogenic and anchorage-independent growth of EwS *in vitro*.

### 4.3.3 Knockdown of *SOX6* inhibits tumorigenicity *in vivo*

To assess the contribution of *SOX6* to tumor growth of EwS cells *in vivo*, xenograft experiments were performed. Thereby, RDES and TC-32 cell lines, each harboring two Dox-inducible shRNAs against *SOX6* and one shCtrl were subcutaneously injected into the flanks of NSG mice. Mice that were injected with EwS cell lines expressing a non-targeting control shRNA (shCtrl) showed no effect of Dox-treatment. Contrarily, mice that harbored a shRNA-mediated *SOX6* knockdown revealed a strong tumor growth reduction in both shRNA constructs and both cell lines compared to the control mice (**Figure 15A**). The knockdown of *SOX6* in these xenograft tumors was confirmed *ex vivo* by qRT-PCR and by immunohistochemistry (IHC) (**Figure 15B**). Immunohistological analysis of these xenografted tumors showed that *SOX6*-silencing was associated with a significant reduction of cell proliferation that was indicated by numbers of mitotic cells per high-power field (HPF) (**Figure 15C**) and Ki67 staining (**Figure 15D**). In contrast, *SOX6*-mediated knockdown in xenografted tumors revealed no significant differences in cleaved caspase 3 staining compared to the corresponding controls (**Figure 15E**), suggesting that the observed reduction of tumor growth was not caused by apoptotic cell death but rather by a cell cycle delay.

To further corroborate the observed subcutaneous effect of *SOX6* in xenograft models, a representative orthotopic tibial bone injection in NSG mice with TC-32 EwS cell lines harboring a shRNA (shSOX6\_2) against *SOX6*, was performed. After intraosseous tibial bone injection, mice were directly treated with or without Dox to induce *SOX6* knockdown.

In analogy to the previously described subcutaneous model, Dox-treatment translated to a reduction of tumor growth and significantly improved mouse survival ( $P \leq 0.0001$ ) in an orthotopic bone model of EwS in mice (**Figure 15F**).

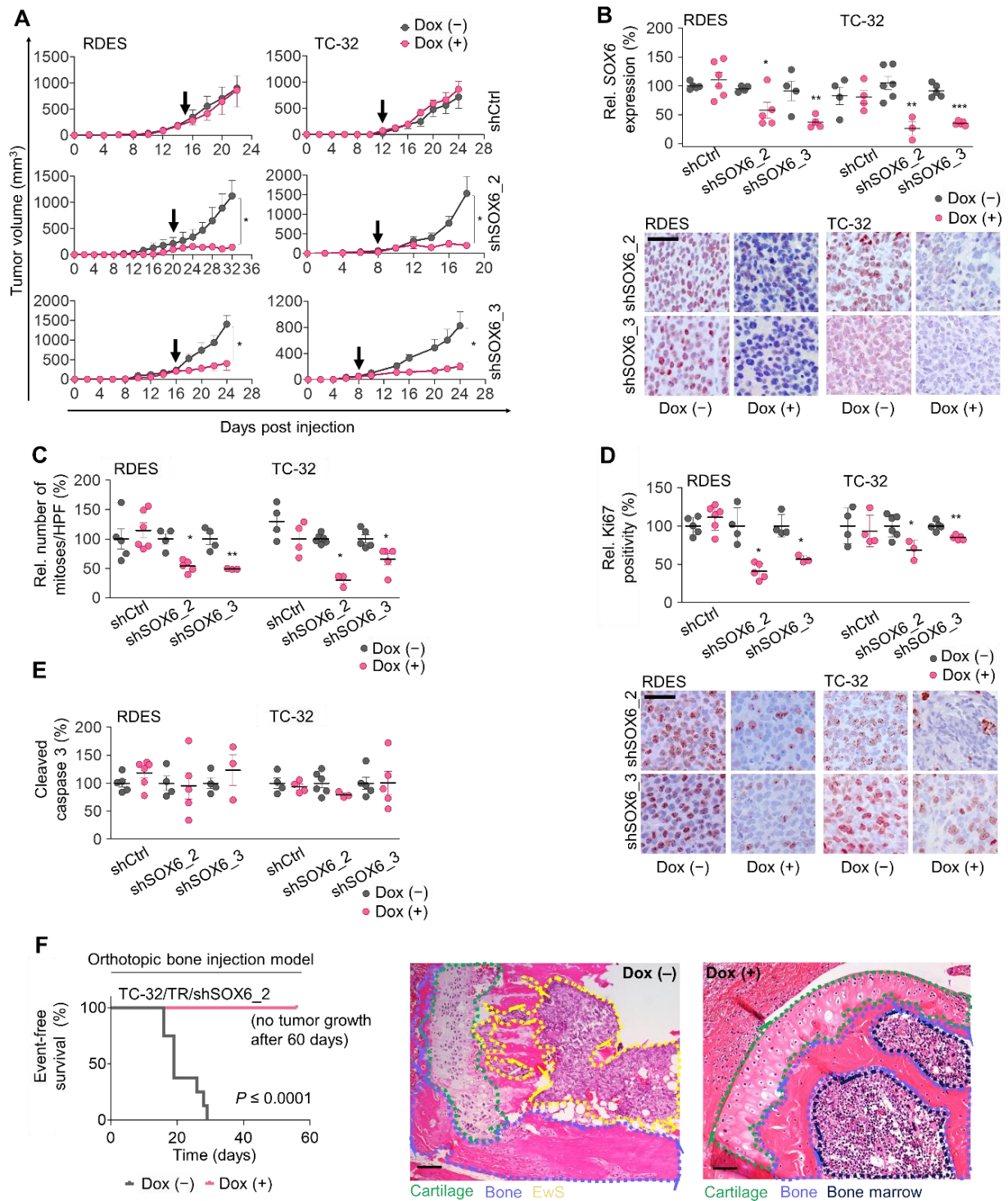


**Figure 15: SOX6 contributes to tumor growth *in vivo*.**

**A)** Analysis of tumor growth of xenografted RDES and TC-32 EwS cells harboring a shRNA against *SOX6* (shSOX6\_2/shSOX6\_3) or a non-targeting control shRNA (shCtrl). Arrow: start of Dox-treatment. Means and SEM,  $n \geq 3$  mice per condition. **B) Top:** Relative *SOX6* expression measured *ex vivo* by qRT-PCR from RDES and TC-32 EwS cells shown in **(A)**. Means and SEM,  $n \geq 3$  mice per condition. **Bottom:** Representative pictures of xenografts stained for *SOX6*; scale bar = 20  $\mu$ m. **C)** Quantification of the relative number of mitoses per high-power field (HPF) of xenografts shown in **(A)**. Means and SEM,  $n \geq 3$ . **D) Top:** Quantification of the relative Ki67 positive cells of xenografts shown in **(A)**. Means and SEM,  $n \geq 3$ . **Bottom:** Representative pictures of xenografts stained for Ki67; scale bar = 20  $\mu$ m **E) Top:** Quantification of cleaved caspase 3 cells of xenografts shown in **(A)**. Mean and SEM,  $n \geq 3$ . **Bottom:**

Representative pictures of xenografts stained for cleaved caspase 3; scale bar = 20  $\mu\text{m}$ . **F)** Kaplan-Meier analysis of event-free survival of mice orthotopically xenografted with TC-32/TR/shSOX6\_2 cells with/without Dox-inducible SOX6 silencing.  $n = 8$  animals per group.  $P$  values were determined via Mantel-Haenszel test. Representative pictures of tibial orthotopic injection with/without Dox. Scale bar = 1000  $\mu\text{m}$ . \*\*\*\* $P < 0.0001$ , \*\*\* $P < 0.001$ , \*\* $P < 0.01$ , \* $P < 0.05$ .

Taken together, these results depict a contribution of SOX6 to tumor growth in xenografted mice with EwS cell lines.

#### 4.3.4 Correlation of tumor growth in PDX of EwS patients with SOX6 expression

To further validate the tumorigenicity of SOX6 expression in EwS, eight patient-derived xenografts (PDX) were subcutaneously grown in the mice, which included high, intermediate and low SOX6 expression. The analysis of the PDX staining revealed that high SOX6 expression (validated by IHC), was associated with high positive Ki67 staining resulting in a positive correlation between SOX6 expression and Ki67 staining ( $r_{\text{pearson}} = 0.856$ ;  $P \leq 0.007$ ). Furthermore, a negative correlation was observed between the tumor growth and the corresponding SOX6 expression ( $r_{\text{pearson}} = -0.752$ ,  $P = 0.013$ ) (**Figure 16**).

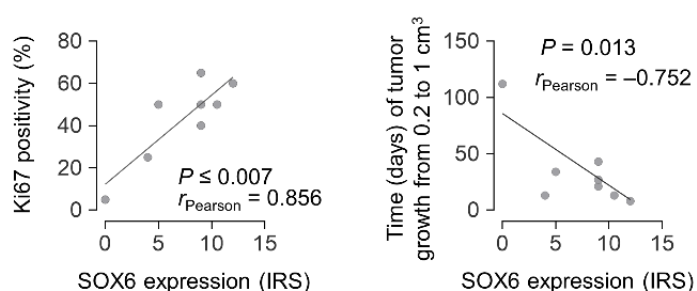


**Figure 16: Correlation of tumor growth in patient-derived EwS xenografts (PDX) with SOX6 expression.**

Correlation of the tumor growth or Ki67 positive staining with SOX6 expression in PDX tumors,  $n = 8$ . Lines indicate linear regression of the data.

#### 4.4 Therapeutic aspect of SOX6

Next to its role in the development of the CNS, the developmental transcription factor *SOX6* is known to be mostly expressed during endochondral ossification in adolescents. This fact makes *SOX6* a suitable biomarker, as the direct targeting of a developmental factor with inhibitors would cause severe side effects in the bone formation and nervous system of growing children (Smits et al., 2001). The author aimed to explore whether high *SOX6* levels in EwS may constitute a specific vulnerability of EwS that may be exploited therapeutically.

##### 4.4.1 *SOX6* expression confers sensitivity toward small-molecule Elesclomol

A published gene expression dataset with matched drug-response data comprising 22 EwS cell lines (Iorio et al., 2016) and 250 drugs was interrogated. The Pearson correlation coefficient and the statistical significance of the corresponding IC50 values were calculated for all tested drugs with the observed *SOX6* expression levels across all 22 EwS cell lines (**Figure 17A**). Subsequently, the results were filtered for the significance of the median IC50 values ( $P$  value  $\leq 0.05$ ) and afterwards sorted by their Pearson correlation coefficient (**see list 8.6**).

Among the top 7 drugs with the highest Pearson correlation coefficient, the small-molecule Elesclomol (N-malonyl-bis (N-methyl-N-thiobenzoyl hydrazide) ( $r_{\text{Pearson}} = -0.565$ ;  $P = 0.014$ ) was the only drug inhibiting EwS cell line growth at a nanomolar range (IC50  $\sim 25$  nM) (**Figure 17B**). Elesclomol is known to be a potent oxidative stress inducer leading cells to apoptosis if levels of oxidative stress rise beyond a tolerable threshold (Kirshner et al., 2008). In order to verify these observations a validation drug-response assay with Elesclomol was carried out in EwS cell lines with high *SOX6* levels (TC-32 and RDES) as well as in an osteosarcoma cell line (SAOS-2) and a non-transformed human primary mesenchymal stem-cell cell line (MSC-52), both exhibiting low *SOX6* expression levels. In agreement to the above-stated assumptions, *SOX6*-low expressing cell lines were more resistant, while EwS cell lines were more sensitive toward Elesclomol treatment (**Figure 17C, D**).

As previously reported, *SOX6* knockdown contributes to proliferation and cell cycle progression in EwS cell lines. This might raise the question whether the reduced sensitivity toward Elesclomol in *SOX6*-low expressing cell lines might result from the reduced proliferation rate upon *SOX6* knockdown. The analysis of the proliferation rate via Resazurin assay of the involved cell lines revealed that the higher sensitivity of EwS cells toward Elesclomol appeared to be independent of proliferation since the osteosarcoma cell line SAOS-2 proliferated even more than the tested EwS cells in Resazurin assays (**Figure 17E**).

Interestingly, the imitation of a *SOX6*-low expressing EwS cell line was mediated through the knockdown of *SOX6* in the Dox-inducible RDES and TC-32 EwS cell lines. This experiment revealed that *SOX6* withdrawal diminished the sensitivity toward Elesclomol pointing to a functional role of *SOX6* in Elesclomol sensitivity (**Figure 17F**).

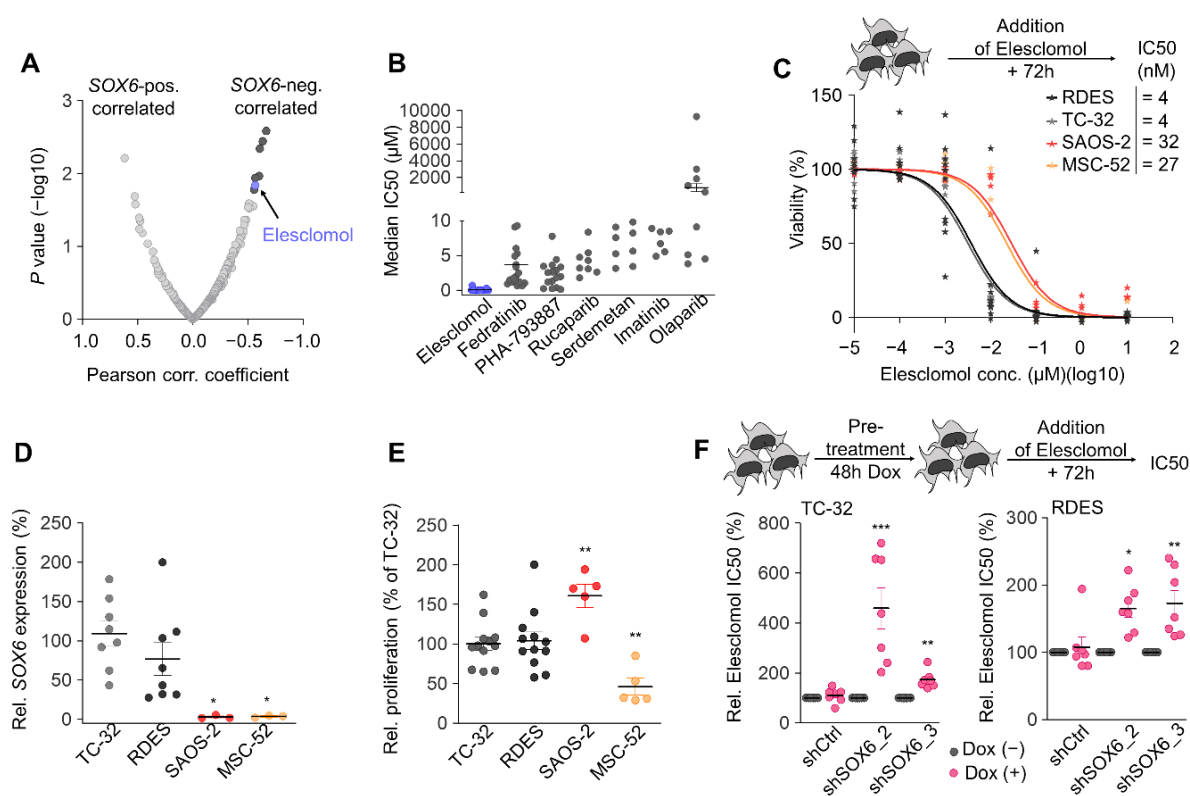


**Figure 17: *SOX6* confers to Elesclomol sensitivity.**

**A)** Analysis of publicly available matched gene expression and drug-response data (Iorio et al., 2016) of up to 22 EwS cell lines per drug. Dark grey: top 7 drugs with  $P < 0.02$ ; pink: Elesclomol. **B)** Median IC50 values (µM) of the top 7 drugs with  $P < 0.02$ . Means and SEM,  $n \geq 18$  EwS cell lines. **C)** Resazurin assays of different cell lines after treatment with Elesclomol at indicated concentrations for 72h. Black and grey: *SOX6*-high (RDES and TC-32), dark and light red: *SOX6*-low (SAOS-2, MSC-52),  $n \geq 3$ . **D)**

Analysis of relative *SOX6* expression in TC-32, RDES, SAOS-2 and MSC-52 cell lines by qRT-PCR. Means and SEM,  $n \geq 3$ . **E**) Quantification of relative proliferation rate by a Resazurin assay. Means and SEM,  $n \geq 5$ . **F**) Resazurin assay in TC-32 and RDES cell lines with Elesclomol. Pre-treatment with Dox for 48h and subsequent addition of Dox and Elesclomol for 72h. Means and SEM,  $n = 7$ . \*\*\* $P < 0.001$ , \*\* $P < 0.01$ , \* $P < 0.05$ .

In sum, these results demonstrate that *SOX6* confers a proliferation-independent sensitivity toward Elesclomol in EwS cell lines.

#### 4.4.2 Elesclomol induces apoptosis *in vitro* and necrosis *in vivo*

Prior reports showed that Elesclomol inhibits cancer cell growth in breast, melanoma and leukemia cell lines (Alli and Ford, 2012; Nagai et al., 2012; Qu et al., 2010; Yadav et al., 2013). It is known that Elesclomol elevates oxidative stress-levels beyond a certain threshold, thus triggering the cells into apoptosis (Kirshner et al., 2008). In fact, Elesclomol treatment *in vitro* induced apoptosis in EwS cell lines when treated with the corresponding IC50 concentrations (**Figure 18A**), without affecting *SOX6* expression levels (**Figure 18B**).

Furthermore, the effect of Elesclomol *in vivo* in NGS mice was further investigated. Accordingly, TC-32 EwS xenografts were administrated intravenously with Elesclomol for 9 days with 5 mg/kg Elesclomol or with vehicle (DMSO). The analysis of the tumor volume resulted in reduced local tumor growth of these xenografts compared to the DMSO-treated control (**Figure 18C**). The subsequent immunohistological analysis of the extracted tumors showed an increased apoptosis rate evidenced by positive cells for cleaved caspase 3 (**Figure 18D**) and necrotic tumor area (**Figure 18E**) compared to the control tumors treated with DMSO. Noticeably, Elesclomol treatment did not affect mice well-being as they did not show any differences in weight-loss (**Figure 18F**). Elesclomol administration also did not exert histo-morphological changes in the inner organs (data not shown).

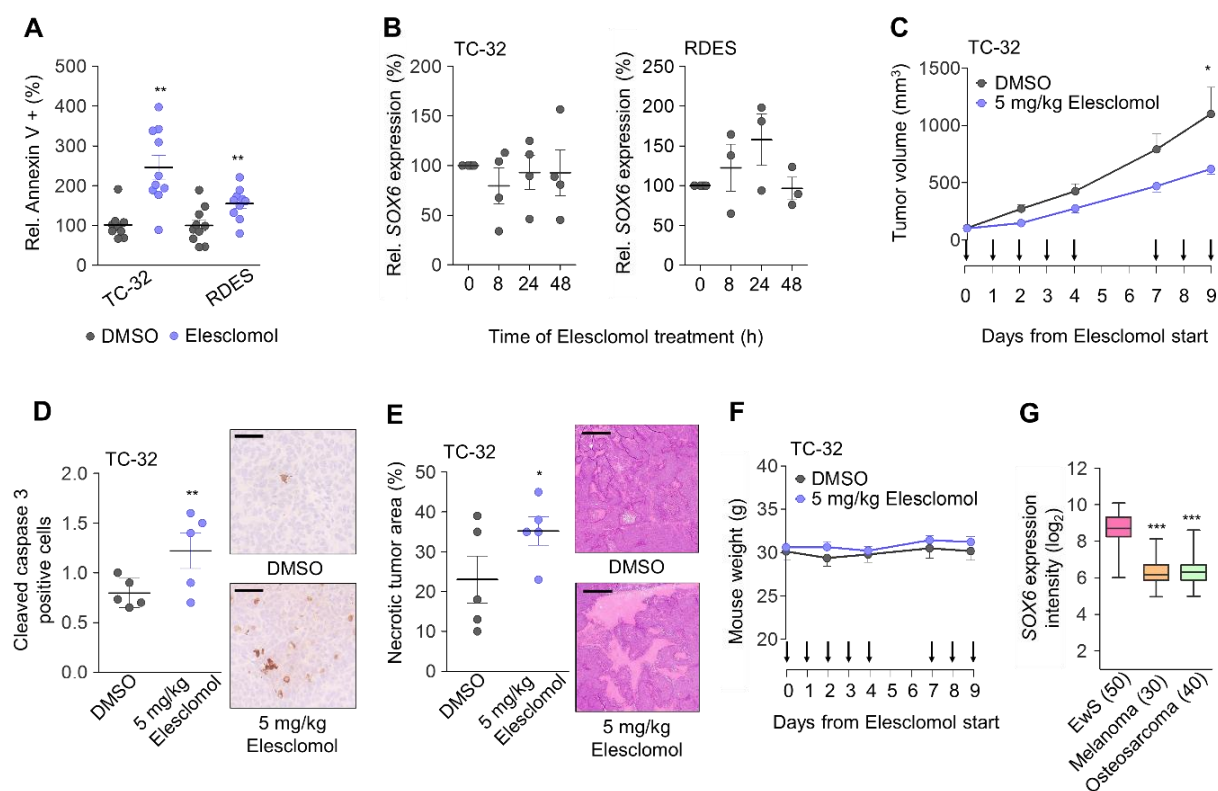


**Figure 18: Elesclomol induces apoptosis *in vitro* and *in vivo*.**

**A**) Quantification of relative Annexin V positivity of TC-32 and RDES cell lines 48h after Elesclomol treatment (10 nM). Mean and SEM,  $n = 10$ .  $P$  values were determined via unpaired two-sided  $t$ -test with Welch's correction. **B**) Quantification of relative SOX6 expression levels in RDES and TC-32 cells at different time points after start of Elesclomol treatment (10 nM). Means and SEM,  $n \geq 3$ . **C**) Tumor volumes of TC-32 EwS xenografts in mice treated once per day (day 0 – 4 and day 7 – 9) with Elesclomol intravenously (5 mg/kg). Means and SEM,  $n = 5$  mice per condition. **D**) **Left:** Quantification of cleaved caspase 3 positive cells/ 3 HPF in TC-32 xenografts shown in **(C)** by IHC staining. Means and SEM,  $n = 5$  per condition. **Right:** Representative pictures; scale bar = 100  $\mu\text{m}$ . **E**) **Left:** Quantification of necrotic area in TC-32 xenografts shown in **(C)** by H&E staining. Means and SEM,  $n = 5$  per condition. **Right:** Representative pictures; scale bar = 900  $\mu\text{m}$ . **F**) Mouse weight over the time during intravenous Elesclomol administration (5 mg/kg). Means and SEM,  $n = 5$ . **G**) Analysis of SOX6 expression intensities (log<sub>2</sub>) of primary EwS tumors, melanomas and osteosarcomas (Baldauf et al., 2018b). \*\*\* $P < 0.001$ , \*\* $P < 0.01$ , \* $P < 0.05$ .

In summary, these results demonstrate that Elesclomol contributes to tumor growth reduction in mice xenografted with EwS cell lines.

#### 4.4.3 *SOX6* expression is associated with oxidative stress levels in EwS

It has been previously reported by Kirshner and colleagues that Elesclomol is able to induce oxidative stress (Kirshner et al., 2008). This is due to the ability of Elesclomol to bind and transfer serum Cu(II) into mitochondria, where it accumulates and subsequently undergoes a redox reaction. During this process, copper is reduced from Cu(II) to Cu(I) thereby releasing free radicals by a Fenton reaction (Nagai et al., 2012; Yadav et al., 2013). The precise mechanism of how copper-ligated Elesclomol is leading to oxidative stress within the human cell still needs to be elucidated but it has been reported in *yeast S. cerevisiae*, that Elesclomol interacts with the electron transfer chain leading to mitochondrial apoptosis (Blackman et al., 2012). In this regard, it has been investigated whether Elesclomol treatment could modulate oxidative stress levels in EwS cell lines in the cytosol by DCF-DA and in mitochondria by MitoSOX Red fluorescence measurement. A further question was to investigate why EwS cells are sensitive to Elesclomol.

With this objective, EwS cell lines RDES and TC-32 were treated with Elesclomol (10 nM) to investigate changes in the oxidative stress levels, both in the cytosol and mitochondria, showing a significant induction of oxidative stress level in both EwS cell lines compared to control (DMSO) when quantified by DCF-DA and MitoSOX Red fluorescence measurement, respectively (**Figure 19A, B**). In line with this finding, a strong increase of the immunoreactivity for 8-hydroxyguanosine (8-OHG), which is a marker for the rate of oxidative damage to nucleic acids (Curtis et al., 2010; Kasai, 1997) were observed in xenografts of mice treated with 5 mg/kg Elesclomol compared to the corresponding DMSO treated controls (**Figure 19C**).

Since the production of Elesclomol has been discontinued, another known oxidative stress-inducing agent called Menadione was used to further explore if the elevated oxidative stress is capable of inducing apoptosis in EwS cells. Indeed, drug-response assays reduced sensitivity toward Menadione upon *SOX6* knockdown in RDES and TC-32 EwS cells compared to the control (**Figure 19D**).

To further confirm that elevated oxidative stress levels are responsible for killing EwS cells, two experiments with two antioxidants namely N-acetylcysteine (Nac) (Ezeriņa et al., 2018; Zafarullah et

al., 2003) and Tiron (Krishna et al., 1992) were carried out. Firstly, cytosolic oxidative stress levels were measured by DCF-DA fluorescence and revealed a decrease of oxidative stress levels upon treatment with the antioxidants Nac and Tiron (**Figure 19E**). Secondly, drug-response assays of Elesclomol with pre-treatment of antioxidants significantly increased IC50 values (**Figure 19F**).

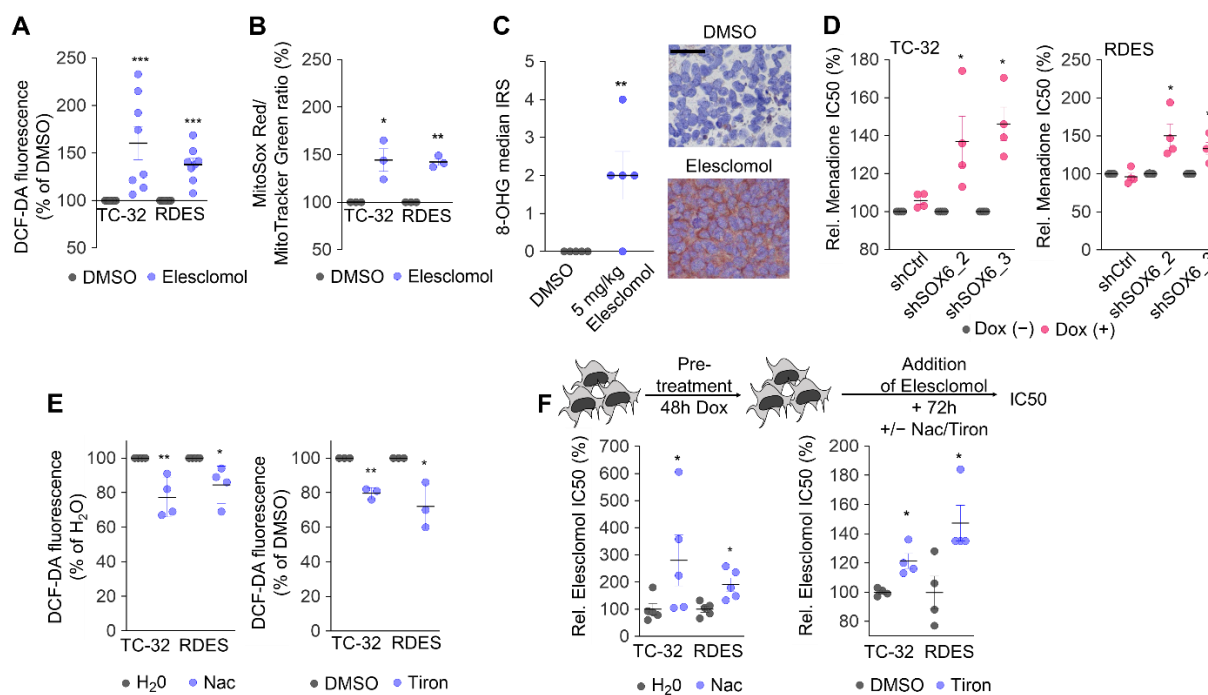


**Figure 19: Elesclomol confers oxidative stress *in vitro* and *in vivo* in EwS.**

**A)** Quantification of relative DCF-DA fluorescence in TC-32 and RDES cells after Elesclomol treatment (10 nM) compared to DMSO control. Means and SEM,  $n = 8$ .  $P$  values were determined via an independent one sample  $t$ -test. **B)** Quantification of MitoSOX Red/MitoTracker Green ratio in TC-32 and RDES cells after Elesclomol treatment (10 nM) compared to DMSO control. Means and SEM,  $n = 3$ .  $P$  values were determined via an independent one sample  $t$ -test. **C) Left:** IRS of 8-OHG staining are presented as dot plots. Horizontal bars represent means.  $P$  values determined via two-sided Mann Whitney test. **Right:** Representative picture of 8-OHG staining. Scale bar = 10  $\mu\text{m}$ . **D)** Quantification of relative Elesclomol IC50 values by a Resazurin assay in TC-32 and RDES cell lines after 48h of Dox treatment and subsequent addition of Menadione treatment and concomitant SOX6 knockdown for 72h. **E)** Quantification of relative DCF-DA fluorescence in TC-32 and RDES cells upon Nac (0.01 mM) or Tiron (0.1 mM) treatment compared to control. Means and SEM,  $n \geq 3$ .  $P$  values determined via independent one sample  $t$ -test. **F) Top:** Schematic illustration of the experiment procedure. **Bottom:** Quantification of relative IC50 concentrations in TC-32 and RDES cells by a Resazurin assays after pre-treatment with either the antioxidant Nac or Tiron compared to DMSO control. Horizontal bars indicate means and whiskers SEM,  $n \geq 4$ . \*\*\* $P < 0.001$ , \*\* $P < 0.01$ , \* $P < 0.05$ .

These results were in line with the assumption that Elesclomol exert its pro-apoptotic effect in EwS cells partly by induction of oxidative stress beyond a tolerable threshold.

In order to evaluate if *SOX6* expression is linked to oxidative stress levels, RDES and TC-32 EwS cell lines were treated with Dox to ensure *SOX6* knockdown and subsequently oxidative stress level changes were measured by flow cytometric analysis. The resulting DCF-DA and MitoSOX Red fluorescence was reduced upon *SOX6* knockdown in both EwS cell lines compared to the corresponding control (**Figure 20A, B**). To test whether oxidative stress-dependent sensitivity toward Elesclomol is conferred by *SOX6* expression, rescue experiments with a potent oxidative stress-inducer such as  $H_2O_2$  were performed. Therefore,  $H_2O_2$  was added to *SOX6*-silenced EwS cells in a drug-response assay with Elesclomol to rescue the *SOX6*-mediated resistance toward Elesclomol. Indeed, *SOX6*-silenced EwS cells, treated with  $H_2O_2$ , could fully restore the sensitivity of these cell lines toward Elesclomol compared to *SOX6*-silenced cells alone (**Figure 20C**). The  $H_2O_2$  treatment itself did not have any effect on the cell viability of EwS cells (**Figure 20D**).

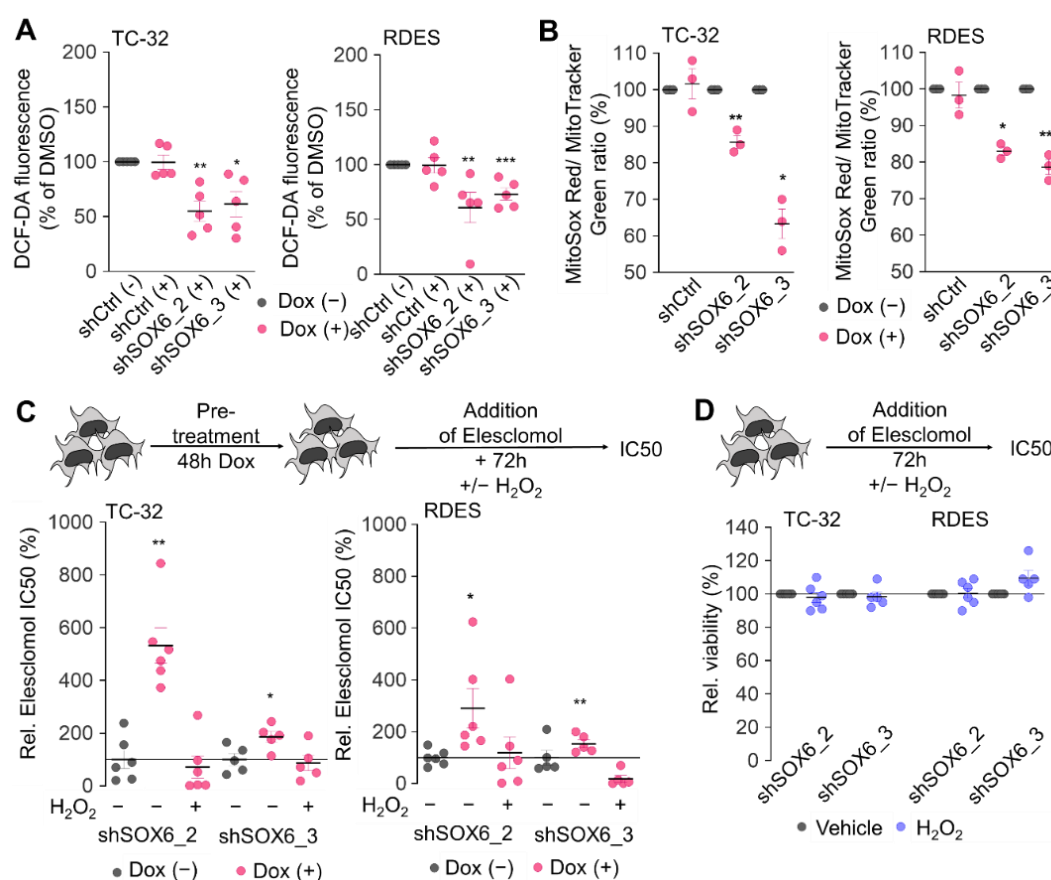


**Figure 20: Elesclomol induces *SOX6*-mediated oxidative stress-levels in EwS cells.**

**A)** Quantification of relative DCF-DA fluorescence in TC-32 and RDES cells after Dox-induced *SOX6* knockdown. Means and SEM,  $n = 5$ .  $P$  values were determined via a one-sample  $t$ -test. **B)** Quantification

---

of MitoSOX Red/MitoTracker Green ratio in TC-32 and RDES cells after dox-induced *SOX6* knockdown compared to the shCtrl. Means and SEM,  $n = 3$ .  $P$  values were determined via an independent one sample  $t$ -test. **C) Top:** Schematic illustration of the experimental procedure. **Bottom:** Resazurin assays of TC-32 and RDES cell lines after Dox-induced *SOX6* knockdown with Elesclomol and with  $H_2O_2$  (30 mM) treatment for 72h. Means and SEM,  $n \geq 5$ . **D) Top:** Schematic illustration of experimental procedure. **Bottom:** Analysis of cell viability of indicated cell lines treated with either vehicle ( $H_2O$ ) or  $H_2O_2$  (30 mM) by a Resazurin assay. Means and SEM,  $n \geq 5$ . \*\*\* $P < 0.001$ , \*\* $P < 0.01$ , \* $P < 0.05$ .

The above-stated results suggest that *SOX6* modulates oxidative stress-dependent sensitivity toward Elesclomol.

#### 4.4.4 SOX6 regulates Elesclomol sensitivity via TXNIP

So far, data obtained from previous experiments suggest that *SOX6* is involved in oxidative stress metabolism. This led to further analysis of the generated microarray data obtained from EwS cells with/without *SOX6* knockdown (see list 8.4). The microarray data did not show any evidence for a systematic enrichment or depletion of oxidative stress-associated pathways in the GSEA (see list 8.5). Among the DEGs after *SOX6*-silencing, thioredoxin interacting protein (*TXNIP*) was identified (see list 8.4) as the second most downregulated gene. *TXNIP* is involved in the thioredoxin antioxidant system, where it inhibits the antioxidative function of the redox-protein thioredoxin resulting in an accumulation of oxidative stress within the cell (Collet and Messens, 2010).

To validate the results of the microarray data, *SOX6* was silenced in EwS cells for 96h in multiple independent experiments. It could be shown that *TXNIP* levels were indeed reduced at mRNA and protein level after this duration (Figure 21A).

To corroborate the potential link between *SOX6* and *TXNIP* another microarray data set that was generated on the same microarray platform, with 18 EwS cell lines with/without *EWSR1-FLI1* knockdown was analyzed (in-house generated data, not published). This dataset revealed a significant positive correlation ( $r_{\text{Pearson}} = 0.559$ ,  $P = 0.016$ ) of *SOX6* and *TXNIP* mRNA expression (Figure 21B). Furthermore, *TXNIP* was downregulated in xenografted tumors with/without *SOX6* knockdown at protein level *in vivo* (Figure 21C), an observation that strengthens the possible link between *SOX6* and *TXNIP*.

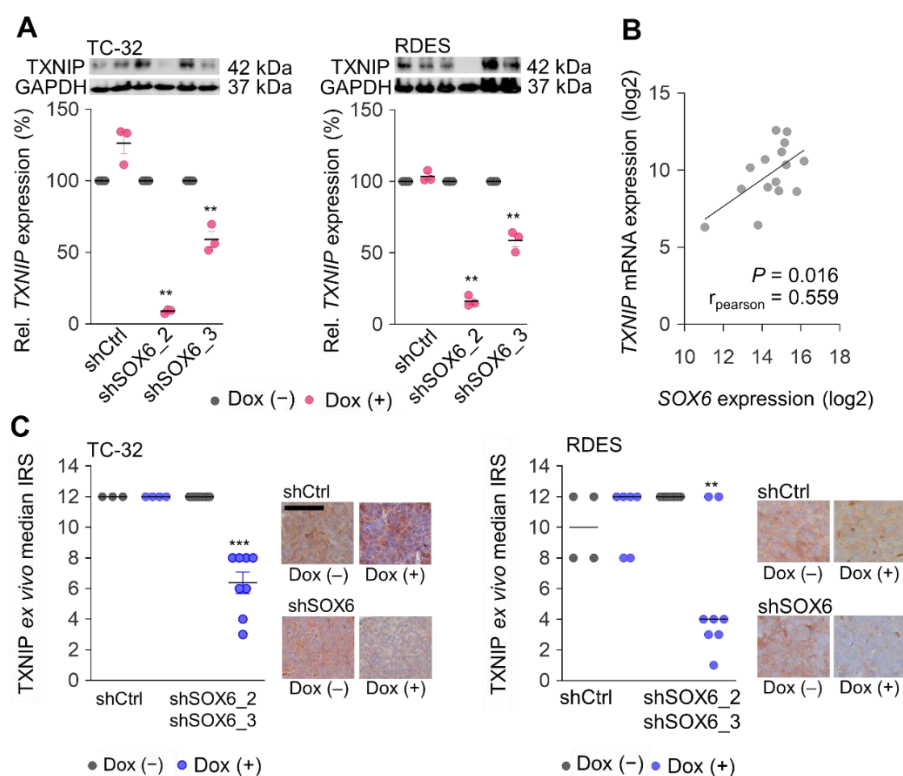


**Figure 21: SOX6 mediates TXNIP expression.**

**A) Top:** Representative Western blots of TXNIP expression 96h after induction of SOX6 knockdown in TC-32 and RDES cells. GAPDH was used as loading control. **Bottom:** Quantification of relative TXNIP mRNA expression by qRT-PCR. Means and SEM,  $n = 3$ . **B)** Correlation of TXNIP and SOX6 mRNA expression from 18 EwS cells performed on an Affymetrix Clariom D array. Lines indicate linear regression. **C)** Quantification of the IRS for TXNIP in EwS xenografts with/without SOX6 knockdown in TC-32 and RDES cell lines. Data are represented as median IRS,  $n \geq 4$ .  $P$  values were determined by two-sided unpaired student's  $t$ -test. Representative micrographs are depicted, scale bar = 20  $\mu\text{m}$ . \*\*\* $P < 0.001$ , \*\* $P < 0.01$ , \* $P < 0.05$ .

As TXNIP is involved in the antioxidant system, its possible function as oxidative stress-regulator was further explored. In order to evaluate if TXNIP is indeed modulating oxidative stress levels in EwS cell lines, flow cytometric analysis with DCF-DA and MitoSOX Red fluorescence labeling in TC-32 cell lines were performed. Indeed, the knockdown of TXNIP in TC-32 cells (**Figure 22A**) reduced cytoplasmic (**Figure 22B**) and mitochondrial oxidative stress levels (**Figure 22C**).

To further validate if TXNIP plays an important role in oxidative stress-mediated sensitivity toward Elesclomol, EwS cells were transiently transfected with a siRNA against TXNIP and a drug-response

assay was carried out. The knockdown of *TXNIP* reduced the sensitivity of EwS cells toward Elesclomol (**Figure 22D**).

For rescue experiments, Dox-inducible *SOX6* knockdown EwS cell lines were additionally transduced with a cumate-inducible overexpression system that contains a full-length cDNA of *TXNIP*. Dox addition induced 80% knockdown of *SOX6* in TC-32 EwS cells and a subsequent reduction of *TXNIP* onto 10%. The cumate-inducible re-expression of *TXNIP* in *SOX6*-silenced cells could restore the physiological concentration of *TXNIP* at the mRNA level (**Figure 22E**). Drug-response assays with Elesclomol revealed that the inducible re-expression of *TXNIP* in *SOX6*-silenced EwS cells was sufficient to restore ~ 66% of the sensitivity toward Elesclomol (**Figure 22F**).

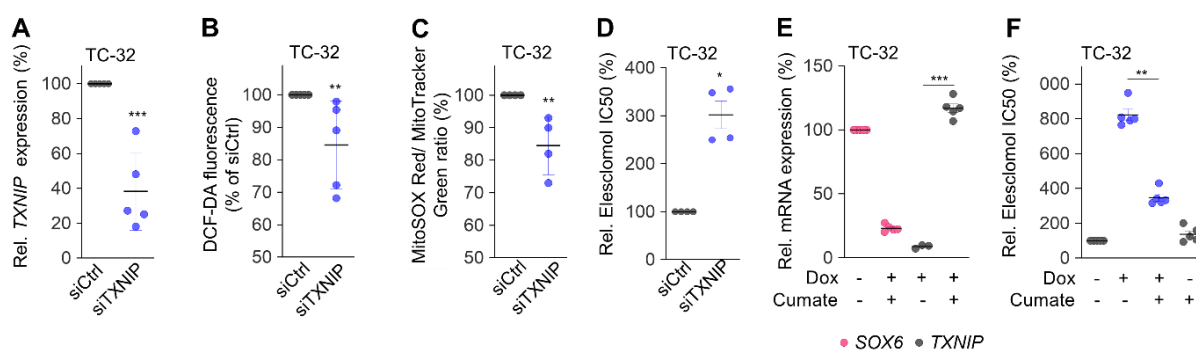


**Figure 22: *SOX6*-mediated *TXNIP* expression links oxidative stress to Elesclomol sensitivity.**

**A)** Analysis of relative *TXNIP* mRNA expression by qRT-PCR in TC-32 cells 96h after siRNA-mediated *TXNIP* knockdown. Means and SEM,  $n = 5$ .  $P$  value was determined via unpaired two-sided  $t$ -test with Welch's correction. **B) + C)** Analysis of oxidative stress levels by flow cytometric measurement of DCF-DA fluorescence or MitoSOX Red/MitoTracker Green ratio in TC-32 cells after siRNA-mediated *TXNIP* knockdown. Means and SEM,  $n \geq 4$ .  $P$  value was determined via independent one sample  $t$ -test. **D)** Quantification of relative Elesclomol IC50 after siRNA-mediated *TXNIP* knockdown in TC-32 EwS cells. Mean and SEM,  $n = 4$ . **E)** Relative mRNA expression of *SOX6* and *TXNIP* after 96h of Dox and/or Cumate treatment in TC-32 EwS cells. Means and s SEM,  $n \geq 3$ . **F)** Quantification of relative Elesclomol IC50 values measured by a Resazurin assay in TC-32 cells harboring a shRNA against *SOX6* and/or re-expression of *TXNIP* after 72h of Elesclomol treatment. Mean and SEM,  $n \geq 5$ . \*\*\* $P < 0.001$ , \*\* $P < 0.01$ , \* $P < 0.05$ .

In summary, this data implies a possible link between *SOX6*, oxidative stress and Elesclomol. This corroborates the assumption that *SOX6* might increase oxidative stress levels through upregulation of *TXNIP* and thus promotes sensitivity toward Elesclomol in EwS cells.

In conclusion, the presented data in this thesis offer an insight into the regulation of the transcription factor *SOX6* via the fusion protein EWSR1-FLI1 binding to an intronic GGAA-mSat of the *SOX6* gene. On the one hand *SOX6* confers proliferation and tumor growth by upregulating cell cycle-related genes. On the other side *SOX6* interferes with TXNIP, that in turn increases intracellular oxidative stress levels and thus promotes Elesclomol sensitivity in EwS cells (**Figure 23**).

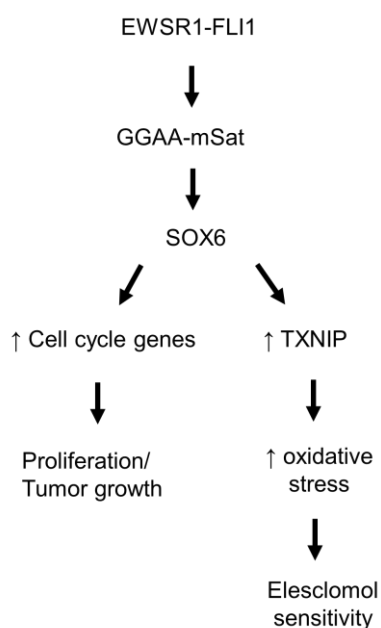


**Figure 23:** Schematic illustration of the EWSR1-FLI1-mediated *SOX6* expression and its function in EwS.

## 5. Discussion

EwS is a highly aggressive cancer of bone or soft-tissues that might arise from osteo-chondrogenic progenitors. As the developmental transcription factor *SOX6* is crucial for endochondral ossification and thus for bone development (Hagiwara, 2011; Smits et al., 2001), the aim of this thesis was to analyze the role of *SOX6* in bone-associated EwS.

This thesis showed that *SOX6* is regulated by the fusion oncogene *EWSR1-FLI1* in EwS, resulting in high but heterogeneous expression at the mRNA and protein level compared to most normal tissues and other cancers. Further analyses revealed that the high *SOX6* expression in EwS tumors did not result from CNV or differences in promoter methylation.

Through analysis of publicly available ChIP-seq data, an intronic *SOX6*-associated GGAA-mSat was found to be bound by *EWSR1-FLI1*. Interestingly, this mSat revealed strong length- and *EWSR1-FLI1*-dependent enhancer activity in EwS cell lines. This was supported by the fact, that the maternal and paternal alleles from the *SOX6*-associated mSat revealed that the allele with the higher consecutive GGAA-repeats exerted the higher enhancer activity. This result gives rise to the assumption that the observed inter-tumor heterogeneity of *SOX6* expression in EwS is probably due to different repeat numbers of consecutive GGAA-repeats at the *SOX6*-associated GGAA-mSat locus. These findings are in accordance with previously published data, stating that target genes of the fusion oncogene such as *EGR2* and *NROB1* also showed variable expression most likely caused by differences in the consecutive GGAA-repeats at the corresponding GGAA-mSat (Grünwald et al., 2018; Monument et al., 2014).

The *SOX6* gene can act as a splicing factor (Ohe et al., 2002, 2009) or as a transcription factor (Hagiwara, 2011) depending on the cellular requirement. Transcriptome profiling experiments that contained > 285,000 transcripts and isoforms did not reveal a strong contribution of *SOX6* to alternative splicing in EwS. Instead, a combination of microarray data with a GSEA analysis identified a large number of deregulated genes after *SOX6*-silencing. Those genes were significantly enriched for gene sets involved in proliferation and cell cycle progression. This finding, is in line with the known role of *SOX6* in proliferation of chondroblasts and oligodendrocytes. Furthermore, the changes in the cellular

transcriptome were verified and observed in functional *in vitro* and *in vivo* experiments in frame of this thesis.

*SOX6*-silencing reduced clonogenic and anchorage-independent growth as well as tumorigenicity in EwS cells, probably through the observed delayed transition of the cell cycle and the reduced expression of the proliferation marker Ki67 in xenografts. Interestingly, these findings suggest that *SOX6* acts as an oncogene in EwS, while it also has been reported that *SOX6* can act as tumor suppressor, for instance in esophageal squamous cell carcinoma and hepatocellular carcinoma (Guo et al., 2013; Qin et al., 2011). The actual function of *SOX6* in tumors might depend on the cellular requirements of the tumor entity.

Even though treatment options for EwS patients have improved over the last years and mortality could subsequently be reduced, novel therapeutic options are still urgently required (Grünewald et al., 2018; Thiel et al., 2011). In this regard, this thesis aimed at investigating whether the observed overexpression of *SOX6* in EwS compared to other sarcomas and normal tissues provides vulnerabilities that could be exploited therapeutically. Indeed, analysis of published gene expression data with drug-response data revealed seven drugs whose potency was highly dependent on *SOX6* expression. Revising all the listed drugs by their Pearson correlation coefficient and the statistical significance of the corresponding IC50 value, those with clinically unrealistic high IC50 values were excluded, ending up with the small-molecule Elesclomol.

Elesclomol is known to be an oxidative-stress inducer as it binds and transports copper across biological membranes into the mitochondria, there generating oxidative stress by its redox properties (Nagai et al., 2012). Previous reports showed that Elesclomol is able to increase oxidative stress even beyond a tolerable threshold, triggering cells into apoptosis (Gibellini et al., 2010; Kirshner et al., 2008; Nagai et al., 2012). It has already been shown that Elesclomol inhibits cancer cell growth *in vitro* at micro-molar concentrations in melanoma, breast cancer and leukemia cell lines (Alli and Ford, 2012; Nagai et al., 2012; Qu et al., 2010; Yadav et al., 2013).

Actually, in drug-response analyses *SOX6*-high expressing EwS cell lines showed sensitivity toward the small-molecule Elesclomol, whereas *SOX6* knockdown led to resistance of these cells. Interestingly, *SOX6* itself regulated oxidative stress in EwS cell lines, as oxidative stress and mito-ROS was reduced in EwS cell lines upon *SOX6* knockdown. Hence, it is tempting to speculate that the sensitivity of EwS toward Elesclomol is due to the relatively high *SOX6* expression and thereby elevated basic oxidative stress level in EwS. An increase of oxidative stress and mito-ROS levels upon Elesclomol-treatment was mirrored in functional *in vitro* and *in vivo* experiments in EwS cells. The apoptotic effect of Elesclomol was again dependent on *SOX6* expression. In line, Elesclomol-treatment in *SOX6*-high expressing cell lines with two antioxidants diminished the sensitivity toward Elesclomol, as previously observed in case of *SOX6* knockdown. Consequently, treatment with an oxidative stress-inducer rescued the Elesclomol sensitivity in *SOX6* knockdown EwS cell lines.

Additional analysis of the microarray data revealed a decreased *TXNIP* expression upon *SOX6* knockdown in EwS suggesting a *SOX6*-mediated upregulation of *TXNIP*. This observation could at least in part explain the elevated intracellular oxidative stress and mito-ROS levels that are linked to the sensitivity of *SOX6*-high expressing EwS cells toward Elesclomol. Interestingly, *TXNIP* is an inhibitor of the thioredoxin (TRX) antioxidant system that plays an essential role in buffering intracellular oxidative stress levels (Burke-Gaffney et al., 2005; Hwang et al., 2014).

Worth to mention, in a phase II and III of clinical trials, Elesclomol was administered in combination with paclitaxel to patients suffering from malignant melanoma (O'Day et al., 2009, 2013). However, the Elesclomol-treatment did not exert the desired effect as the outcomes could only be moderately improved in unselected patients (O'Day et al., 2009, 2013). This might have been circumvented if there would have been a preselection of patients with higher *SOX6* levels or higher intracellular oxidative stress levels. Yet, not only the sensitivity toward Elesclomol is higher in EwS cells, but also primary EwS present higher *SOX6* expression compared to melanoma or other cancers such as osteosarcoma (**Figure 18G**). Furthermore, Elesclomol mainly targets actively respiring mitochondria, a feature that

may reduce its effectiveness in predominantly hypoxic tumors (Yadav et al., 2013). Hypoxic tumors are under the control of the hypoxia-inducible factor 1 alpha (HIF-1 $\alpha$ ), a main response gene that in turn leads to an increase of Lactate dehydrogenase (LDH) levels (Semenza, 2000). This might also be an explanation why a subgroup analysis showed a more favorable outcome from Elesclomol treatment in patients with normal versus elevated baseline LDH levels in the phase III clinical trial (O'Day et al., 2013).

So far, Elesclomol has only been used as an enhancer in combination with other chemotherapeutic drugs such as Doxorubicin and Paclitaxel. Doxorubicin competes with the coenzyme Q<sub>10</sub> in the mitochondria. Treatment of breast cancer cells with a combination of Elesclomol and Doxorubicin enhanced the apoptosis effect (Qu et al., 2010). Paclitaxel, as Vincristin, are known to inhibit microtubule formation and both promote the release of cytochrome *c* from the mitochondria. Both pathways (Doxorubicin and Paclitaxel/Vincristin) lead to a rise in oxidative stress levels. Actually, standard treatment options for EwS include the chemotherapeutic agents Doxorubicin and Vincristin. The author of this thesis speculates whether Doxorubicin and Vincristin (besides Etoposide and Ifosfamide), could enhance their treatment potency when combined with Elesclomol in EwS. As mentioned before, *SOX6* is heterogeneously expressed in EwS with certain inter- and intra-tumoral differences meaning that even patients with lower *SOX6* expression could potentially benefit from this new treatment approach.

The observations and results of this thesis suggest that the oxidative stress-inducing reagent Elesclomol could be considered as a new therapeutic option for a subgroup of EwS patients with high levels of *SOX6*. Additionally, the author of this thesis suggests *SOX6* as a biomarker for prediction of Elesclomol efficacy in EwS. The application of *SOX6* as a biomarker in other cancer types needs to be further validated.

## 6. Conclusions and limitations

### 6.1 Conclusions

This PhD thesis investigated the tumorigenic role of SOX6 in EwS. This project revealed that SOX6 expression is regulated by EWSR1-FLI1 in EwS. Additionally, this project demonstrated that the overexpression of the transcription factor SOX6 contributes to proliferation *in vitro* and *in vivo*, anchorage-independent clonogenic growth as well as tumorigenicity of EwS.

SOX6 is highly expressed in EwS and other cancer entities. Although its expression does not correlate with survival in EwS patients, SOX6 might still serve as a biomarker and drug enhancer for targeted therapy. Supporting this, the underlying thesis elucidated the links between SOX6-mediated TXNIP expression, oxidative stress and Elesclomol sensitivity in EwS.

### 6.2 Limitations

The result of this PhD thesis illuminated a functional role of SOX6 in EwS progression and its capability as a biomarker for Elesclomol treatment in EwS patients. Nevertheless, the complex role of the developmental transcription factor SOX6 in EwS need to be further investigated. In the following section some open question resulting from this thesis were addressed:

#### **How exactly does SOX6 interfere with TXNIP in EwS?**

This thesis demonstrated that SOX6 in EwS somehow interferes with TXNIP repressing Trx and thereby increasing intrinsic oxidative stress levels. It is still unclear how exactly SOX6 interacts with TXNIP on the molecular level as unpublished ChIP-seq data for SOX6 (not shown in the thesis) in wildtype and SOX6-knockdown EwS cells did not hint to a direct regulation of TXNIP by SOX6. Interestingly, SOX6 does not possess an own trans-activation domain and its activation is dependend the interaction with other proteins. This thesis hint to the fact that SOX6 needs to bind a co-factor, which than in turn directly interacts with TXNIP. The full mechanism of how SOX6 interacts with TXNIP and contributes to oxidative stress levels in EwS cells needs to be further elucidated.

**Which role holds SOX6 in endochondral ossification during EwS progression?**

This project pointed out that SOX6 is involved in proliferation, anchorage-independent clonogenic growth and tumorigenesis of EwS cells. As a member of the SOX-trio, SOX6 is mainly involved in the proliferation of chondroblasts during endochondral ossification. So far, the role of SOX6 in the genesis of Ewing sarcoma is unknown. This is partly due to the still unknown cellular origin of EwS and due to the lack of an appropriate EwS model mimicking the real EwS from the beginning.

The analysis of the differentiation capacity with/without SOX6 *in vitro* by measuring for differentiation specific markers or stainings for mineralization did not hint at a differentiation capacity of EwS cells.

Interestingly, subcutaneous injection of SOX6-silenced EwS cells in mice showed that these knockdown cells were able to attract mouse-derived osteoblasts into the EwS tumor environment, which then differentiated into woven bone (data not shown in this thesis). Hence, further analysis of the tumor microenvironment of SOX6-expressing and SOX6-knockdown cells could reveal important insights into the mechanisms of SOX6 acting in EwS, such as by secretory proteins.

**Is SOX6-mediated Elesclomol sensitivity to other tumor entities with increased SOX6 levels (melanoma or glioma) improving clinical output for patients beyond EwS?**

This thesis demonstrated that SOX6 is linked to Elesclomol sensitivity in EwS cells. Overexpression experiments of SOX6 in SOX6-low expressing osteosarcoma cell lines U2OS and SAOS-2 were performed attempting to restore Elesclomol sensitivity (data not shown). Despite all effort, these experiments only revealed restricted effects suggesting other factors might be involved in the SOX6-mediated Elesclomol sensitivity at least in osteosarcoma. Thus, it remains unclear if the SOX6-mediated Elesclomol sensitivity is a phenomenon specific for EwS cells or if this given Elesclomol sensitivity could also be a predictive biomarker for other tumor entities. Treatment possibilities for SOX6-positive melanoma and glioblastoma patients could thus be improved potentially.

## 7. References

- Ahrens, S., Hoffmann, C., Jabar, S., Braun-Munzinger, G., Paulussen, M., Dunst, J., Rube, C., Winkelmann, W., Heinecke, A., Göbel, U., et al. (1999). Evaluation of prognostic factors in a tumor volume-adapted treatment strategy for localized Ewing sarcoma of bone: the CESS 86 experience. Cooperative Ewing Sarcoma Study. *Med. Pediatr. Oncol.* *32*, 186–195.
- Akiyama, H., Chaboissier, M.-C., Martin, J.F., Schedl, A., and de Crombrughe, B. (2002). The transcription factor Sox9 has essential roles in successive steps of the chondrocyte differentiation pathway and is required for expression of Sox5 and Sox6. *Genes Dev* *16*, 2813–2828.
- Alli, E., and Ford, J.M. (2012). Breast cancers with compromised DNA repair exhibit selective sensitivity to elesclomol. *DNA Repair (Amst)* *11*, 522–524.
- Anderson, N.D., de Borja, R., Young, M.D., Fuligni, F., Rosic, A., Roberts, N.D., Hajjar, S., Layeghifard, M., Novokmet, A., Kowalski, P.E., et al. (2018). Rearrangement bursts generate canonical gene fusions in bone and soft tissue tumors. *Science* *361*.
- Ayad, N.G., Rankin, S., Murakami, M., Jebanathirajah, J., Gygi, S., and Kirschner, M.W. (2003). Tome-1, a trigger of mitotic entry, is degraded during G1 via the APC. *Cell* *113*, 101–113.
- Azim, E., Jabaudon, D., Fame, R., and Macklis, J.D. (2009). SOX6 controls dorsal-ventral progenitor parcellation and interneuron diversity during neocortical development. *Nat Neurosci* *12*, 1238–1247.
- Baldauf, M.C., Orth, M.F., Dallmayer, M., Marchetto, A., Gerke, J.S., Rubio, R.A., Kiran, M.M., Musa, J., Knott, M.M.L., Ohmura, S., et al. (2018a). Robust diagnosis of Ewing sarcoma by immunohistochemical detection of super-enhancer-driven EWSR1-ETS targets. *Oncotarget* *9*, 1587–1601.
- Baldauf, M.C., Gerke, J.S., Kirschner, A., Blaesche, F., Effenberger, M., Schober, K., Rubio, R.A., Kanaseki, T., Kiran, M.M., Dallmayer, M., et al. (2018b). Systematic identification of cancer-specific MHC-binding peptides with RAVEN. *Oncoimmunology* *7*, e1481558.
- Bartel, D.P. (2009). MicroRNA Target Recognition and Regulatory Functions. *Cell* *136*, 215–233.
- Batista-Brito, R., Rossignol, E., Hjerling-Leffler, J., Denaxa, M., Wegner, M., Lefebvre, V., Pachnis, V., and Fishell, G. (2009). The cell-intrinsic requirement of Sox6 for cortical interneuron development. *Neuron* *63*, 466–481.
- Beck, R., Monument, M.J., Watkins, W.S., Smith, R., Boucher, K.M., Schiffman, J.D., Jorde, L.B., Randall, R.L., and Lessnick, S.L. (2012). EWS/FLI-responsive GGAA microsatellites exhibit polymorphic differences between European and African populations. *Cancer Genet* *205*, 304–312.
- Ben-David, Y., Giddens, E.B., Letwin, K., and Bernstein, A. (1991). Erythroleukemia induction by Friend murine leukemia virus: insertional activation of a new member of the ets gene family, Fli-1, closely linked to c-ets-1. *Genes Dev.* *5*, 908–918.
- Benz, C.C., and Yau, C. (2008). Ageing, oxidative stress and cancer: paradigms in parallax. *Nat. Rev. Cancer* *8*, 875–879.
- Berta, P., Hawkins, J.R., Sinclair, A.H., Taylor, A., Griffiths, B.L., Goodfellow, P.N., and Fellous, M. (1990). Genetic evidence equating SRY and the testis-determining factor. *Nature* *348*, 448–450.

- Bertolotti, A., Lutz, Y., Heard, D.J., Chambon, P., and Toral, L. (1996). hTAF<sub>168</sub>, a novel RNA/ssDNA-binding protein with homology to the pro-oncoproteins TLS/FUS and EWS is associated with both TFIID and RNA polymerase 1. *Binding Protein* 10.
- Bi, W., Deng, J.M., Zhang, Z., Behringer, R.R., and de Crombrughe, B. (1999). Sox9 is required for cartilage formation. *Nat. Genet.* 22, 85–89.
- Blackman, R.K., Cheung-Ong, K., Gebbia, M., Proia, D.A., He, S., Kepros, J., Jonneaux, A., Marchetti, P., Kluza, J., Rao, P.E., et al. (2012). Mitochondrial electron transport is the cellular target of the oncology drug elesclomol. *PLoS One* 7, e29798.
- Boulay, G., Sandoval, G.J., Riggi, N., Iyer, S., Buisson, R., Naigles, B., Awad, M.E., Rengarajan, S., Volorio, A., McBride, M.J., et al. (2017). Cancer-Specific Retargeting of BAF Complexes by a Prion-like Domain. *Cell* 171, 163-178.e19.
- Bradford, M.M. (1976). A rapid and sensitive method for the quantitation of microgram quantities of protein utilizing the principle of protein-dye binding. *Analytical Biochemistry* 72, 248–254.
- Burke-Gaffney, A., Callister, M.E.J., and Nakamura, H. (2005). Thioredoxin: friend or foe in human disease? *Trends Pharmacol. Sci.* 26, 398–404.
- Castillero-Trejo, Y., Eliazer, S., Xiang, L., Richardson, J.A., and Ilaria, R.L. (2005). Expression of the *EWS/FLI-1* Oncogene in Murine Primary Bone-Derived Cells Results in EWS/FLI-1–Dependent, Ewing Sarcoma–Like Tumors. *Cancer Res* 65, 8698–8705.
- Chen, J., and Wu, X. (2019). MicroRNA-103 contributes to osteoarthritis development by targeting Sox6. *Biomed. Pharmacother.* 118, 109186.
- Chen, K.-S., and DeLuca, H.F. (1994). Isolation and characterization of a novel cDNA from HL-60 cells treated with 1,25-dihydroxyvitamin D-3. *Biochimica et Biophysica Acta (BBA) - Gene Structure and Expression* 1219, 26–32.
- Chen, C., Deng, L., Nie, D.-K., Jia, F., Fu, L.-S., Wan, Z.-Q., and Lan, Q. (2019). Circular RNA Pleiotrophin promotes carcinogenesis in glioma via regulation of microRNA-122/SRY-box transcription factor 6 axis. *Eur. J. Cancer Prev.*
- Christensen, J., Cloos, P., Toftegaard, U., Klinkenberg, D., Bracken, A.P., Trinh, E., Heeran, M., Di Stefano, L., and Helin, K. (2005). Characterization of E2F8, a novel E2F-like cell-cycle regulated repressor of E2F-activated transcription. *Nucleic Acids Res* 33, 5458–5470.
- Cohen-Barak, O., Hagiwara, N., Arlt, M.F., Horton, J.P., and Brilliant, M.H. (2001). Cloning, characterization and chromosome mapping of the human SOX6 gene. *Gene* 265, 157–164.
- Cohen-Barak, O., Erickson, D.T., Badowski, M.S., Fuchs, D.A., Klassen, C.L., Harris, D.T., and Brilliant, M.H. (2007). Stem cell transplantation demonstrates that Sox6 represses  $\epsilon$  globin expression in definitive erythropoiesis of adult mice. *Experimental Hematology* 35, 358–367.
- Collet, J.-F., and Messens, J. (2010). Structure, function, and mechanism of thioredoxin proteins. *Antioxid. Redox Signal.* 13, 1205–1216.
- Cotterill, S.J., Ahrens, S., Paulussen, M., Jurgens, H.F., Voute, P.A., Gadner, H., and Craft, A.W. (2000). Prognostic factors in Ewing’s tumor of bone: analysis of 975 patients from the European Intergroup Cooperative Ewing’s Sarcoma Study Group. *J Clin Oncol* 18, 3108–3114.

- Crompton, B.D., Stewart, C., Taylor-Weiner, A., Alexe, G., Kurek, K.C., Calicchio, M.L., Kiezun, A., Carter, S.L., Shukla, S.A., Mehta, S.S., et al. (2014). The Genomic Landscape of Pediatric Ewing Sarcoma. *Cancer Discovery* 4, 1326–1341.
- Curtis, C.D., Thorngren, D.L., and Nardulli, A.M. (2010). Immunohistochemical analysis of oxidative stress and DNA repair proteins in normal mammary and breast cancer tissues. *BMC Cancer* 10, 9.
- Dai, M., Wang, P., Boyd, A.D., Kostov, G., Athey, B., Jones, E.G., Bunney, W.E., Myers, R.M., Speed, T.P., Akil, H., et al. (2005). Evolving gene/transcript definitions significantly alter the interpretation of GeneChip data. *Nucleic Acids Res* 33, e175.
- Das, A.T., Tenenbaum, L., and Berkhout, B. (2016). Tet-On Systems For Doxycycline-inducible Gene Expression. *Curr Gene Ther* 16, 156–167.
- De Biasi, S., Gibellini, L., Bianchini, E., Nasi, M., Pinti, M., Salvioli, S., and Cossarizza, A. (2016). Quantification of mitochondrial reactive oxygen species in living cells by using multi-laser polychromatic flow cytometry. *Cytometry Part A* 89, 1106–1110.
- Delattre, O., Zucman, J., Plougastel, B., Desmaze, C., Melot, T., Peter, M., Kovar, H., Joubert, I., de Jong, P., Rouleau, G., et al. (1992). Gene fusion with an ETS DNA-binding domain caused by chromosome translocation in human tumours. *Nature* 359, 162–165.
- Delattre, O., Zucman, J., Melot, T., Garau, X.S., Zucker, J.M., Lenoir, G.M., Ambros, P.F., Sheer, D., Turc-Carel, C., and Triche, T.J. (1994). The Ewing family of tumors--a subgroup of small-round-cell tumors defined by specific chimeric transcripts. *N. Engl. J. Med.* 331, 294–299.
- Denny, P., Swift, S., Brand, N., Dabhade, N., Barton, P., and Ashworth, A. (1992). A conserved family of genes related to the testis determining gene, *SRY*. *Nucl Acids Res* 20, 2887–2887.
- Dittmer, J. (2011). Ets Transcription Factors. In *Encyclopedia of Cancer*, M. Schwab, ed. (Berlin, Heidelberg: Springer Berlin Heidelberg), pp. 1339–1343.
- Dong, P., Xiong, Y., Yu, J., Chen, L., Tao, T., Yi, S., Hanley, S.J.B., Yue, J., Watari, H., and Sakuragi, N. (2018). Control of PD-L1 expression by miR-140/142/340/383 and oncogenic activation of the OCT4–miR-18a pathway in cervical cancer. *Oncogene* 37, 5257–5268.
- Dugas, J.C., Cuellar, T.L., Scholze, A., Ason, B., Ibrahim, A., Emery, B., Zamanian, J.L., Foo, L.C., McManus, M.T., and Barres, B.A. (2010). Dicer1 and miR-219 Are Required for Normal Oligodendrocyte Differentiation and Myelination. *Neuron* 65, 597–611.
- Dumitriu, B. (2006). Sox6 cell-autonomously stimulates erythroid cell survival, proliferation, and terminal maturation and is thereby an important enhancer of definitive erythropoiesis during mouse development. *Blood* 108, 1198–1207.
- Dumitriu, B., Bhattaram, P., Dy, P., Huang, Y., Quayum, N., Jensen, J., and Lefebvre, V. (2010). Sox6 Is Necessary for Efficient Erythropoiesis in Adult Mice under Physiological and Anemia-Induced Stress Conditions. *PLoS ONE* 5, e12088.
- Esiashvili, N., Goodman, M., and Marcus, R. (2008). Changes in Incidence and Survival of Ewing Sarcoma Patients Over the Past 3 Decades. *Journal of Pediatric Hematology/Oncology* 30, 425–430.
- Ewing, J. (1921). Diffuse endothelioma of bone. *Proc NY Pathol Soc* 12:17-24.

- Ezeriņa, D., Takano, Y., Hanaoka, K., Urano, Y., and Dick, T.P. (2018). N-Acetyl Cysteine Functions as a Fast-Acting Antioxidant by Triggering Intracellular H<sub>2</sub>S and Sulfane Sulfur Production. *Cell Chem Biol* 25, 447-459.e4.
- Feng, X., Zhang, C., Zhu, L., Zhang, L., Li, H., He, L., Mi, Y., Wang, Y., Zhu, J., and Bu, Y. (2017). DEPDC1 is required for cell cycle progression and motility in nasopharyngeal carcinoma. *Oncotarget* 8, 63605–63619.
- Folpe, A.L., Hill, C.E., Parham, D.M., O’Shea, P.A., and Weiss, S.W. (2000). Immunohistochemical detection of FLI-1 protein expression: a study of 132 round cell tumors with emphasis on CD99-positive mimics of Ewing’s sarcoma/primitive neuroectodermal tumor. *Am. J. Surg. Pathol.* 24, 1657–1662.
- Gangwal, K., and Lessnick, S.L. (2008). Microsatellites are EWS/FLI response elements: genomic “junk” is EWS/FLI’s treasure. *Cell Cycle* 7, 3127–3132.
- Gangwal, K., Sankar, S., Hollenhorst, P.C., Kinsey, M., Haroldsen, S.C., Shah, A.A., Boucher, K.M., Watkins, W.S., Jorde, L.B., Graves, B.J., et al. (2008). Microsatellites as EWS/FLI response elements in Ewing’s sarcoma. *Proc Natl Acad Sci U S A* 105, 10149–10154.
- Gaspar, N., Hawkins, D.S., Dirksen, U., Lewis, I.J., Ferrari, S., Le Deley, M.-C., Kovar, H., Grimer, R., Whelan, J., Claude, L., et al. (2015). Ewing Sarcoma: Current Management and Future Approaches Through Collaboration. *J. Clin. Oncol.* 33, 3036–3046.
- Giard, D.J., Aaronson, S.A., Todaro, G.J., Arnstein, P., Kersey, J.H., Dosik, H., and Parks, W.P. (1973). In vitro cultivation of human tumors: establishment of cell lines derived from a series of solid tumors. *J. Natl. Cancer Inst.* 51, 1417–1423.
- Gibellini, L., Pinti, M., Nasi, M., De Biasi, S., Roat, E., Bertoncelli, L., and Cossarizza, A. (2010). Interfering with ROS Metabolism in Cancer Cells: The Potential Role of Quercetin. *Cancers (Basel)* 2, 1288–1311.
- Gordon, D.J., Motwani, M., and Pellman, D. (2016). Modeling the initiation of Ewing sarcoma tumorigenesis in differentiating human embryonic stem cells. *Oncogene* 35, 3092–3102.
- Grier, H.E., Krailo, M.D., Tarbell, N.J., Link, M.P., Fryer, C.J.H., Pritchard, D.J., Gebhardt, M.C., Dickman, P.S., Perlman, E.J., Meyers, P.A., et al. (2003). Addition of Ifosfamide and Etoposide to Standard Chemotherapy for Ewing’s Sarcoma and Primitive Neuroectodermal Tumor of Bone. *New England Journal of Medicine* 348, 694–701.
- Grünewald, T.G., Diebold, I., Esposito, I., Plehm, S., Hauer, K., Thiel, U., da Silva-Buttkus, P., Neff, F., Unland, R., Muller-Tidow, C., et al. (2012). STEAP1 is associated with the invasive and oxidative stress phenotype of Ewing tumors. *Mol Cancer Res* 10, 52–65.
- Grünewald, T.G., Bernard, V., Gilardi-Hebenstreit, P., Raynal, V., Surdez, D., Aynaud, M.M., Mirabeau, O., Cidre-Aranaz, F., Tirode, F., Zaidi, S., et al. (2015). Chimeric EWSR1-FLI1 regulates the Ewing sarcoma susceptibility gene EGR2 via a GGAA microsatellite. *Nat Genet* 47, 1073–1078.
- Grünewald, T.G.P., Cidre-Aranaz, F., Surdez, D., Tomazou, E.M., de Alava, E., Kovar, H., Sorensen, P.H., Delattre, O., and Dirksen, U. (2018). Ewing sarcoma. *Nat Rev Dis Primers* 4, 5.
- Gubbay, J., Collignon, J., Koopman, P., Capel, B., Economou, A., Münsterberg, A., Vivian, N., Goodfellow, P., and Lovell-Badge, R. (1990). A gene mapping to the sex-determining region of the mouse Y chromosome is a member of a novel family of embryonically expressed genes. *Nature* 346, 245–250.

- Guillon, N., Tirode, F., Boeva, V., Zynovyev, A., Barillot, E., and Delattre, O. (2009). The oncogenic EWS-FLI1 protein binds in vivo GGAA microsatellite sequences with potential transcriptional activation function. *PLoS One* 4, e4932.
- Guo, X., Yang, M., Gu, H., Zhao, J., and Zou, L. (2013). Decreased expression of SOX6 confers a poor prognosis in hepatocellular carcinoma. *Cancer Epidemiol* 37, 732–736.
- Hagiwara, N. (2011). Sox6, jack of all trades: a versatile regulatory protein in vertebrate development. *Dev Dyn* 240, 1311–1321.
- Hagiwara, N., Yeh, M., and Liu, A. (2007). Sox6 is required for normal fiber type differentiation of fetal skeletal muscle in mice. *Dev. Dyn.* 236, 2062–2076.
- Han, Y., and Lefebvre, V. (2008). L-Sox5 and Sox6 Drive Expression of the Aggrecan Gene in Cartilage by Securing Binding of Sox9 to a Far-Upstream Enhancer. *Mol Cell Biol* 28, 4999–5013.
- Han, Y., Fan, T.B., Peng, B.T., Li, B., Cheng, J.T., Xu, H.D., Gao, C.Y., and Cheng, Z.Y. (2018). [Effect of miR-19b on the proliferation and apoptosis of P19CL6 cells during the late-stage of cardiac differentiation]. *Zhonghua Yi Xue Za Zhi* 98, 617–621.
- Hannus, M., Beitzinger, M., Engelmann, J.C., Weickert, M.T., Spang, R., Hannus, S., and Meister, G. (2014). siPools: highly complex but accurately defined siRNA pools eliminate off-target effects. *Nucleic Acids Res* 42, 8049–8061.
- Hauer, K., Calzada-Wack, J., Steiger, K., Grunewald, T.G.P., Baumhoer, D., Plehm, S., Buch, T., da Costa, O.P., Esposito, I., Burdach, S., et al. (2013). DKK2 Mediates Osteolysis, Invasiveness, and Metastatic Spread in Ewing Sarcoma. *Cancer Research* 73, 967–977.
- von Hofsten, J., Elworthy, S., Gilchrist, M.J., Smith, J.C., Wardle, F.C., and Ingham, P.W. (2008). Prdm1- and Sox6-mediated transcriptional repression specifies muscle fibre type in the zebrafish embryo. *EMBO Rep* 9, 683–689.
- Horton, W.A., Hood, O.J., Machado, M.A., Ahmed, S., and Griffey, E.S. (1988). Abnormal ossification in thanatophoric dysplasia. *Bone* 9, 53–61.
- Hwang, J., Suh, H.-W., Jeon, Y.H., Hwang, E., Nguyen, L.T., Yeom, J., Lee, S.-G., Lee, C., Kim, K.J., Kang, B.S., et al. (2014). The structural basis for the negative regulation of thioredoxin by thioredoxin-interacting protein. *Nature Communications* 5, 2958.
- Iguchi, H., Ikeda, Y., Okamura, M., Tanaka, T., Urashima, Y., Ohguchi, H., Takayasu, S., Kojima, N., Iwasaki, S., Ohashi, R., et al. (2005). SOX6 Attenuates Glucose-stimulated Insulin Secretion by Repressing PDX1 Transcriptional Activity and Is Down-regulated in Hyperinsulinemic Obese Mice. *J. Biol. Chem.* 280, 37669–37680.
- Iguchi, H., Urashima, Y., Inagaki, Y., Ikeda, Y., Okamura, M., Tanaka, T., Uchida, A., Yamamoto, T.T., Kodama, T., and Sakai, J. (2007). SOX6 Suppresses Cyclin D1 Promoter Activity by Interacting with  $\beta$ -Catenin and Histone Deacetylase 1, and Its Down-regulation Induces Pancreatic  $\beta$ -Cell Proliferation. *J. Biol. Chem.* 282, 19052–19061.
- Ikeda, K., Horie-Inoue, K., Suzuki, T., Hobo, R., Nakasato, N., Takeda, S., and Inoue, S. (2019). Mitochondrial supercomplex assembly promotes breast and endometrial tumorigenesis by metabolic alterations and enhanced hypoxia tolerance. *Nat Commun* 10, 4108.

- Iorio, F., Knijnenburg, T.A., Vis, D.J., Bignell, G.R., Menden, M.P., Schubert, M., Aben, N., Goncalves, E., Barthorpe, S., Lightfoot, H., et al. (2016). A Landscape of Pharmacogenomic Interactions in Cancer. *Cell* 166, 740–754.
- Irizarry, R.A., Hobbs, B., Collin, F., Beazer-Barclay, Y.D., Antonellis, K.J., Scherf, U., and Speed, T.P. (2003). Exploration, normalization, and summaries of high density oligonucleotide array probe level data. *Biostatistics* 4, 249–264.
- Jin, R.-H., Yu, D.-J., and Zhong, M. (2018). MiR-1269a acts as an onco-miRNA in non-small cell lung cancer via down-regulating SOX6. *European Review for Medical and Pharmacological Sciences* 22, 4888–4897.
- Kamachi, Y., Uchikawa, M., and Kondoh, H. (2000). Pairing SOX off: with partners in the regulation of embryonic development. *Trends Genet.* 16, 182–187.
- Kasai, H. (1997). Analysis of a form of oxidative DNA damage, 8-hydroxy-2'-deoxyguanosine, as a marker of cellular oxidative stress during carcinogenesis. *Mutation Research/Reviews in Mutation Research* 387, 147–163.
- Khoury, J.D. (2005). Ewing sarcoma family of tumors. *Adv Anat Pathol* 12, 212–220.
- Kinsey, M., Smith, R., and Lessnick, S.L. (2006). NROB1 Is Required for the Oncogenic Phenotype Mediated by EWS/FLI in Ewing's Sarcoma. *Molecular Cancer Research* 4, 851–859.
- Kirshner, J.R., He, S., Balasubramanyam, V., Kepros, J., Yang, C.Y., Zhang, M., Du, Z., Barsoum, J., and Bertin, J. (2008). Elesclomol induces cancer cell apoptosis through oxidative stress. *Mol Cancer Ther* 7, 2319–2327.
- Koopman, P., Schepers, G., Brenner, S., and Venkatesh, B. (2004). Origin and diversity of the SOX transcription factor gene family: genome-wide analysis in *Fugu rubripes*. *Gene* 328, 177–186.
- Kovar, H. (1998). Progress in the Molecular Biology of Ewing Tumors. *Sarcoma* 2, 3–17.
- Krishna, C.M., Liebmann, J.E., Kaufman, D., DeGraff, W., Hahn, S.M., McMurry, T., Mitchell, J.B., and Russo, A. (1992). The catecholic metal sequestering agent 1,2-dihydroxybenzene-3, 5-disulfonate confers protection against oxidative cell damage. *Archives of Biochemistry and Biophysics* 294, 98–106.
- Le Deley, M.-C., Delattre, O., Schaefer, K.-L., Burchill, S.A., Koehler, G., Hogendoorn, P.C.W., Lion, T., Poremba, C., Marandet, J., Ballet, S., et al. (2010). Impact of *EWS-ETS* Fusion Type on Disease Progression in Ewing's Sarcoma/Peripheral Primitive Neuroectodermal Tumor: Prospective Results From the Cooperative Euro-E.W.I.N.G. 99 Trial. *Journal of Clinical Oncology* 28, 1982–1988.
- Le Douarin, N.M., and Kalcheim, C. (1999). *The Neural Crest* (Cambridge: Cambridge University Press).
- Lefebvre, V., and Smits, P. (2005). Transcriptional control of chondrocyte fate and differentiation. *Birth Defects Res C Embryo Today* 75, 200–212.
- Lefebvre, V., Li, P., and de Crombrughe, B. (1998). A new long form of Sox5 (L-Sox5), Sox6 and Sox9 are coexpressed in chondrogenesis and cooperatively activate the type II collagen gene. *EMBO J* 17, 5718–5733.
- Lefebvre, V., Dumitriu, B., Penzo-Méndez, A., Han, Y., and Pallavi, B. (2007). Control of Cell Fate and Differentiation by Sry-related High-mobility-group Box (Sox) Transcription Factors. *Int J Biochem Cell Biol* 39, 2195–2214.

- Li, Z., and Wang, Y. (2017). miR-96 targets SOX6 and promotes proliferation, migration, and invasion of hepatocellular carcinoma. *Biochem. Cell Biol.* *96*, 365–371.
- Li, C., Li, Y., Chen, L., Li, D., Yang, L., Jin, J., and Zhang, B. (2015). MicroRNA-766 targeting regulation of SOX6 expression promoted cell proliferation of human colorectal cancer. *OTT* 2981.
- Li, H., Zheng, D., Zhang, B., Liu, L., Ou, J., Chen, W., Xiong, S., Gu, Y., and Yang, J. (2014). Mir-208 promotes cell proliferation by repressing SOX6 expression in human esophageal squamous cell carcinoma. *J Transl Med* *12*, 196.
- Li, W., Fang, J., Shen, J., Liu, X., Hou, J., Zhu, Y., and Ma, X. (2019). MicroRNA-135a-5p promotes neuronal differentiation of pluripotent embryonal carcinoma cells by repressing Sox6/CD44 pathway. *Biochemical and Biophysical Research Communications* *509*, 603–610.
- Li, X., Wang, J., Jia, Z., Cui, Q., Zhang, C., Wang, W., Chen, P., Ma, K., and Zhou, C. (2013). MiR-499 Regulates Cell Proliferation and Apoptosis during Late-Stage Cardiac Differentiation via Sox6 and Cyclin D1. *PLoS ONE* *8*, e74504.
- Liu, B., Zhang, J., Yang, S., Ji, K., Liu, X., Du, B., Jia, Q., Qi, S., Li, X., and Fan, R. (2018). Effect of silencing microRNA-508 by STTM on melanogenesis in alpaca (*Vicugna pacos*). *Gene* *678*, 343–348.
- Livak, K.J., and Schmittgen, T.D. (2001). Analysis of Relative Gene Expression Data Using Real-Time Quantitative PCR and the  $2^{-\Delta\Delta CT}$  Method. *Methods* *25*, 402–408.
- Long, S., Long, S., He, H., and Chen, G. (2019). MicroRNA-765 is preregulated in multiple myeloma and serves an oncogenic role by directly targeting SOX6. *Exp Ther Med* *17*, 4741–4747.
- Machiela, M.J., Grünewald, T.G.P., Surdez, D., Reynaud, S., Mirabeau, O., Karlins, E., Rubio, R.A., Zaidi, S., Grossetete-Lalami, S., Ballet, S., et al. (2018). Genome-wide association study identifies multiple new loci associated with Ewing sarcoma susceptibility. *Nat Commun* *9*, 3184.
- May, W.A., Grigoryan, R.S., Keshelava, N., Cabral, D.J., Christensen, L.L., Jenabi, J., Ji, L., Triche, T.J., Lawlor, E.R., and Reynolds, C.P. (2013). Characterization and drug resistance patterns of Ewing's sarcoma family tumor cell lines. *PLoS One* *8*, e80060.
- Mi, Y., Zhang, C., Bu, Y., Zhang, Y., He, L., Li, H., Zhu, H., Li, Y., Lei, Y., and Zhu, J. (2015). DEPDC1 is a novel cell cycle related gene that regulates mitotic progression. *BMB Rep* *48*, 413–418.
- Mikkelsen, R.B., and Wardman, P. (2003). Biological chemistry of reactive oxygen and nitrogen and radiation-induced signal transduction mechanisms. *Oncogene* *22*, 5734–5754.
- Monument, M.J., Johnson, K.M., McIlvaine, E., Abegglen, L., Watkins, W.S., Jorde, L.B., Womer, R.B., Beeler, N., Monovich, L., Lawlor, E.R., et al. (2014). Clinical and biochemical function of polymorphic NROB1 GGAA-microsatellites in Ewing sarcoma: a report from the Children's Oncology Group. *PLoS ONE* *9*, e104378.
- Mullick, A., Xu, Y., Warren, R., Koutroumanis, M., Guilbault, C., Broussau, S., Malenfant, F., Bourget, L., Lamoureux, L., Lo, R., et al. (2006). The cumate gene-switch: a system for regulated expression in mammalian cells. *BMC Biotechnol* *6*, 43.
- Musa, J., Cidre-Aranaz, F., Aynaud, M.-M., Orth, M.F., Knott, M.M.L., Mirabeau, O., Mazor, G., Varon, M., Hölting, T.L.B., Grossetête, S., et al. (2019). Cooperation of cancer drivers with regulatory germline variants shapes clinical outcomes. *Nat Commun* *10*, 4128.

- Nagai, M., Vo, N.H., Shin Ogawa, L., Chimmanamada, D., Inoue, T., Chu, J., Beaudette-Zlatanova, B.C., Lu, R., Blackman, R.K., Barsoum, J., et al. (2012). The oncology drug elesclomol selectively transports copper to the mitochondria to induce oxidative stress in cancer cells. *Free Radic Biol Med* 52, 2142–2150.
- O’Day, S., Gonzalez, R., Lawson, D., Weber, R., Hutchins, L., Anderson, C., Haddad, J., Kong, S., Williams, A., and Jacobson, E. (2009). Phase II, randomized, controlled, double-blinded trial of weekly elesclomol plus paclitaxel versus paclitaxel alone for stage IV metastatic melanoma. *J Clin Oncol* 27, 5452–5458.
- O’Day, S.J., Eggermont, A.M., Chiarion-Sileni, V., Kefford, R., Grob, J.J., Mortier, L., Robert, C., Schachter, J., Testori, A., Mackiewicz, J., et al. (2013). Final results of phase III SYMMETRY study: randomized, double-blind trial of elesclomol plus paclitaxel versus paclitaxel alone as treatment for chemotherapy-naïve patients with advanced melanoma. *J Clin Oncol* 31, 1211–1218.
- Ohe, K., Lalli, E., and Sassone-Corsi, P. (2002). A direct role of SRY and SOX proteins in pre-mRNA splicing. *Proc Natl Acad Sci U S A* 99, 1146–1151.
- Ohe, K., Tamai, K.T., Parvinen, M., and Sassone-Corsi, P. (2009). DAX-1 and SOX6 molecular interplay results in an antagonistic effect in pre-mRNA splicing. *Dev Dyn* 238, 1595–1604.
- Paulussen, M., Bielack, S., Jürgens, H., and Jost, L. (2008a). Ewing’s sarcoma of the bone: ESMO Clinical Recommendations for diagnosis, treatment and follow-up. *Ann Oncol* 19, ii97–ii98.
- Paulussen, M., Craft, A.W., Lewis, I., Hackshaw, A., Douglas, C., Dunst, J., Schuck, A., Winkelmann, W., Köhler, G., Poremba, C., et al. (2008b). Results of the EICESS-92 Study: Two Randomized Trials of Ewing’s Sarcoma Treatment—Cyclophosphamide Compared With Ifosfamide in Standard-Risk Patients and Assessment of Benefit of Etoposide Added to Standard Treatment in High-Risk Patients. *Journal of Clinical Oncology* 26, 4385–4393.
- Paulussen, M., Bielack, S., Jürgens, H., and Casali, P.G. (2009). Ewing’s sarcoma of the bone: ESMO Clinical Recommendations for diagnosis, treatment and follow-up. *Ann Oncol* 20, iv140–iv142.
- Pevny, L.H., and Lovell-Badge, R. (1997). Sox genes find their feet. *Curr. Opin. Genet. Dev.* 7, 338–344.
- Qin, Y.R., Tang, H., Xie, F., Liu, H., Zhu, Y., Ai, J., Chen, L., Li, Y., Kwong, D.L., Fu, L., et al. (2011). Characterization of tumor-suppressive function of SOX6 in human esophageal squamous cell carcinoma. *Clin Cancer Res* 17, 46–55.
- Qu, X., Chen, Z., Fan, D., Sun, C., and Zeng, Y. (2016). MiR-132-3p Regulates the Osteogenic Differentiation of Thoracic Ligamentum Flavum Cells by Inhibiting Multiple Osteogenesis-Related Genes. *IJMS* 17, 1370.
- Qu, Y., Wang, J., Sim, M.S., Liu, B., Giuliano, A., Barsoum, J., and Cui, X. (2010). Elesclomol, counteracted by Akt survival signaling, enhances the apoptotic effect of chemotherapy drugs in breast cancer cells. *Breast Cancer Res Treat* 121, 311–321.
- Quintana, L., zur Nieden, N.I., and Semino, C.E. (2009). Morphogenetic and Regulatory Mechanisms During Developmental Chondrogenesis: New Paradigms for Cartilage Tissue Engineering. *Tissue Eng Part B Rev* 15, 29–41.
- Remmele, W., and Stegner, H.E. (1987). [Recommendation for uniform definition of an immunoreactive score (IRS) for immunohistochemical estrogen receptor detection (ER-ICA) in breast cancer tissue]. *Pathologe* 8, 138–140.
- Resnick, D., and Kransdorf, M.J. (2005). *Bone and joint imaging* (Philadelphia, Pa.: Elsevier Saunders).

- Riggi, N., and Stamenkovic, I. (2007). The Biology of Ewing sarcoma. *Cancer Lett.* *254*, 1–10.
- Riggi, N., Cironi, L., Provero, P., Suvà, M.-L., Kaloulis, K., Garcia-Echeverria, C., Hoffmann, F., Trumpp, A., and Stamenkovic, I. (2005). Development of Ewing's Sarcoma from Primary Bone Marrow-Derived Mesenchymal Progenitor Cells. *Cancer Res* *65*, 11459–11468.
- Riggi, N., Suvà, M.-L., Suvà, D., Cironi, L., Provero, P., Tercier, S., Joseph, J.-M., Stehle, J.-C., Baumer, K., Kindler, V., et al. (2008). EWS-FLI-1 Expression Triggers a Ewing's Sarcoma Initiation Program in Primary Human Mesenchymal Stem Cells. *Cancer Res* *68*, 2176–2185.
- Riggi, N., Knoechel, B., Gillespie, S.M., Rheinbay, E., Boulay, G., Suva, M.L., Rossetti, N.E., Boonseng, W.E., Oksuz, O., Cook, E.B., et al. (2014). EWS-FLI1 utilizes divergent chromatin remodeling mechanisms to directly activate or repress enhancer elements in Ewing sarcoma. *Cancer Cell* *26*, 668–681.
- Sarkar, A., and Hochedlinger, K. (2013). The Sox Family of Transcription Factors: Versatile Regulators of Stem and Progenitor Cell Fate. *Cell Stem Cell* *12*, 15–30.
- Semenza, G.L. (2000). HIF-1: using two hands to flip the angiogenic switch. *Cancer Metastasis Rev.* *19*, 59–65.
- Sheffield, N.C., Pierron, G., Klughammer, J., Datlinger, P., Schonegger, A., Schuster, M., Hadler, J., Surdez, D., Guillemot, D., Lapouble, E., et al. (2017). DNA methylation heterogeneity defines a disease spectrum in Ewing sarcoma. *Nat Med* *23*, 386–395.
- Sluijter, J.P.G., van Mil, A., van Vliet, P., Metz, C.H.G., Liu, J., Doevendans, P.A., and Goumans, M.-J. (2010). MicroRNA-1 and -499 regulate differentiation and proliferation in human-derived cardiomyocyte progenitor cells. *Arterioscler. Thromb. Vasc. Biol.* *30*, 859–868.
- Smits, P., Li, P., Mandel, J., Zhang, Z., Deng, J.M., Behringer, R.R., de Crombrughe, B., and Lefebvre, V. (2001). The transcription factors L-Sox5 and Sox6 are essential for cartilage formation. *Dev Cell* *1*, 277–290.
- Smits, P., Dy, P., Mitra, S., and Lefebvre, V. (2004). Sox5 and Sox6 are needed to develop and maintain source, columnar, and hypertrophic chondrocytes in the cartilage growth plate. *J Cell Biol* *164*, 747–758.
- Soci, U.P.R., Fernandes, T., Barauna, V.G., Hashimoto, N.Y., de Fatima Alves Mota, G., Rosa, K.T., Irigoyen, M.C., Philips, M.I., and de Oliveira, E.M. (2016). Epigenetic control of exercise training-induced cardiac hypertrophy by miR-208. *Clinical Science* *130*, 2005–2015.
- Sorensen, P.H., Lessnick, S.L., Lopez-Terrada, D., Liu, X.F., Triche, T.J., and Denny, C.T. (1994). A second Ewing's sarcoma translocation, t(21;22), fuses the EWS gene to another ETS-family transcription factor, ERG. *Nat. Genet.* *6*, 146–151.
- Stewart, E., Goshorn, R., Bradley, C., Griffiths, L.M., Benavente, C., Twarog, N.R., Miller, G.M., Caufield, W., Freeman, B.B., Bahrami, A., et al. (2014). Targeting the DNA Repair Pathway in Ewing Sarcoma. *Cell Reports* *9*, 829–840.
- Stewart, E., Federico, S.M., Chen, X., Shelat, A.A., Bradley, C., Gordon, B., Karlstrom, A., Twarog, N.R., Clay, M.R., Bahrami, A., et al. (2017). Orthotopic patient-derived xenografts of paediatric solid tumours. *Nature* *549*, 96–100.

- Stolt, C.C., Schlierf, A., Lommes, P., Hillgartner, S., Werner, T., Kosian, T., Sock, E., Kessar, N., Richardson, W.D., Lefebvre, V., et al. (2006). SoxD proteins influence multiple stages of oligodendrocyte development and modulate SoxE protein function. *Dev Cell* *11*, 697–709.
- Storey, J., Bass, A., Dabney, A., and Robinson, D. (2019). qvalue: Q-value estimation for false discovery rate control. R package version 2.16.0.
- Stros, M., Launholt, D., and Grasser, K.D. (2007). The HMG-box: a versatile protein domain occurring in a wide variety of DNA-binding proteins. *Cell. Mol. Life Sci.* *64*, 2590–2606.
- Subramanian, A., Tamayo, P., Mootha, V.K., Mukherjee, S., Ebert, B.L., Gillette, M.A., Paulovich, A., Pomeroy, S.L., Golub, T.R., Lander, E.S., et al. (2005). Gene set enrichment analysis: a knowledge-based approach for interpreting genome-wide expression profiles. *Proc Natl Acad Sci U S A* *102*, 15545–15550.
- Tanaka, M., Yamazaki, Y., Kanno, Y., Igarashi, K., Aisaki, K., Kanno, J., and Nakamura, T. (2014). Ewing's sarcoma precursors are highly enriched in embryonic osteochondrogenic progenitors. *J Clin Invest* *124*, 3061–3074.
- Thiel, U., Wawer, A., Wolf, P., Badoglio, M., Santucci, A., Klingebiel, T., Basu, O., Borkhardt, A., Laws, H.-J., Kodera, Y., et al. (2011). No improvement of survival with reduced- versus high-intensity conditioning for allogeneic stem cell transplants in Ewing tumor patients. *Annals of Oncology* *22*, 1614–1621.
- Tirode, F., Laud-Duval, K., Prieur, A., Delorme, B., Charbord, P., and Delattre, O. (2007). Mesenchymal stem cell features of Ewing tumors. *Cancer Cell* *11*, 421–429.
- Tirode, F., Surdez, D., Ma, X., Parker, M., Le Deley, M.C., Bahrami, A., Zhang, Z., Lapouble, E., Grossetete-Lalami, S., Rusch, M., et al. (2014). Genomic landscape of Ewing sarcoma defines an aggressive subtype with co-association of STAG2 and TP53 mutations. *Cancer Discov* *4*, 1342–1353.
- Trachootham, D., Alexandre, J., and Huang, P. (2009). Targeting cancer cells by ROS-mediated mechanisms: a radical therapeutic approach? *Nat Rev Drug Discov* *8*, 579–591.
- Turc-Carel, C., Aurias, A., Mugneret, F., Lizard, S., Sidaner, I., Volk, C., Thiery, J.P., Olschwang, S., Philip, I., and Berger, M.P. (1988). Chromosomes in Ewing's sarcoma. I. An evaluation of 85 cases of remarkable consistency of t(11;22)(q24;q12). *Cancer Genet. Cytogenet.* *32*, 229–238.
- Ueda, R., Yoshida, K., Kawakami, Y., Kawase, T., and Toda, M. (2004a). Expression of a transcriptional factor, SOX6, in human gliomas. *Brain Tumor Pathol* *21*, 35–38.
- Ueda, R., Iizuka, Y., Yoshida, K., Kawase, T., Kawakami, Y., and Toda, M. (2004b). Identification of a human glioma antigen, SOX6, recognized by patients' sera. *Oncogene* *23*, 1420–1427.
- Wang, X.Y., Chen, X.L., Huang, Z.Q., Chen, D.W., Yu, B., He, J., Luo, J.Q., Luo, Y.H., Chen, H., Zheng, P., et al. (2017). MicroRNA-499-5p regulates porcine myofiber specification by controlling Sox6 expression. *Animal* *11*, 2268–2274.
- Wegner, M. (1999). From head to toes: the multiple facets of Sox proteins. *Nucleic Acids Res* *27*, 1409–1420.
- Wiederschain, D., Wee, S., Chen, L., Loo, A., Yang, G., Huang, A., Chen, Y., Caponigro, G., Yao, Y.M., Lengauer, C., et al. (2009). Single-vector inducible lentiviral RNAi system for oncology target validation. *Cell Cycle* *8*, 498–504.

- Womer, R.B., West, D.C., Krailo, M.D., Dickman, P.S., Pawel, B.R., Grier, H.E., Marcus, K., Sailer, S., Healey, J.H., Dormans, J.P., et al. (2012). Randomized Controlled Trial of Interval-Compressed Chemotherapy for the Treatment of Localized Ewing Sarcoma: A Report From the Children's Oncology Group. *Journal of Clinical Oncology* 30, 4148–4154.
- Xie, Q., Chen, X., Lu, F., Zhang, T., Hao, M., Wang, Y., Zhao, J., McCrae, M.A., and Zhuang, H. (2012). Aberrant expression of microRNA 155 may accelerate cell proliferation by targeting sex-determining region Y box 6 in hepatocellular carcinoma. *Cancer* 118, 2431–2442.
- Xu, J., Sankaran, V.G., Ni, M., Menne, T.F., Puram, R.V., Kim, W., and Orkin, S.H. (2010). Transcriptional silencing of  $\gamma$ -globin by BCL11A involves long-range interactions and cooperation with SOX6. *Genes & Development* 24, 783–798.
- Yadav, A.A., Patel, D., Wu, X., and Hasinoff, B.B. (2013). Molecular mechanisms of the biological activity of the anticancer drug elesclomol and its complexes with Cu(II), Ni(II) and Pt(II). *J Inorg Biochem* 126, 1–6.
- Yamashita, A., Ito, M., Takamatsu, N., and Shiba, T. (2000). Characterization of Solt, a novel SoxLZ/Sox6 binding protein expressed in adult mouse testis. *FEBS Letters* 481, 147–151.
- Yi, Z., Cohen-Barak, O., Hagiwara, N., Kingsley, P.D., Fuchs, D.A., Erickson, D.T., Epner, E.M., Palis, J., and Brilliant, M.H. (2006). Sox6 Directly Silences Epsilon Globin Expression in Definitive Erythropoiesis. *PLoS Genetics* 2, 11.
- Yu, Y., Wang, Z., Sun, D., Zhou, X., Wei, X., Hou, W., Ding, Y., Ma, Y., and Hou, Y. (2018). miR-671 promotes prostate cancer cell proliferation by targeting tumor suppressor SOX6. *European Journal of Pharmacology* 823, 65–71.
- Zafarullah, M., Li, W.Q., Sylvester, J., and Ahmad, M. (2003). Molecular mechanisms of N-acetylcysteine actions. *Cell. Mol. Life Sci.* 60, 6–20.
- Zeng, Z., Liu, Y., Zheng, W., Liu, L., Yin, H., Zhang, S., Bai, H., Hua, L., Wang, S., Wang, Z., et al. (2019). MicroRNA-129-5p alleviates nerve injury and inflammatory response of Alzheimer's disease via downregulating SOX6. *Cell Cycle* 1–16.
- Zhang, D., Li, Y., Tian, J., Zhang, H., and Wang, S. (2015). MiR-202 promotes endometriosis by regulating SOX6 expression. *Int J Clin Exp Med* 8(10):17757-17764, 8.
- Zhao, X., He, X., Han, X., Yu, Y., Ye, F., Chen, Y., Hoang, T., Xu, X., Mi, Q.-S., Xin, M., et al. (2010). MicroRNA-Mediated Control of Oligodendrocyte Differentiation. *Neuron* 65, 612–626.
- Zhou, J., and Chng, W.-J. (2013). Roles of thioredoxin binding protein (TXNIP) in oxidative stress, apoptosis and cancer. *Mitochondrion* 13, 163–169.
- Zhou, Y., Zheng, X., Chen, L., Xu, B., and Jiang, J. (2019). microRNA-181b suppresses the metastasis of lung cancer cells by targeting sex determining region Y-related high mobility group-box 6 (Sox6). *Pathology - Research and Practice* 215, 335–342.
- Zhu, Y., Xia, Y., Niu, H., and Chen, Y. (2014). MiR-16 induced the suppression of cell apoptosis while promote proliferation in esophageal squamous cell carcinoma. *Cell. Physiol. Biochem.* 33, 1340–1348.

## 8. Appendix

### 8.1 1-kb sequence from the reference genome containing SOX6-mSat

1-kb sequence of the microsatellite (mSat) of *SOX6*, including 500 bp up- and downstream, from the human reference genome (Hg19: chr11:16,371,142-16,371,383).

```

...GAGATGTGTCAGCAGTCAATCCAAGCAAACGGGTCTTCTTCAGTTTCTGTCCCACTGTTTCAGATGCCCTGTCTTACCTCACTCT
TCCTTTCACACTTTGTTTTGTTCCATTGGTCTAACTTCTTCTTGGGGTTACTCTTTCACACTAAATAAACTTAACTCCTACAATATT
AGATAGTTCTTATCATCTGTAACATCTTCCCTTACAGCTCTAGAAAACAGTAAATCTTGCAAGTAAGTGATGCAGTATCACACTTGAGA
ATTTAATTTATAGGTTTCTATAATTTCCAGAGATACAATCATACCCAGGCATTGTCAATTTTTATTGCAAAAAGTTTGTAGGTTTTCTG
GTTGATATGTGCTTAACTCTAATCCTTAAGAATAAAAGTAAACAACAAATACATTGAATAAACACATATGTGTATACATATTATATGT
TCTGAACATTATTAGGTCATAACCATGCTGAAATGAAAAGAAAGGGGGAGGGAGGGAGGGAGGAGAGAGGAAGGAAGGAAGGAAG
GAAGGAAGGAAGGAAGGAAGGAAGGAAGGAAGGAAGGAAGGAAGGAAGGGAGGGAGGGAGGAAGGGAGGGAGGAAGGGG
AAGGGAGGGAGGAAGGGGAAGGAAGAAGGAAGGAAGGCTAACTTATCTTTATTAATACAGAAATGTAGCCCTCAGTATAGCTAAT
AAATACTCAAGGCTGTACATCATTGACCCATCTTAACTCAATACAGTTACTACAGCTTCCATGCAGATATTATCTCAAATATTATG
CTATATCATACTGACTTAAGTCATAAAGCCAAATCTTCTTCTCTGAACTCCCTTATGTGCTCTTCATTATTCAGAACATCCTGGAC
TGCC...

```

### 8.2 List of GGAA-repeats of the *SOX6*-associated GGAA-mSat with different *SOX6* expressions and its corresponding enhancer activity

The *SOX6* expression level of the following EwS cell lines were measured by RT-qPCR. Three *SOX6*-high expressing cell lines (TC-32, RDES and POE) as well as three *SOX6*-intermediate expressing cell lines (ORS, SK-N-MC and EW17) and two *SOX6*-low expressing cell lines (EW7 and A673) were separated into their maternal and paternal GGAA-mSat alleles (Allele A and B). The amount of consecutive GGAA-repeats within each allele was determined by Sanger sequencing and their corresponding enhancer activity was measured in a luciferase assay.

Cell line	Average <i>SOX6</i> expression (%)	GGAA-repeats			Enhancer activity			
		Allele A	Allele B	Average number of GGAA-repeats	Allele A	Allele B	Average enhancer activity	Rel. to TC-32 Enhancer activity
TC-32	100	11	13	12	82	175	129	100
RDES	77	10	11	10.5	73	127	100	78
POE	62	10	14	12	48	93	70	54
ORS	32	10	10	10	50	45	48	37
SK-N-MC	30	8	11	9.5	36	76	56	44
EW17	26	9	10	9.5	25	50	38	29
EW7	7	10	11	10.5	76	86	81	63
A673	7	8	11	9.5	32	41	37	28

### 8.3 List of analyzed splicing events by microarray

As SOX6 was reported to be a DNA- and RNA-binding transcription factor, a Human Affymetrix Clariom D microarray was performed, that also measured splicing events. An independent one sample *t*-test was applied to determine significance and furthermore corrected for Bonferroni.

Probe set region	Gene Symbol	P value
		Bonferroni corrected
PSR1600175052.hg.1	EARS2	0.161
PSR0200222926.hg.1	CCDC138	0.555
PSR1500157474.hg.1	MORF4L1	1
PSR0600180336.hg.1	MDGA1	1
PSR0300170031.hg.1	ABCF3	1
PSR0300204354.hg.1	SEMA3B	1
PSR0200225812.hg.1	SMC6	1
PSR0800178860.hg.1	ENPP2	1
PSR0200197661.hg.1	EIF2AK3	1
PSR0200172036.hg.1	GULP1	1
PSR1000144236.hg.1	GTPBP4	1
PSR0600148118.hg.1	JARID2	1
PSR1200167634.hg.1	ACADS	1
PSR0700194571.hg.1	MLL3	1
PSR1100200312.hg.1	NDUFS3	1
PSR0800179609.hg.1	MTSS1	1
PSR0100163643.hg.1	CLCA1	1
PSR1500169532.hg.1	MYO5C	1
PSR0400184559.hg.1	SPOCK3	1
PSR1200191400.hg.1	NUAK1	1

### 8.4 List of differentially expressed genes (DEGs)

Represented are the DEGs of TC-32 and RDES cell lines (including only genes with minimally expression of > 7) sorted by the mean log<sub>2</sub>-fold change (FC). An independent one sample *t*-test was applied to determine significance and further corrected for Bonferroni correction for multiple testing. As statistical power for four samples reached no significance for any gene when applying Bonferroni correction for multiple testing, FDR estimation was applied for comparison. Genes that have been further validated by qRT-PCR are highlighted.

Gene symbol	ENTREZG	Mean_log <sub>2</sub> _FC	P value	P value Bonferroni corrected	FDR_estimate
<b>CDCA3</b>	83461	-2.420	0.012	1	0.237
<b>TXNIP</b>	10628	-2.339	0.084	1	0.315
<b>RHOB</b>	388	-2.308	0.003	1	0.197
<b>PKP2</b>	5318	-2.226	0.173	1	0.435
<b>CRIP1</b>	1396	-2.216	0.010	1	0.235
<b>ANLN</b>	54443	-2.192	0.098	1	0.332
<b>KIF20A</b>	10112	-2.185	0.078	1	0.309
<b>SHMT2</b>	6472	-2.110	0.167	1	0.426
<b>KIF4A</b>	24137	-2.108	0.080	1	0.311

USE1	55850	-2.071	0.146	1	0.397
ESYT1	23344	-2.041	0.141	1	0.391
RAC1	5879	-2.040	0.174	1	0.436
SKP2	6502	-2.037	0.123	1	0.366
SHISA5	51246	-2.015	0.033	1	0.259
RPS16	6217	-1.960	0.184	1	0.449
EPB41	2035	-1.959	0.215	1	0.489
CDK2	1017	-1.958	0.052	1	0.280
CENPM	79019	-1.957	0.054	1	0.282
C11orf24	53838	-1.950	0.058	1	0.287
ID1	3397	-1.934	0.003	1	0.198
FOX M1	2305	-1.930	0.076	1	0.306
DCTPP1	79077	-1.930	0.152	1	0.406
ARHGEF39	84904	-1.921	0.071	1	0.301
UCP2	7351	-1.918	0.160	1	0.417
<b>E2F8</b>	79733	-1.898	0.047	1	0.274
FKBP1A	2280	-1.896	0.179	1	0.443
MICB	4277	-1.887	0.021	1	0.246
CDCA7	83879	-1.886	0.059	1	0.288
SLC29A2	3177	-1.884	0.099	1	0.334
SLC1A5	6510	-1.883	0.108	1	0.345
PSRC1	84722	-1.865	0.038	1	0.265
BIRC5	332	-1.846	0.039	1	0.266
UBE2S	27338	-1.843	0.015	1	0.240
HN1	51155	-1.838	0.259	1	0.540
PLP2	5355	-1.836	0.158	1	0.414
CCNA2	890	-1.832	0.124	1	0.366
MEGF9	1955	-1.831	0.011	1	0.235
CCNK	8812	-1.829	0.108	1	0.346
EPHA2	1969	-1.826	0.016	1	0.241
LRP8	7804	-1.825	0.030	1	0.256
SRM	6723	-1.821	0.147	1	0.399
CD99	4267	-1.809	0.230	1	0.507
CCNB2	9133	-1.805	0.047	1	0.274
PMAIP1	5366	-1.803	0.065	1	0.294
<b>DEPDC1</b>	55635	-1.801	0.030	1	0.256
TMEM97	27346	-1.786	0.032	1	0.257
AURKB	9212	-1.784	0.147	1	0.399
TK1	7083	-1.763	0.107	1	0.344
NROB1	190	-1.759	0.341	1	0.622
ZFP36L2	678	-1.747	0.020	1	0.245
HIST2H3A	333932	-1.744	0.145	1	0.396
HIST1H4L	8368	-1.734	0.094	1	0.328
TFDP1	7027	-1.710	0.057	1	0.285
C14orf119	55017	-1.697	0.121	1	0.362
FADS1	3992	-1.692	0.171	1	0.432
DNAJB1	3337	-1.679	0.004	1	0.201
E2F2	1870	-1.678	0.030	1	0.256
CDC20	991	-1.677	0.083	1	0.314
SLC39A14	23516	-1.671	0.025	1	0.250
HIST1H2BI	8346	-1.650	0.106	1	0.342
SLC35A4	113829	-1.650	0.156	1	0.411
ARPC1A	10552	-1.638	0.237	1	0.515
MKI67	4288	-1.635	0.115	1	0.354
C1QL1	10882	-1.634	0.049	1	0.277
DIXDC1	85458	-1.622	0.006	1	0.222
IAH1	285148	-1.620	0.042	1	0.269
MYBL2	4605	-1.603	0.112	1	0.350
GNG4	2786	-1.601	0.050	1	0.278
HIST1H2BL	8340	-1.597	0.091	1	0.323

AHNAK	79026	-1.588	0.073	1	0.303
CTGF	1490	-1.586	0.052	1	0.280
GIN52	51659	-1.584	0.095	1	0.329
FAM96A	84191	-1.583	0.194	1	0.462
NRM	11270	-1.581	0.009	1	0.231
MLX	6945	-1.581	0.074	1	0.304
ABCB10	23456	-1.571	0.030	1	0.256
ERH	2079	-1.571	0.181	1	0.445
CHAC1	79094	-1.570	0.122	1	0.363
NRSN2	80023	-1.564	0.206	1	0.477
ACOT7	11332	-1.554	0.033	1	0.259
KIFC1	3833	-1.542	0.063	1	0.293
ERHP1	100507125	-1.540	0.150	1	0.403
TLCD1	116238	-1.533	0.115	1	0.354
SREBF2	6721	-1.527	0.062	1	0.292
FAM111B	374393	-1.522	0.050	1	0.278
SMC2	10592	-1.521	0.061	1	0.290
CCNB1	891	-1.514	0.061	1	0.290
CHCHD10	400916	-1.511	0.030	1	0.256
GPN1	11321	-1.507	0.069	1	0.298
RNU1-122P	106480190	-1.505	0.045	1	0.272
ARHGDI1	396	-1.504	0.127	1	0.371
RANGAP1	5905	-1.504	0.102	1	0.337
CDK5	1020	-1.503	0.160	1	0.417
SYTL5	94122	-1.501	0.115	1	0.354
RRM2	6241	-1.497	0.074	1	0.304
ITPRIPL1	150771	-1.493	0.096	1	0.330
GNG10	2790	-1.491	0.016	1	0.241
HIST1H2BJ	8970	-1.486	0.115	1	0.354
SOX6	55553	-1.486	0.006	1	0.220

### 8.5 List of Gene Set Enrichment Analysis of DEGs

GSEA results of DEGs (including only genes with minimally gene expression of > 7) are sorted by NES values.

NAME	NES	NOM p-value	FDR q-value
ROSTY_CERVICAL_CANCER_PROLIFERATION_CLUSTER	-2.652	0	0
GAVIN_FOXP3_TARGETS_CLUSTER_P6	-2.528	0	0
KOBAYASHI_EGFR_SIGNALING_24HR_DN	-2.501	0	0
WHITEFORD_PEDIATRIC_CANCER_MARKERS	-2.498	0	0
DUTERTRE_ESTRADIOL_RESPONSE_24HR_UP	-2.475	0	0
BURTON_ADIPOGENESIS_3	-2.461	0	0
ZHOU_CELL_CYCLE_GENES_IN_IR_RESPONSE_24HR	-2.456	0	0
NAKAYAMA_SOFT_TISSUE_TUMORS_PCA2_UP	-2.456	0	0
CROONQUIST_IL6_DEPRIVATION_DN	-2.447	0	0
SOTIRIOU_BREAST_CANCER_GRADE_1_VS_3_UP	-2.444	0	0
TANG_SENESCENCE_TP53_TARGETS_DN	-2.438	0	0
ISHIDA_E2F_TARGETS	-2.436	0	0
GRAHAM_NORMAL_QUIESCENT_VS_NORMAL_DIVIDING_DN	-2.422	0	0
CHANG_CYCLING_GENES	-2.421	0	0
LEE_EARLY_T_LYMPHOCYTE_UP	-2.409	0	0
FRASOR_RESPONSE_TO_SERM_OR_FULVESTRANT_DN	-2.407	0	0
KONG_E2F3_TARGETS	-2.397	0	0
ZHOU_CELL_CYCLE_GENES_IN_IR_RESPONSE_6HR	-2.393	0	0

## 8.6 List of matched gene expression data with drug response data

Represented are the Pearson correlation coefficients with the corresponding *P* value calculated by the *SOX6* expression and their matching IC50 value (Iorio et al., 2016). An independent one sample *t*-test was applied to determine significance. The list is sorted by the median IC50 values.

Name	Description	Median IC50	Pearson corr. coefficient	<i>P</i> value
<b>Elesclomol (STA-4783)</b>	Oxidative stress inducer	25 nM	−0.565	0.014
Fedratinib	JAK2 inhibitor	2 μM	−0.569	0.012
PHA-793887	CDK2, CDK5, CDK7 inhibitor	3 μM	−0.633	0.004
Serdemetan	HDM2 ubiquitin ligase antagonist	11 μM	−0.600	0.011
Rucaparib	PARP inhibitor	12 μM	−0.665	0.003
Imatinib	v-Abl, c-Kit, PDGFR inhibitor	15 μM	−0.556	0.017
Olaparib	PARP1/2 inhibitor	32 μM	−0.607	0.005

## 8.7 List of figures

Figure 1: Main steps in endochondral ossification.....	9
Figure 2: The pGL3-mSat plasmid with the pGL3-Promoter vector as backbone and the microsatellite (mSat).....	27
Figure 3: The pLKO-shSOX6 plasmid with the Tet-pLKO-puro vector as backbone with shRNA against SOX6 as insert.....	30
Figure 4: Cumate-inducible pCDH-TXNIP vector.....	33
Figure 5: Gating strategy for cell cycle analysis with Propidium Iodide.....	45
Figure 6: Gating strategy for apoptosis analysis with Annexin V staining.....	45
Figure 7: Gating strategy for oxidative stress analysis with DCF-DA staining.....	47
Figure 8: Gating strategy for mito-ROS by MitoSOX Red and MitoTracker Green staining.....	48
Figure 9: SOX6 is highly but variably expressed in EwS.....	59
Figure 10: SOX6 is heterogeneously expressed in EwS cell lines.....	60
Figure 11: Kaplan-Maier curves comprising 161 primary tumors of EwS patients.....	61
Figure 12: EWSR1-FLI1 induces SOX6 expression via an intronic enhancer-like GGAA-mSat.....	64
Figure 13: SOX6 promotes proliferation and anchorage-independent growth <i>in vitro</i> in EwS cells. ...	66
Figure 14: SOX6 promotes cell cycle progression.....	68
Figure 15: SOX6 contributes to tumor growth <i>in vivo</i> .....	70
Figure 16: Correlation of tumor growth in patient-derived EwS xenografts (PDX) with SOX6 expression. .....	71
Figure 17: SOX6 confers to Elesclomol sensitivity.....	73
Figure 18: Elesclomol induces apoptosis <i>in vitro</i> and <i>in vivo</i> .....	75
Figure 19: Elesclomol confers oxidative stress <i>in vitro</i> and <i>in vivo</i> in EwS.....	77
Figure 20: Elesclomol induces SOX6-mediated oxidative stress-levels in EwS cells.....	78
Figure 21: SOX6 mediates TXNIP expression.....	81
Figure 22: SOX6-mediated TXNIP expression links oxidative stress to Elesclomol sensitivity.....	82
Figure 23: Schematic illustration of the EWSR1-FLI1-mediated SOX6 expression and its function in EwS. .....	83

## 8.8 List of tables

Table 1: Overview of microRNAs (miRNA) that regulate SOX6 expression in different tissues or tumor entities.....	6
Table 2: Sox6 function in mesenchymal differentiation, development of the CNS or in differentiation of different tissues.....	8
Table 3: Digestion protocol of pGL3-Promotor vector and gDNA.....	25
Table 4: Protocol for Gotaq PCR-amplification from gDNA. ....	25
Table 5: Thermal cycling conditions for Gotaq-mediated mSat-PCR-amplification.....	26
Table 6: “In-Fusion HD cloning” reactions according to manufacturer’s protocol. ....	26
Table 7: Design of shRNAs against SOX6 or control.....	28
Table 8: Double digestion protocol. ....	29
Table 9: Ligation protocol of Tet-pLKO-puro with shRNAs. ....	30
Table 10: Customized dsDNA (5' → 3'). ....	31
Table 11: Ligation protocol of pCDH vector with dsDNA oligonucleotide sequence.....	31
Table 12: Primer for eGFP amplification from pCMV-GFP vector.....	32
Table 13: Primer for cDNA TXNIP amplification. ....	32
Table 14: Protocol for colony-PCR of pGL3-mSat (*)– and pLKO-shSOX6/shCtrl (#)-insert amplification. ....	34
Table 15: Protocol for PCR-amplification of eGFP (***) or cDNA TXNIP (###) from pCMV-GFP or TXNIP ORF vector, respectively and protocol for colony-PCR of pCDH-TXNIP-insert (###) amplification. ....	34
Table 16: Thermal cycling conditions for colony-TD-PCR of pLKO-Tet and pGL3 vectors.....	35
Table 17: Thermal cycling conditions for (colony)-TD-PCR for pCMV-GFP/ TXNIP ORF vector and pCDH-TXNIP vectors. ....	36
Table 18: Origin of the mostly used EwS cell lines in this thesis.....	37
Table 19: Reverse transcription protocol for EwS cells.....	40
Table 20: qRT-PCR protocol with SYBR green master mix. ....	40
Table 21: Thermal cycling conditions for qRT-PCR.....	41
Table 22: Pre-dilutions and final concentration of sipool-mediated transfection.....	43
Table 23: Transfection protocol for sipool-mediated knockdown.....	43
Table 24: Transient transfection protocol of pGL3-mSat* or pCAG-YFP* in A673/TR/shEF1 cells for luciferase assay.....	49

## 8.9 List of abbreviations

3'/5' –LTR	Long Terminal Repeat
AmpR	Ampicillin Resistance gene
BCS	Body Condition Score
BMP	Bone Morphogenic Protein
CAP	Catabolite Activator Protein binding site
cDNA	Complementary DNA
ChIP	Chromatin Immunoprecipitation
cPPT/CTS	Central PolyPurine Tract/ Central Termination Sequence
DAB+	3, 3 -diaminobenzidine
DCF-DA	2',7'-dichlorodihydrofluorescein diacetate
DMSO	Dimethylsulfoxid
Dox	Doxycycline
EwS	Ewing sarcoma
EWSR1-FLI1	Ewing sarcoma breakpoint region 1 / friend leukemia virus integration 1
f1 ori	Filamentous phage derived origin of replication
FC	Fold Change
FCS	Fetal Calf Serum
GEO	Gene Expression Omnibus
GSEA	Gene-Set Enrichment Analysis
H&E	Hematoxylin and Eosin
H <sub>2</sub> O <sub>2</sub>	Hydrogen peroxide
HIV-1	Human Immunodeficiency Virus-1
hPGK	Human PhosphoGlycerate Kinase
HRP	Horseradish peroxidase
ICGC	International Cancer Genome Consortium
IHC	Immunohistochemistry
IRS	Immune Reactivity Score
lac	lactose
miRNA	Micro RNA
Mito-ROS	Mitochondrial Reactive Oxygen Species
mRNA	Messenger RNA
mSat	Microsatellite
MSC	Mesenchymal Stem Cells
Nac	N-acetyl-cysteine

---

NCBI	National Center for Biotechnology Information
NSG	NOD/Scid/Gamma
ori	Origin of replication in <i>E.coli</i>
OSX	Osterix
PI	Propidium Iodide
Poly (A) signal	Polyadenylation signal
PSR	Probe Selection Region
PuroR	Puromycin resistance
qRT-PCR	Quantitative Real-Time PCR
RMA	Robust Multiarray Average
RRE	Rev Response Element
RSV	Rous Sarcoma Virus
RT	Room Temperature
RUNX2	Runt-related transcription factor 2
SDS-PAGE	Sodium-dodecylsulfate-polyacrylamid-gelelectrophoresis
SEM	Standard error of the mean
shRNA	Short hairpin RNA
siRNA	Small interfering RNA
STR	Short Tandem Repeat
SOX6	SRY-Box 6
SV40	Simian Virus 40
TetR	Tetracycline Resistance
TGF- $\beta$	Transforming Growth Factor beta
TMA	Tissue Microarray
TXNIP	Thioredoxin binding protein
UCSC	University of California Santa Cruz )
VBA	Visual Basic for Applications
WB	Western blot

## 9. Acknowledgement

First, I would like to express my deepest appreciation to my supervisor Dr. Thomas Grünewald, PhD who taught me valuable scientific knowledge at each of our many meetings and believed in me and in my work from the very first beginning.

I am especially grateful to Prof. Dr. Kirchner for being part of my Thesis Advisory Committee and agreeing to be a reviewer of my PhD thesis.

I owe my deepest gratitude to the Matthias Lackas-Stiftung for their financial support, a help without which I would never have been able to complete this work.

I am indebted to Dr. Shunya Ohmura for his commitment in carrying out my mouse experiments and the many weekends he has sacrificed for this.

Special thanks to Anja Heier and Andrea Sendelhofert for excellent technical assistance and their support during my thesis.

A special thanks goes to the whole AG Grünewald for their technical support and joyful moments that we shared in the lab. I would particularly thank my colleague Giusy for her great supervision, Steffi for her technical assistance and Martin for scientific discussions.

I would like to thank Laura, Martin and the family Helm-Finck for proof-reading of my manuscript and their helpful feedback.

My deepest heartfelt appreciation goes to my parents who, not only during my studies, but throughout my entire life have always been there for me and always encouraged me in everything I am doing.

From the bottom of my heart I would like to thank my beloved fiance Tom for his love, patience and support over the last years.

## 10. Publications

Parts of this thesis have been published in:

- **Aruna Marchetto**, Shunya Ohmura, Martin F Orth, Maximilian M L Knott, Maria V Colombo, Chiara Arrigoni, Victor Bardinet, David Saucier, Fabienne S Wehweck, Jing Li, Stefanie Stein, Julia S Gerke, Michaela C Baldauf, Julian Musa, Marlene Dallmayer, Laura Romero-Pérez, Tilman L B Hölting, James F Amatruda, Andrea Cossarizza, Anton G Henssen, Thomas Kirchner, Matteo Moretti, Florencia Cidre-Aranaz, Giuseppina Sannino, Thomas G P Grünewald.

*Oncogenic hijacking of a developmental transcription factor evokes vulnerability toward oxidative stress in Ewing sarcoma.* Nat Commun. 2020;11(1):2423. Published 2020 May 15. doi:10.1038/s41467-020-16244-2

Additionally, I contributed to following publications during my thesis that were not further described:

- Baldauf MC\*, Orth MF\*, Dallmayer M\*, **Marchetto A**, Gerke JS, Rubio RA, Kiran MM, Musa J, Knott MML, Ohmura S, Li J, Akpolat N, Akatli AN, Özen Ö, Dirksen U, Hartmann W, de Alava E, Baumhoer D, Sannino G, Kirchner T, Grünewald TGP.  
*Robust diagnosis of Ewing sarcoma by immunohistochemical detection of super-enhancer-driven EWSR1-ETS targets.* Oncotarget. 2017 Aug 4;9(2):1587-1601
- Sannino G, **Marchetto A**, Kirchner T, Grünewald TGP.  
*Epithelial-to-Mesenchymal and Mesenchymal-to-Epithelial Transition in Mesenchymal Tumors: A ParaDox in Sarcomas?* Cancer Res. 2017 Sep 1;77(17):4556-4561. doi: 10.1158/0008-5472.CAN-17-0032. Epub 2017 Aug 15.
- Baldauf MC, Gerke JS, Kirschner A, Blaeschke F, Effenberger M, Schober K, Rubio RA, Kanaseki T, Kiran MM, Dallmayer M, Musa J, Akpolat N, Akatli AN, Rosman FC, Özen Ö, Sugita S, Hasegawa T, Sugimura H, Baumhoer D, Knott MML, Sannino G, **Marchetto A**, Li J, Busch DH, Feuchtinger T, Ohmura S, Orth MF, Thiel U, Kirchner T, Grünewald TGP.  
*Systematic identification of cancer-specific MHC-binding peptides with RAVEN.* Oncoimmunology. 2018 Jul 23;7(9):e1481558. doi: 10.1080/2162402X.2018.1481558. eCollection 2018.
- Orth MF, Gerke JS, Knösel T, Altendorf-Hofmann A, Musa J, Alba-Rubio R, Stein S, Hölting TLB, Cidre-Aranaz F, Romero-Pérez L, Dallmayer M, Baldauf MC, **Marchetto A**, Sannino G, Knott MLK, Wehweck F, Ohmura S, Li J, Hakozaiki M, Kirchner T, Dandekar T, Butt E, Grünewald TGP.  
*Functional genomics identifies AMPD2 as a new prognostic marker for undifferentiated pleomorphic sarcoma.* Int J Cancer. 2018 Sep 28.
- Dallmayer M, Li J, Ohmura S, Alba-Rubio R, Baldauf MC, Hölting TLB, Musa J, Knott MLK, Stein S, Cidre-Aranaz F, Wehweck F, Romero-Pérez L, Gerke JS, Orth MF, **Marchetto A**, Kirchner T, Bach H, Sannino G, Grünewald TGP.  
*Targeting the CALCB/CGRP-receptor axis inhibits growth of Ewing sarcoma.* Cell Death Dis. 2019 Feb 11;10(2):116

- Shannan B, Matschke J, Chauvistre H, Vogel F, Klein D, Meier F, Westphal D, Bruns J, Rauschenberg R, Utikal J, Forschner A, Berking C, Terheyden P, Dabrowski E, Gutzmer R, Rafei-Shamsabadi D, Meiss F, Heinzerling L, Zimmer L, Varaljai R, Hoewner A, Horn S, Klode J, Stuschke M, Scheffler B, **Marchetto A**, Sannino G, Grünewald TGP, Schadendorf D, Jendrossek V, Roesch A.  
*Sequence-dependent cross-resistance of combined radiotherapy plus BRAFV600E-inhibition in melanoma.* Eur J Cancer. 2019 Mar; 109:137-153.
- Sannino G, **Marchetto A**, Ranft A, Jabar S, Zacherl C, Alba-Rubio R, Stein S, Wehweck F, Kiran MM, Hölting TLB, Musa J, Romero-Pérez L, Cidre-Aranaz F, Knott MML, Li J, Jürgens H, Sastre A, Alonso J, Da Silveira W, Hardiman G, Gerke JS, Orth MF, Hartmann W, Kirchner T, Ohmura S, Dirksen U and Grünewald TGP.  
*Gene expression and immunohistochemical analyses identify SOX2 as major risk factor for overall survival and relapse in Ewing sarcoma patients.* EBioMedicine. 2019 Aug 16. pii: S2352-3964(19)30518-3.
- Musa J, Cidre-Aranaz F, Aynaud MM, Orth MF, Knott MML, Mirabeau O, Mazor G, Varon M, Hölting TLB, Grossetête S, Gartlgruber M, Surdez D, Gerke JS, Ohmura S, **Marchetto A**, Dallmayer M, Baldauf MC, Stein S, Sannino G, Li J, Romero-Pérez L, Westermann F, Hartmann W, Dirksen U, Gymrek M8, Anderson ND, Shlien A, Rotblat B, Kirchner T, Delattre O, Grünewald TGP.  
*Cooperation of cancer drivers with regulatory germline variants shapes clinical outcomes.* Nat Commun. 2019 Sep 11;10(1):4128. doi: 10.1038/s41467-019-12071-2.
- Gerke JS, Orth MF, Tolkach Y, Romero-Pérez L, Wehweck FS, Stein S, Musa J, Knott MML, Hölting TLB, Li J, Sannino G, **Marchetto A**, Ohmura S, Cidre-Aranaz F, Müller-Nurasyid M, Strauch K, Stief C, Kristiansen G, Kirchner T, Buchner A, Grünewald TGP.  
*Integrative clinical transcriptome analysis reveals TMPRSS2-ERG dependency of prognostic biomarkers in prostate adenocarcinoma.* Int J Cancer. 2020 Apr 1;146(7):2036-2046. doi: 10.1002/ijc.32792. Epub 2019 Nov 29. PMID: 31732966.
- Orth MF, Hölting TLB, Dallmayer M, Wehweck FS, Paul T, Musa J, Baldauf MC, Surdez D, Delattre O, Knott MML, Romero-Pérez L, Kasan M, Cidre-Aranaz F, Gerke JS, Ohmura S, Li J, **Marchetto A**, Henssen AG, Özen Ö, Sugita S, Hasegawa T, Kanaseki T, Bertram S, Dirksen U, Hartmann W, Kirchner T, Grünewald TGP.  
*High Specificity of BCL11B and GLG1 for EWSR1-FLI1 and EWSR1-ERG Positive Ewing Sarcoma.* Cancers (Basel). 2020 Mar 10;12(3):644. doi: 10.3390/cancers12030644. PMID: 32164354; PMCID: PMC7139395.